

**Mechanistic Insight into the Effect of Polymer and NOM Coatings on
Adhesion and Interactions between Nanoparticles and Bacteria**

Zhiqiang Li

B.E., Tongji University, Shanghai, P.R. China, 2003
M.S., the University of Vermont, Burlington, VT, USA, 2006

A DISSERTATION
SUBMITTED IN PARTIAL FULFILLMENT
OF THE REQUIREMENTS
FOR THE DEGREE OF

Doctor of Philosophy

in

Civil and Environmental Engineering

Carnegie Mellon University

Pittsburgh, PA

August, 2011

Copyright © 2011

ABSTRACT

Engineered nanomaterials may be released to the environment and adversely affect the microbial community. Three generalized modes of interaction between NPs and bacteria that lead to observed toxicity are commonly described: physical contact between nanoparticles and cells (Type I), production of reactive oxygen species (ROS) (Type II), and release of toxic metal ions (Type III). Previous studies demonstrated that polymeric coatings and natural organic matter (NOM) may reduce antibacterial activities of nanoparticles. Thus, application of coatings is a mean to mitigate nanoparticle toxicity. However, coatings may have different effects depending on the mode of interaction between the NP and bacteria and the toxicity mechanism. The reasons for the different effects of coatings observed on nanoparticles having these different modes are still unclear.

The primary objectives of this thesis are (i) to assess the effect that organic macromolecular coatings such as synthetic polymers and natural organic matter have on nanoparticle-microorganism interactions with type I, II, and III mode of action, and (ii) to determine the reasons for these effects.

NZVI (type I), nano-TiO₂ (type II), and AgNPs (type III) were studied as representative nanoparticles. Poly(styrene sulfonate) (PSS), polyaspartate (PAP), humic acid, and carboxy methyl cellulose (sodium salt) (CMC) were used to coat nanoparticles. *E. coli* was exposed to bare and coated nanoparticles, and the bacterial concentration was determined at specific times using a plate counting technique. By observing different effects for the same coating on each type of nanoparticle, conclusions are made regarding

the exact nature by which the adsorbed coatings (or in solution) are affecting the observed growth inhibition of *E. coli* (toxicity).

For NZVI (type I), exposure to 100 mg/L of bare NZVI with 28% Fe⁰ content resulted in a 2.2-log inhibition after 10 minutes and a 5.2-log growth inhibition after 60 minutes. Adsorbed poly(styrene sulfonate) (PSS), poly(aspartate) (PAP), or NOM on NZVI with the same Fe⁰ content significantly decreased its toxicity, causing less than 0.2-log inhibition after 60 minutes. TEM images and heteroaggregation studies indicate that bare NZVI adheres significantly to cells, and that the adsorbed polyelectrolyte or NOM prevents adhesion. This is the proposed mechanism for decreasing NZVI toxicity.

For nano-TiO₂ (type II), exposure to 100 mg/L bare and PAP coated nano-TiO₂ with UV irradiation resulted in 5-log growth inhibition after 3 hours. Thus, PVP, a coating that prevents direct contact between *E. coli* and the TiO₂ was not sufficient to decrease the toxicity of TiO₂ as it did for NZVI. However, adsorbed NOM significantly decreased nano-TiO₂ toxicity, causing less than 0.3-log inhibition with UV irradiation for 3 hours. It was demonstrated that NOM scavenged ROS produced by the TiO₂ and thereby decreased its toxicity. The other coating evaluated (PAP) could not scavenge ROS produced by TiO₂. This study suggests that NOM, or other coatings capable of scavenging ROS may be used to mitigate the toxic effects of nano-TiO₂.

For AgNPs, exposure of cells to 1 mg/L bare AgNP resulted in 6-log inhibition after 3 hours. Dissolved coal-derived humic acid at 100 mg/L decreased AgNP toxicity, resulting in less than 1-log inhibition over the same period. However, dissolved polyvinylpyrrolidone (PVP) and carboxy methyl cellulose (CMC) had no impact on the toxicity of AgNP. Results show that NOM scavenges Ag⁺ ion released by AgNP more

than CMC and PVP. A correlation between sulfur content and NOM effects on AgNP toxicity is observed. Humic acid containing higher sulfur content resulted in less toxicity. This suggests that Ag^+ scavenging by NOM, and the resulting decrease in toxicity, may be correlated with its ability to complex with NOM through thiol type interactions with Ag ion. These findings suggest that the potential for detrimental impacts of nanoparticles that interact with bacteria through the release of toxic metal ions can be decreased by NOM or other polymeric coatings that scavenge toxic metal ions.

Our results show that the presence of natural organic matter, ubiquitous in terrestrial systems, greatly reduces the toxicity of the nanoparticles, regardless of the mode of toxicity. We demonstrate that the decrease of toxicity is closely tied to the chemistry of both the coating and nanoparticle.

ACKNOWLEDGEMENTS

I have been eager to write the acknowledgements to express my deep gratitude to the following people. Without the guidance, help, encouragement and support from them the completion of this work would not have been possible.

I owe my deepest gratitude to my co-advisors Dr. Kelvin Gregory (chair of the doctoral committee) and Greg Lowry. Their constant guidance and advising is extremely helpful. Their enthusiasm and dedication to science, patience, understanding, not-judging, support, trust, have set a role model for me. It is my fortune to have them as my advisors during my years as a graduate student. Thanks go to my doctoral committee members, Dr. Jeanne VanBriesen and Dr. Claudia Gunsch for their prompt, valuable suggestions and supports over the years.

Many thanks go to the past and present group members in the 207 Lab, for their help, advice, accompany and support.

I also would like to thank my family especially my parents for their comfort and encouragement. I thank my dear friends both here in Pittsburgh and all over the world for their constant support, help and accompany during hard times.

I want to thank my wife, Xinyu Wei, for her encouragement, company, patience, and unconditional support. Without her, it would be much more difficult to complete my study and this PhD thesis.

Lastly, thanks go to the funding agencies: the National Science Foundation (BES-0608646 and EF-0830093) and the U.S. EPA R833326.

DEDICATION

To my parents

Haizhou Li and Xiying Zhang

and to

My Wife

Xinyu Wei

for their deep, unconditional love and support

TABLE OF CONTENTS

Chapter 1: Introduction	1
1.1 Engineered Nanomaterials	1
1.2 Nanoparticle-Microbe Interactions and Nanomaterial Cytotoxicity	3
1.2.1 Metal Nanoparticles.....	3
1.2.2 Fullerene and Carbon Nanotubes	5
1.2.3 Metal Oxide Nanoparticles	6
1.2.4 Effect of Nanoparticle Size.....	7
1.3 Effect of Polymeric Coatings and NOM on Nanoparticle-Microbe Interactions.....	8
1.4 Hypothesis: Nanoparticle-Microbe Modes of Interaction	11
1.5 Research Approach	17
1.5.1 Nanoparticles.....	17
1.5.2 Nanoparticle Modification	18
1.5.3 Nanoparticle Characterization	18
1.5.4 <i>E. coli</i> Culture	18
1.5.5 Coatings	19
1.5.6 Transmission Electron Microscopy (TEM).....	20
1.5.7 Experimental Design	20
1.6 Research Objectives	21
1.7 Dissertation Overview.....	22
1.8 References	24

Chapter 2: Adsorbed Polymer and NOM Limits Adhesion and Toxicity of Nano

Scale Zero-valent Iron (NZVI) to <i>E. coli</i>	29
2.1 Abstract	29
2.2 Introduction	30
2.3 Materials and Methods	32
2.3.1 Chemicals and NZVI	32
2.3.2 NZVI Preparation.....	33
2.3.3 <i>E. coli</i> Culture	34
2.3.4 Exposure Experiments and Minimal Inhibitory Concentration	
(MIC) Determination	34
2.3.5 Measuring the Dispersed Iron Concentration in Culture Tubes ...	36
2.3.6 Transmission Electron Microscopy (TEM).....	36
2.4 Results and Discussion	37
2.4.1 NZVI Cytotoxicity Assessment.....	37
2.4.2 Effect of Coatings.....	39
2.4.3 Effect of Fe⁰ Content	43
2.4.4 Effect of Aerobic and Anaerobic Conditions	44
2.4.5 Minimum Inhibitory Concentrations (MIC).....	45
2.5 Acknowledgements.....	47
2.6 References	47

Chapter 3: Obstruction of Cytotoxicity by Natural Organic Matter Coatings on

Titanium Dioxide Nanoparticles.....	52
3.1 Abstract	52

3.2 Introduction	53
3.3 Materials and Methods	54
3.3.1 Chemicals and TiO ₂ Nanoparticles	54
3.3.2 TiO ₂ Nanoparticle Dispersion Preparation	55
3.3.3 <i>E. coli</i> Culture Preparation.....	56
3.3.4 UV Irradiation and Intensity Measurements.....	56
3.3.5 Exposure Experiments	57
3.3.6 Reactive Oxygen Species Scavenging Experiments	57
3.3.7 Hydroxyl Radical Measurement	58
3.3.8 NOM and Hydroxyl Radicals Reaction Constant.....	59
3.4 Results and Discussion	59
3.4.1 Growth Inhibition by Nano-TiO ₂	59
3.4.2 Reactive Oxygen Species	61
3.4.3 Hydroxyl Radical	64
3.4.4 Hydrogen Peroxide	65
3.4.5 Coating Effects	66
3.5 Supporting Information Available	68
3.6 Literature Cited.....	68
 Chapter 4: Obstruction of Cytotoxicity by Dissolved Natural Organic Matter on	
Silver Nanoparticles.....	71
4.1 Abstract	71
4.2 Introduction	72
4.3 Materials and Methods	74

4.3.1 Chemicals and Silver Nanoparticles	74
4.3.2 Silver Nanoparticle Synthesis and Dispersion Preparation.....	74
4.3.3 <i>E. coli</i> Culture Preparation.....	75
4.3.4 Exposure Experiments	76
4.4 Results and Discussions	77
4.4.1 Growth Inhibition by AgNP	77
4.4.2 Silver Ions	78
4.4.3 Dissolved Humic Acid Effects.....	82
4.5 References	84
 Chapter 5: Natural Organic Matter Coatings Eliminate Cytotoxicity of Nanoscale Zero-valent Iron and Titanium Dioxide Nanoparticles to <i>Shewanella oneidensis</i>	
5.1 Abstract	86
5.2 Introduction	87
5.3 Materials and Methods	89
5.3.1 Chemicals and Nanoparticles	89
5.3.2 NZVI Preparation.....	90
5.3.3 TiO ₂ Nanoparticle Dispersion Preparation	90
5.3.4 <i>S. oneidensis</i> Culture Preparation.....	91
5.3.5 UV Irradiation and Intensity Measurements.....	91
5.3.6 Exposure Experiments	92
5.3.7 Hydroxyl Radical Measurement	92
5.3.8 NOM and Hydroxyl Radicals Reaction Constant.....	93
5.4 Results and Discussion	94

5.4.1 Growth Inhibition by NZVI.....	94
5.4.2 Growth Inhibition by Nano-TiO ₂	95
5.4.3 Coating Effects	96
5.5 Conclusions	100
5.6 References	101
 Chapter 6: Summary, Conclusions, Recommendations for Future Research and Implications	104
6.1 Summary	104
6.2 Conclusions	105
6.2.1 NZVI	105
6.2.2 Titanium Dioxide Nanoparticles	107
6.2.3 Silver Nanoparticle	108
6.2.4 Inorganic coatings: Sulfidation Effects on AgNP Cytotoxic Properties	109
6.3 Recommendations for Future Research.....	110
6.3.1 Model Microorganisms	110
6.3.2 Metal Ion Releasing Nanoparticles	110
6.4 Implications.....	111
6.5 References	113
 APPENDIX A: Notation.....	116
A.1 Abbreviations.....	116
A.2 Symbols.....	118

APPENDIX B: Supporting Information for Chapter 2	119
APPENDIX C: Supporting Information for Chapter 3	120
APPENDIX D: Methods.....	122
D.1 Coating Adsorption Protocol.....	122
D.2 Culture Preparation	125
D.3 Plate Count.....	126
APPENDIX E: Microbial Electricity Generation via Microfluidic Flow Control..	128
E.1 Abstract	128
E.2 Introduction	129
E.3 Materials and Methods	132
E.3.1 Bacterial Strains and Culture Media	132
E.3.2 Fabrication of Microfluidic Fuel Cells	132
E.3.3 Inoculation and Operation of Microfluidic Microbial Fuel Cells	134
E.3.4 Imaging of Microfluidics and Biofilm Cultures	135
E.3.5 Current Dependence on Electron Donor Concentrations	136
E.3.6 Analytical Methods	137
E.4 Results and Discussion	137
E.4.1 <i>Geobacter sulfurreducens</i>: Current Production and Sensing.....	137
E.4.2 <i>Shewanella oneidensis</i>: Current Production and Biofilm Imaging	
.....	140
E.5 Conclusions.....	143
E.6 Acknowledgements	146

E.7 References.....	146
APPENDIX F: Supporting Information for Appendix D	150

LIST OF FIGURES

Figure 1.1. Number of total products listed, by date of inventory update, with regression analysis.....	2
(Image source: http://www.nanotechproject.org/inventories/consumer/analysis_draft/)...	2
Figure 1.2. TEM images show bacteria-nanoparticle interactions. (a) Bare NZVI strongly associated to <i>E. coli</i> cells (31). (b) AgNP caused cell membrane damage (32). (c) Fullerene attached to bacterial cells and damaged the cell membrane (33). (d) ZnO nanoparticle damaged the cell membrane (34).	5
Figure 1.3. Schematic of nanoparticle-microorganism modes of interaction. Mode type I requires physical interaction between cells and particles. Mode type II interacts with bacterial cells with generated reactive oxygen species. Mode type III interacts with bacterial cells by releasing cytotoxic metal ions.....	11
Figure 1.4. Hypotheses for interaction between NZVI and bacterial cells and coating effects. Bare NZVI is cytotoxic due to reductive decomposition, requiring physical contact between cell and particle. Coatings may decrease NZVI toxicity by prevent cell-particle interaction.	13
Figure 1.5. Hypotheses for interaction between TiO ₂ and bacterial cells and coating effects. Nano-TiO ₂ inhibits bacterial growth by generating ROS, which is highly reactive. Coatings that can react with the produced ROS will reduce the cytotoxic effects of nano-TiO ₂ . Coatings incapable of reacting with ROS may have little impact on nano-TiO ₂ cytotoxic activities.	15
Figure 1.6. Hypotheses for interaction between AgNP and bacterial cells and coating effects. AgNPs inhibit bacterial growth by released Ag ions. Coatings capable of	

scavenging Ag ions will reduce nanoparticle toxicity. However, this effect may be temporary if the coating becomes saturated with the toxic metal ion..... 16

Figure 1.7. Numbers of products associated with specific materials..... 17

(Image source: http://www.nanotechproject.org/inventories/consumer/analysis_draft/). 17

Figure 2.1. (a) Exposure of *E. coli* to bare NZVI and coated NZVI under anaerobic conditions; (b) Exposure of *E. coli* to aged NZVI, containing 0%, 7%, and 20% Fe⁰ under anaerobic conditions; (c) Exposure of *E. coli* to NZVI and coated NZVI under aerobic conditions; and (d) Fe⁰ content in NZVI as a function of exposure time to air-saturated water (NZVI concentration was approximately 1g/L). Oxygen was continuously bubbled through the vessel during aging. 38

Figure 2.2. TEM images of *E. coli* incubated with (a) 10 mg/L of bare NZVI (20% Fe⁰) and (b) 10 mg/L of MRNIP2 (coated with olefin maleic acid, MW=16, 000 g/mol) for 1 h. The globular material on the cells was observed for all cells that had been exposed to MRNIP2. The chemical composition of the material is not known, but it did not appear to affect cell viability. 40

Figure 2.3. The surface coatings on NZVI may prevent physical interaction with *E. coli*. Higher MW polyelectrolyte coatings provide electrosteric repulsive forces while low MW surfactants and polyelectrolytes provide predominantly electrostatic repulsive forces that are more prone to charge screening with increasing ionic strength. Uncharged polymers provide steric repulsions (not shown). Natural organic matter can act as a polyelectrolyte or surfactant, providing electrostatic or electrosteric repulsive forces. ... 43

Figure 3.1. Exposure of *E. coli* to bare, PAP coated, and NOM coated nano-TiO₂ under UV irradiation, control experiment without nano-TiO₂ under UV irradiation, and control

experiment with 100 mg/L PAP, and 100 mg/L NOM without UV irradiation. Less than 1-log inhibition was observed in the absence of illumination with 1000 mg/L bare nano-TiO ₂ over 3 hours.....	60
Figure 3.2. (a) Exposure of <i>E. coli</i> to 100 mg/L PAP coated nano-TiO ₂ with ROS scavengers: 0.1 and 1.0 mM mannitol, 20-50 units/mL catalase, and 20-75 units/mL superoxide dismutase; (b) <i>p</i> CBA degradation by 100 mg/L bare, PAP coated, and NOM coated nano-TiO ₂ under UV irradiation; (c) first-order fits of <i>p</i> CBA degradation as a function of O ₃ dose and Ω for NOM (10 mg/L).	63
Figure 3.3. Nano-TiO ₂ inhibits bacterial growth by generating hydroxyl radical. Natural organic matter may react with \cdot OH or decrease light intensity reached at the particles and reduces cytotoxic effects of nano-TiO ₂	67
Figure 4.1. Exposure of <i>E. coli</i> to 1 mg/L AgNP, 1 mg/L AgNP with 100 mg/L dissolved CD-HA, 100 mg/L dissolved ES-HA, and 100 mg/L dissolved Anth-SW-HA, 1 mg/L CD-HA coated AgNP, and <i>E. coli</i> control experiment.	78
Figure 4.2. Exposure of <i>E. coli</i> to 0.2 mg/L Ag ⁺ , 0.2 mg/L Ag ⁺ with 100 mg/L dissolved CD-HA, 0.2 mg/L Ag ⁺ with 100 mg/L dissolved ES-HA, and 0.2 mg/L Ag ⁺ with 100 mg/L Anth-SW-HA.	79
Figure 4.3. Exposure of <i>E. coli</i> to 0.2 mg/L Ag ⁺ , 0.2 mg/L Ag ⁺ with 100 mg/L dissolved CMC, and 0.2 mg/L Ag ⁺ with 100 mg/L PVP.....	81
Figure 4.4. Ag ⁺ concentration change over three hours for 0.2 mg/L Ag ⁺ with 100 mg/L CD-HA, 0.2 mg/L Ag ⁺ with 100 mg/L CMC, 1 mg/L AgNP with 100 mg/L CD-HA, and 1 mg/L AgNP.....	81

Figure 4.5. AgNP inhibits bacterial growth by releasing Ag^+ . Natural organic matter may react with Ag^+ and reduces cytotoxic effects of AgNP.	83
Figure 5.1. (a) Exposure of <i>S. oneidensis</i> to 10, 50, 100, 250, and 500 mg/L bare RNIP under anaerobic condition; (b) Exposure of <i>S. oneidensis</i> to 100 mg/L bare, maleic acid co-olefin coated, and NOM coated nano-TiO ₂ under anaerobic condition.	97
Figure 5.2. (a) Exposure of <i>S. oneidensis</i> to 25, 50, 100, 250, and 500 mg/L bare nano-TiO ₂ under UV irradiation; (b) Exposure of <i>S. oneidensis</i> to 100 mg/L bare, PAP coated, and NOM coated nano-TiO ₂ under UV irradiation. Less than 1-log inhibition was observed in the absence of illumination with 1000 mg/L bare nano-TiO ₂ over 3 hours. .	98
Figure 5.3. (left) The surface coatings on NZVI may prevent physical interaction with <i>S. oneidensis</i> , and reduce its cytotoxicity. (right) Nano-TiO ₂ inhibits bacterial growth by generating $\cdot\text{OH}$ (hydroxyl radical). Natural organic matter may react with $\cdot\text{OH}$ or decrease light intensity reached at the particles and reduces cytotoxic effects of nano-TiO ₂	101
Figure B.1. Aggregation and sedimentation of bare and polymer coated NZVI particles in 5 mM sodium bicarbonate. Bare particles rapidly aggregate and sediment without mixing. Particle concentration is 100 mg/L in all cases.	119
Figure C.1. Exposure of <i>E. coli</i> to 10ppm, 100ppm, and 1000ppm bare nano-TiO ₂ under UV irradiation, and exposure to 1000ppm bare nano-TiO ₂ under dark condition.....	120
Figure C.2. Exposure of <i>E. coli</i> to 3, 6, 9, and 12 mM H ₂ O ₂ with 100 mg/L NOM and 100 mg/L PAP.....	121
Figure D.1. The microfluidic microbial fuel cell (μMFC). An illustration of the essential components for μMFC : (A) two inlets and one outlet, two gold microelectrodes	

connected with gold wires, and (B) SEM image of bacteria colonized on the anode. Images of the fabricated μ MFC including (C) the μ MFC with blue dye in one inlet confirming the ability to establish laminar flow conditions in the μ MFC and (D) multiple μ MFC units on one glass wafer confirming our ability to multiplex this system using lithographic techniques. 131

Figure D.2. Schematic of μ MFC fabrication process and laminar flow condition verification. (A) Photolithography and metal etching techniques were employed for fabrication of the gold microelectrodes. A photoresist layer on top of the gold with desired pattern was created by exposing to UV light (step 1 and 2). The gold uncovered with photoresist on a glass wafer was etched off to form the microelectrodes and wires. (B) The microstructure channel was fabricated using conventional soft lithography. PDMS with a 10:1 ratio of base to curing agent was used and cast against the mold (step 3 and 4), which was created by exposing photoresist on a silicon wafer to UV light (steps 1 and 2). (C) Image at the convergence of the anolyte and catholyte channels and (D) the outlet of the microfluidic fuel cell channel showing that the laminar flow separation persists well along the length of the channel. 134

Figure D.3. Electricity production by *G. sulfurreducens* in the μ MFC. (A) Electrical current as a function of time showing microbial growth and adaptation to electrode respiration was dependent on diffusion limited conditions maintained by laminar flow through the fuel cell. (B) Magnification of x axis to show the onset of the earliest current after inoculation of the cells. (C) Electrical current as a function of time with varying concentrations of electron donor (acetate) (i.e. 0 mM, 5 mM, 10 mM and 20 mM). (D) Current response plotted as a function of varying electron donor concentration. 140

Figure D.4. Current production by *S. oneidensis* and SEM images of *S. oneidensis* growing on a gold electrode in a μ MFC. (A) Electrical current as a function of time. Reactors were sacrificed for imaging after 4 days of continuous operation in (A). (B) Anode and cathode at low magnification shows biofilm growth on the anode surface, while almost no biofilm was formed on the cathode. (C) Higher magnification images of the anode and cathode. (D) Higher magnification images of biofilm growth on the anode at a 75° tilted angle view..... 142

Figure E.1. Electricity production by *G. sulfurreducens* in the μ MFC with H₂ as the only electron donor. (A) High current density was observed when medium with acetate replaced with H₂ saturated medium. (B) Magnification of the axes in (A) to better show adaptation to electrode respiration and current production with acetate as electron donor. 150

Figure E.2. SEM images for investigation of cell-like materials on cathode (Fig. 4 B, C1) at higher magnification. 150

LIST OF TABLES

Table 1.1. Coating effects on nanoparticle properties and particle-microorganism interactions (modified from Aruguete and Hochella (6))	11
Table 1.2. Hypothesis for nanoparticle modes of interaction and model coatings	21
Table 2.1. MIC and the change in suspended iron after contact with bacteria cells	42
Table 3.1. Growth inhibition test and ROS concentrations.....	65
Table 3.2. Reaction rate constants between NOM and hydroxyl radical	65
Table 4.1. Humic substances elemental compositions	83
Table 5.1. Reaction rate constants between NOM and hydroxyl radical	100
Table D.1. Plate count agar compositions.....	127

Chapter 1: INTRODUCTION

1.1 Engineered Nanomaterials

During the past decade, progress in the synthesis and application of nanomaterials has been made. Engineered nanomaterials are widely used in consumer products, such as catalyst, semiconductor, opacifiers, and microelectronics. Based on the nanotechnology consumer products inventory, there were 1317 products or product lines using nanotechnology (1) as of March 2011 (Figure 1.1). The inventory has grown over 500% during the past 5 years (1). And the number of applications for new materials is expected to grow continuously and will lead to the production of thousands of tons of nanomaterials in the next decade (2). Based on the current production volume and assumed paths of particle release, a recent risk assessment study suggested that some engineered nanomaterials may enter the environment in significant amounts to pose an ecological risk (2). Measurable release of engineered TiO₂ nanoparticles from products containing them into the environment has been reported (3-4). A detailed understanding of the fate, transport and potential risk of engineered nanoparticles in the environment is needed to make informed decisions about the use and regulation of engineered nanomaterials.

Nanomaterials released to the natural and built environment (e.g. rivers or wastewater treatment plants) will interact with microbial communities. Understanding nanomaterial-microbe interactions is important for determining the potential risks of nanoparticles because nanoparticles have been shown to be toxic to microbes (5-9) and

may adversely affect the microbial communities. These communities are catalysts for environmental processes such as primary production, organic matter decay, and nutrient cycling as well as for engineered systems. As a result, the interactions between microorganisms and nanoparticles may have deleterious effects on important natural processes and human activity.

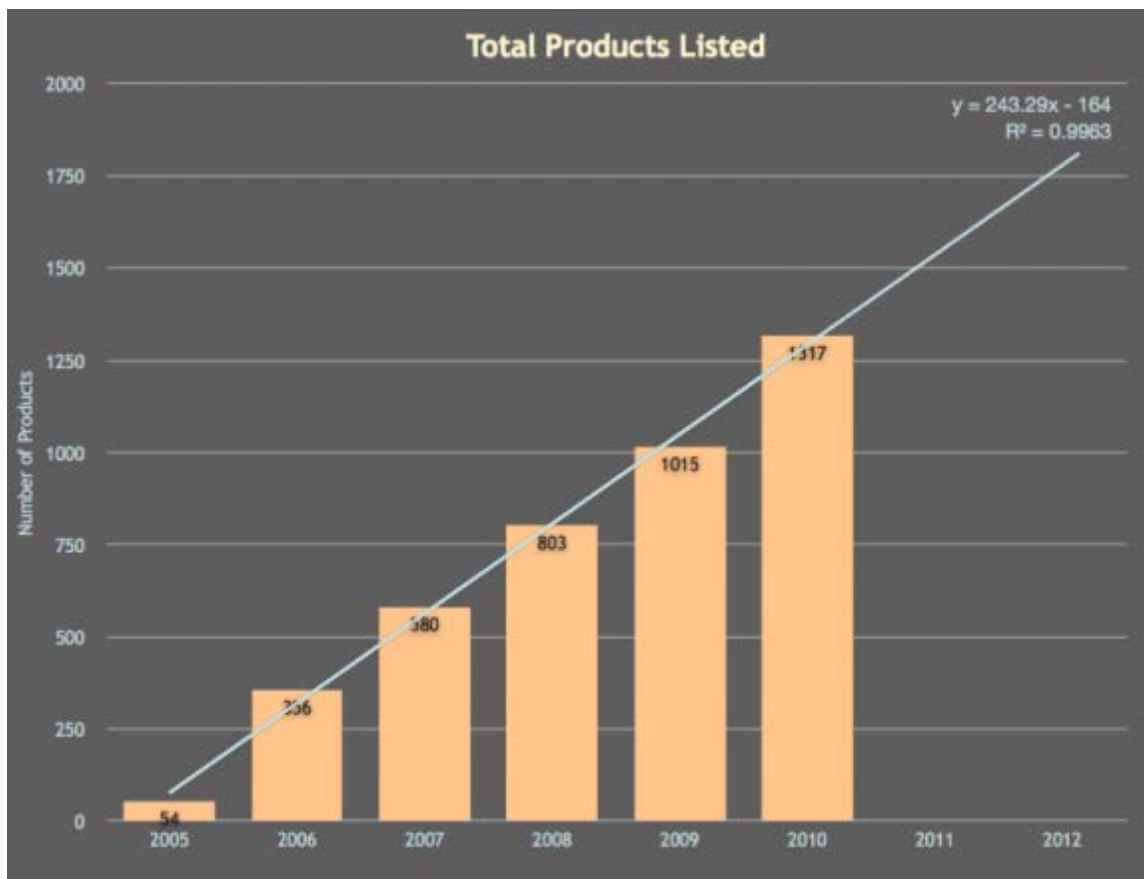


Figure 1.1. Number of total products listed, by date of inventory update, with regression analysis.

(Image source: http://www.nanotechproject.org/inventories/consumer/analysis_draft/)

Nanoparticles used in commercial products are typically coated with polymer to enhance their stability and mobility (10-11). Bare nanoparticles may also become coated with natural organic matter when they are released into the environment (12-14). These

coatings may modify the physicochemical properties of nanoparticles and affect the cell-particle interactions. A number of studies have reported particle-microbe interactions. However, the connections between the physicochemical properties of the particles and coatings and their subsequent interactions with microbes are not clear. For example, little is known about how engineered polymer and NOM coatings affect the cytotoxicity of nanomaterials. The over-arching question addressed in this thesis is whether and how natural and engineered coatings affect the interaction between engineered nanoparticles and microorganisms, as measured by nanoparticle toxicity and other physicochemical measurements (e.g. transmission electron microscopy).

1.2 Nanoparticle-Microbe Interactions and Nanomaterial Cytotoxicity

A number of nanoparticles have been shown to be cytotoxic. The unique physicochemical properties and cytotoxic effects of nanoparticles have been attributed to nanoparticle size, composition, shape, and oxidation state. The nanomaterial toxicity and the nanomaterial-microbe interactions are reviewed in the following paragraphs.

1.2.1 Metal Nanoparticles

Nanoscale Zero-valent Iron (NZVI). NZVI is a highly redox active material used to treat heavy metal and chlorinated organic solvent contaminants found in groundwater and soil (15-21). NZVI reduces contaminants through the oxidation of the metallic iron core of the particle and subsequent transfer of electrons to the contaminant. Recent studies indicate that NZVI is bactericidal in pure cultures at concentrations as low as a few mg/L (22-23), while NZVI is typically injected in to the ground to achieve

porewater concentrations in the grams per liter range (16). Specific modes of action for the bactericidal properties of NZVI have been postulated to be reductive decomposition of protein functional groups in the cell membrane due to strong reducing conditions at the NZVI surface (23), and oxidative damage from intracellular ROS produced from Fenton's chemistry (22-23). Figure 1.2.a shows NZVI associated with the bacterial cell membrane. Without cellular uptake, the oxidation state of iron atoms in NZVI and Fe-oxide nanoparticles have also been shown to correlate with its cytotoxicity to *E. coli* (22); NZVI (Fe(0)/Fe(II)/Fe(III)) being most toxic, magnetite (mixed Fe(II)/Fe(III) particle) being less toxic, while maghemite (all Fe(III)) was non-toxic.

Silver Nanoparticles (AgNP). Silver nanoparticles are one of the most widely used engineered nanomaterials because of their usefulness in antimicrobial applications in consumer products. AgNP have been incorporated in many of products, such as antibacterial washing machines, toothpaste, cookware, and socks (6). AgNPs are also used in medical applications to reduce infection, and inhibit bacterial colonization on catheters. The primary cause of cell death is believed to be the released Ag^+ ions, which may damage protein and DNA (24-26). A proteomic analysis of the interactions between *E. coli* and Ag^+ or AgNP shows similar protein expression profiles (24). Both Ag^+ and AgNP damaged the outer membrane, reduced the plasma membrane potential, and caused ATP depletion (Figure 1.2.b). In addition, Ag^+ has been suggested to be the active toxic agent for AgNP because AgNP toxicity was eliminated by adding NaCl and forming $\text{AgCl}_{(s)}$ to eliminate free Ag^+ (27).

Other cytotoxic mechanisms were also proposed for AgNP. AgNP may be embedded into the lipid bilayer (28-29), causing cell membrane leakage by changing

bilayer fluidity. In addition, Reactive Oxygen Species (ROS) generated by AgNP may also account for its toxicity. Intracellular ROS concentrations were reported to increase in the presence of Ag^+ and AgNP for nitrifying bacteria (30). The toxicity to the nitrifying bacteria was correlated with the concentration of ROS.

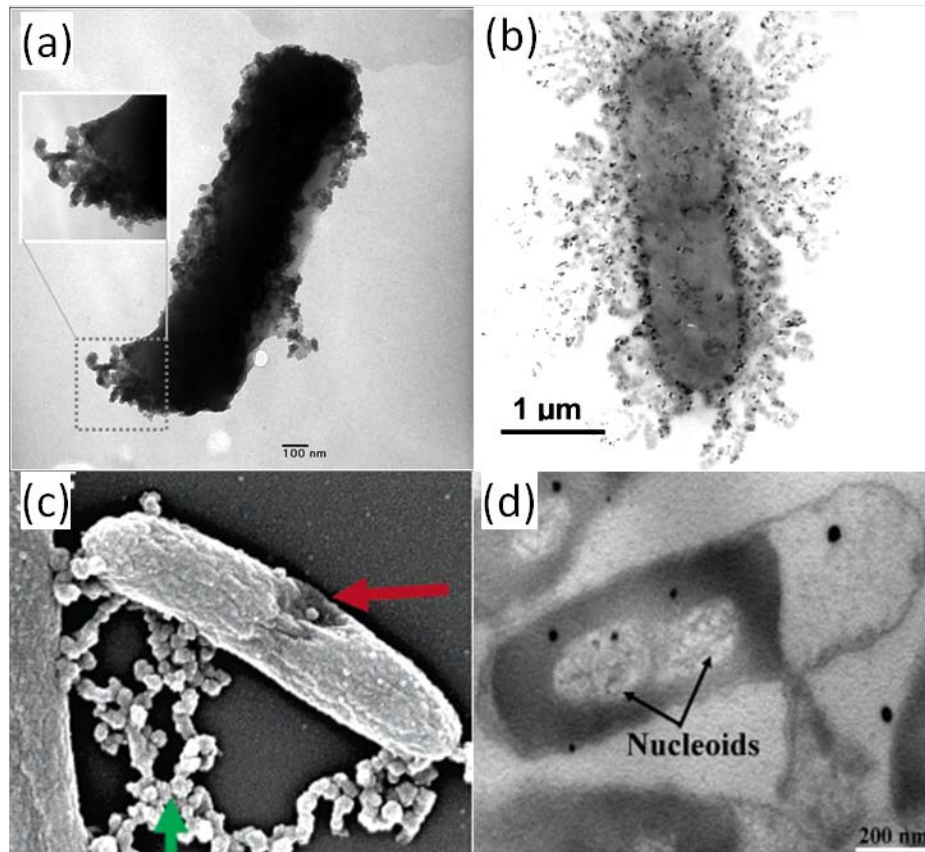


Figure 1.2. TEM images show bacteria-nanoparticle interactions. (a) Bare NZVI strongly associated to *E. coli* cells (31). (b) AgNP caused cell membrane damage (32). (c) Fullerene attached to bacterial cells and damaged the cell membrane (33). (d) ZnO nanoparticle damaged the cell membrane (34).

1.2.2 Fullerene and Carbon Nanotubes

Both C_{60} and carbon nanotubes have been shown to be toxic to bacteria (Figure 1.2.c). The mechanisms of toxicity of C_{60} and carbon nanotubes are still unclear.

Conflicting results have been reported. Earlier studies demonstrated that ROS could be the toxic agent for carbonaceous nanomaterials (35-37). However, Lyon et al. found no evidence of ROS-related damage for C₆₀ (38). It was found that false positives may be yielded for some of the dye-based ROS assay in the presence of C₆₀ (38). Thus C₆₀ was possibly interfering with the ROS assay and produced incorrect results. Direct association between cells and nanoparticles has been shown to cause cell membrane damage for C₆₀ (33). In addition, the presence of impurities (e.g. tetrahydrofuran, THF used in fullerenes preparations) was found to be toxic to bacteria (39). However, how adsorbed macromolecular organic coatings may affect C₆₀ toxicity has not been evaluated.

1.2.3 Metal Oxide Nanoparticles

TiO₂. Nano-TiO₂ is one of the most widely used nanomaterials, with an estimated worldwide production of 5000 t/year (2). Based on the current production volume and assumed paths of particle release, a recent risk assessment study suggested that nano-TiO₂ released to the environment may pose a risk to aquatic organisms (2). Nano-TiO₂ may express toxicity through photocatalytic and non-photocatalytic mechanisms. Reactive oxygen species (ROS) generated from photocatalyzed reactions of TiO₂ in water is the primary route for cytotoxicity towards bacteria. ROS evolved from TiO₂ oxidizes membrane phospholipids and inhibits cellular respiratory processes (40). However, during disinfection with TiO₂, the photocatalyzed toxicity is reduced by aqueous constituents commonly found in natural systems such as sulfate, nitrate, and most importantly for this work, organic matter (41). Recent studies with nano-TiO₂ show that dark interactions between the nanoparticles and cells also inhibit cell growth (5). These

studies suggest that the mechanisms and effectors of cytotoxicity of nano-TiO₂ are more complicated than previously suspected. Further, the exact nature by which adsorbed macromolecules and NOM affect the toxicity potential of nano-TiO₂ has not been reported.

ZnO. The cytotoxic mechanisms of nano-ZnO are still under investigation. Released Zn²⁺ and ROS have been proposed to be the cause of cell death (Figure 1.2.d) (42). However, conflicting results have been reported. Applerot et al. concluded that the ionic Zn had no cytotoxic effect, by comparing the cytotoxicity of nano-ZnO and zinc acetate (34). They suggested that the generated hydroxyl radical is the toxic agent. However, Heinlaan et al. demonstrated that bacteria were exposed to Zn ions released by nano-ZnO, by using bioluminescent indicator bacteria (43). They found that nano-ZnO toxicity correlated with the ionic Zn²⁺ released. While ZnO nanoparticles were not studied in this work, these types of inconsistencies in the literature are numerous and may be attributed to researchers neglecting the presence of polymeric stabilizers on the nanoparticles if these stabilizers are affecting the release of Zn²⁺ ion or interaction of the ZnO particles with the bacteria.

1.2.4 Effect of Nanoparticle Size

Nanoparticle size has been reported to affect cytotoxicity. The size of TiO₂, ZnO, AgNP, and carbon nanotubes has been shown to affect their toxicity (44-50). Generally, smaller nanoparticles display higher cytotoxicity for a given concentration. However, the causes are still unclear. A number of mechanisms have been proposed. For example, the smaller size leads to increased surface area, which may enhance the toxic effects by

affecting nanoparticle dissolution rates (51) or ROS generation. In addition, smaller size nanoparticles may be able to penetrate the cell membrane (52). It is not clear if there is any particle size dependence that is not related to surface area.

1.3 Effect of Polymeric Coatings and NOM on Nanoparticle-Microbe Interactions

Nanoparticles used in commercial products are typically coated with polymer to enhance their stability and mobility. Physisorption of charged macromolecules (polyelectrolytes) has been used to modify nanoparticle surface properties to enhance their stability against aggregation. The physisorption process is governed by the molecular weight, ionization and charge density of the macromolecule, the charge density and polarity of nanoparticles, and solvent ionic strength and ionic composition. Nanoparticles with adsorbed charged macromolecules may have enhanced stability against aggregation, due to the electrosteric repulsive forces provided by the coatings. Furthermore, nanoparticles may become coated with natural organic matter (NOM) after being released to the environment (14). Polymer and NOM coatings may affect the fate and transport and toxicity of nanoparticles, due to the change of their physical and chemical properties. Previous studies demonstrated that polymeric coatings and NOM can reduce antibacterial activities of nanoparticles (31,53-54). Polyelectrolyte and NOM coatings may prevent particle-cell physical interaction by providing electrosteric and electrostatic repulsions, resulting in reduced cytotoxic activities for nanoparticles requiring cell association. Work in this thesis shows that NZVI toxicity toward *E. coli* was significantly reduced by adsorbed polymeric coatings and NOM (31). A recent study

showed that the addition of NOM to AgNP reduced its bacterial toxicity, perhaps due to the sorption of the humic acid on to nanoparticles (8). However, positively-charged coatings have been shown to enhance toxicity in some studies, perhaps due to the affinity between positively charged particles and negatively-charged bacterial membrane (33,55). In addition, coatings were shown to reduce the toxicity of quantum dots to microorganisms by prevent the release of cadmium and selenite ions (54). Application of coatings is proposed as a means to mitigate nanoparticle toxicity. The hypothesized effects of polymeric coatings and NOM on nanoparticle properties and nanoparticle-microorganism interactions are summarized in Table 1.1, but these remain to be confirmed experimentally. Coatings can modify the charge on the particles and provide steric or electrosteric repulsive forces that prevent adhesion to other particles or surfaces (56). This affects the particle's stability against homoaggregation and heteroaggregation, including heteroaggregation with bacteria. Altering the interaction between bacteria and the particles can affect their toxicity. The size (hydrodynamic diameter) of nanoparticles may increase upon modification by coatings. The magnitude of this effect depends on the coating and particle type. This could affect the ability of nanoparticles to penetrate cell walls or to be taken up by cells (28). A very important consideration is the interaction of the coatings on the nanoparticles with reactive oxygen species. Some coatings are potentially capable of scavenging free radicals produced by nanoparticles or by the cell in response to the NPs. This free radical scavenging would effectively decrease the amount of harmful free radicals delivered to bacteria and in turn may decrease toxicity.

The exact nature of how coatings on engineered nanoparticles may affect their interaction with microorganisms is complex and remains unclear. A systematic study

probing the fundamental physicochemical reasons for the beneficial or adverse effects of nanoparticle coatings on their toxicity to bacteria are lacking so it is not yet possible to make predictions of about how specific coatings may affect nanoparticle-bacteria interactions for specific particles. This understanding is needed to design nanoparticles with coatings that prevent adverse effects of nanoparticles to microbial communities in environments impacted by engineered nanoparticles.

To address these data gaps, we investigated the effects of selected polymeric coatings for three commonly used engineered nanoparticles including silver nanoparticles, titanium dioxide nanoparticles, and zerovalent iron nanoparticles. These particles were selected because they represent three different modes of action for toxicity as described in detail later in this thesis. Coatings were selected to test specific hypotheses for how the coating will affect the different modes of interaction between nanoparticles and bacteria, and the subsequent toxic effect. NOM was evaluated for all three particle types given its ubiquity in the environment and the general notion that NOM will be present in all environmental systems. We tested three hypothetical effects listed in Table 1.1, including whether or not 1) steric or electrosteric repulsions can prevent bacteria-nanoparticle interactions and decrease their toxicity, 2) the ability to scavenge free radicals will decrease or prevent toxicity, 3) chemical stabilization of nanoparticles with an inorganic metal sulfide coating that decreases the solubility of the nanoparticles and thereby decrease the toxicity of nanoparticles that release toxic metal ions, and 4) the ability of a coating to complex the toxic metal ions released from the nanoparticles can decrease the toxicity of metal nanoparticles. In the following section,

we will elaborate on these three particle-cell interactions and explain how we selected model particles and coatings.

Table 1.1. Coating effects on nanoparticle properties and particle-microorganism interactions (modified from Aruguete and Hochella (6))

Effect on nanoparticle properties	Effect on particle-microorganism interaction
Surface charge	Stability in solution, affinity for cell surface
Hydrodynamic diameter	Ability of nanoparticle to penetrate cell
Chemical stabilization of nanoparticle	Release of toxic ions from nanoparticle
Ability to scavenge free radicals	Amount of free radicals delivered to bacteria
Steric or electrosteric properties	Stability in solution, affinity for cell surface

1.4 Hypothesis: Nanoparticle-Microbe Modes of Interaction

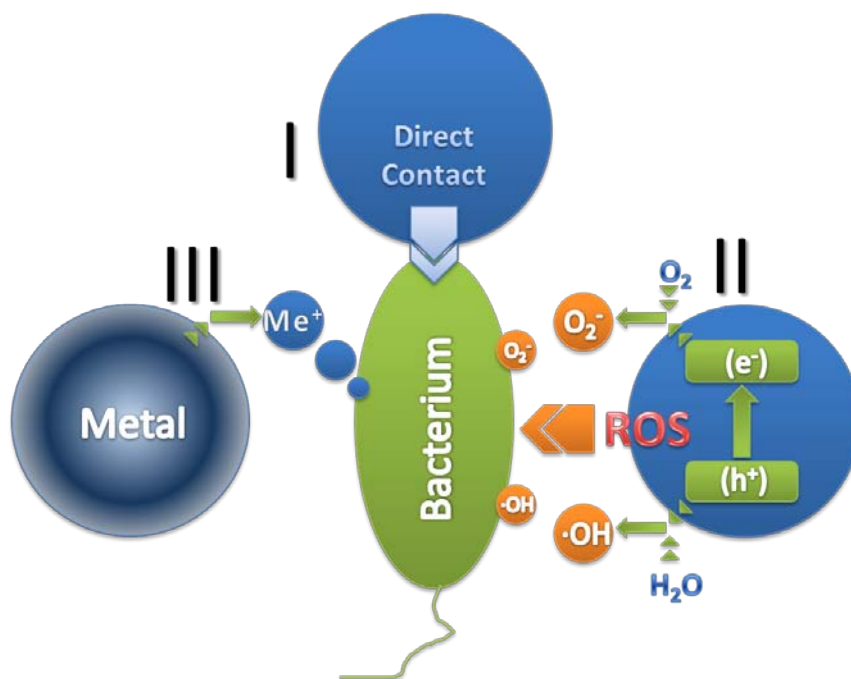


Figure 1.3. Schematic of nanoparticle-microorganism modes of interaction. Mode type I requires physical interaction between cells and particles. Mode type II interacts with bacterial cells with generated reactive oxygen species. Mode type III interacts with bacterial cells by releasing cytotoxic metal ions.

For coated nanoparticles, the underlying nanoparticles may have different modes by which they can interact with bacteria, which could change how the NP coating affects their cytotoxic properties. Figure 1.3 summarizes three generalized representative modes of interaction for nanoparticles that are commonly encountered in the literature. Grouping nanoparticle-microbe interactions into these three modes can aid in understanding coating effects for different types of nanoparticles. In principle, this will enable us to predict the effect of coatings on unstudied nanoparticles by assuming their mode of interaction with bacteria.

In mode type I, physical contact between nanoparticles and cells is required to inhibit bacterial growth. Cell growth inhibited by reductive decomposition of protein functional groups in the cell membrane, nanoparticle uptake by bacteria (57), and nanoparticles trapped in lipid bilayers (28) may be grouped in the type I mode of action. NZVI (23) and fullerene (58) have been proposed to interact with bacteria via mode type I. Figure 1.4 demonstrate the postulated cytotoxic mechanisms for bare NZVI in the literature. Bare NZVI is cytotoxic due to reductive decomposition, requiring physical contact between cell and particle. Coatings may decrease NZVI toxicity by preventing cell-particle interaction. In addition, NZVI may interact with bacteria and exert toxicity by producing ROS, which is the type II mode of action. It should be noted that nanoparticles may exert cytotoxic activities via a combination of these modes and these multiple types of interactions were considered in the study design.

Based upon our hypothesis, we addressed the following questions for NZVI:

- Does NOM and adsorbed polymeric coatings affect NZVI toxicity?

- What are the physicochemical processes responsible for the observed reduced toxicity or for the lack of an effect on toxicity?
- What properties of adsorbed macromolecules enable them to reduce the toxicity?

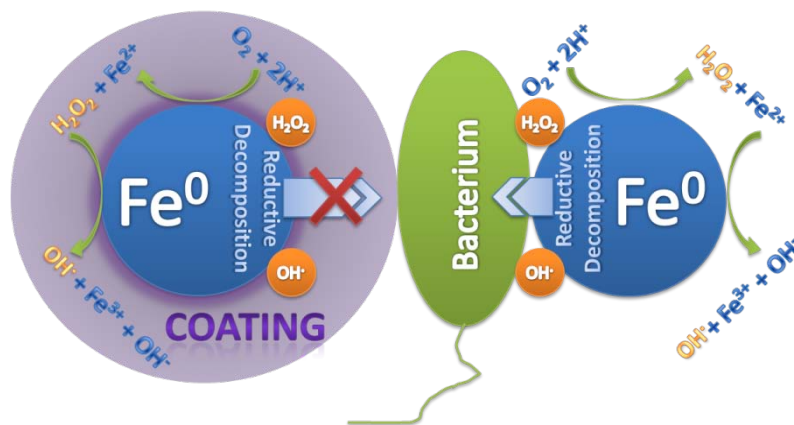
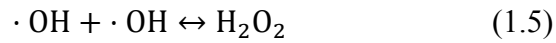
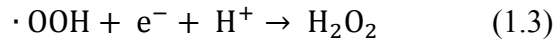


Figure 1.4. Hypotheses for interaction between NZVI and bacterial cells and coating effects. Bare NZVI is cytotoxic due to reductive decomposition, requiring physical contact between cell and particle. Coatings may decrease NZVI toxicity by prevent cell-particle interaction.

For type II mode of action, reactive oxygen species (ROS), usually generated from photocatalytic reactions, may cause cell death. Nano-TiO₂ (40) is known to interact with bacteria and exert toxicity via mode type II. It was indicated that ROS may also account for part of the cytotoxic activities for AgNP (30), NZVI (23), and fullerene (44). Figure 1.5 and equations 1.1-1.5 summarize the reported cytotoxic mechanisms for nano-TiO₂. Nano-TiO₂ inhibits bacterial growth by generating ROS, which is highly reactive. We hypothesize that coatings that can react with the produced ROS will reduce the cytotoxic effects of nano-TiO₂, whereas coatings incapable of reacting with ROS may

have little impact on nano-TiO₂ cytotoxic activities. Particle-cell physical contact is not necessary for type II mode.



Based upon our hypothesis, we addressed the following questions for nano-TiO₂:

- Do polymeric coatings and NOM adsorbed to nano-TiO₂ decrease their toxicity to *E. coli*?
- What physical properties of the coatings enable them to decrease nano-TiO₂ cytotoxicity (e.g. an ability to scavenge ROS produced by TiO₂ or an ability to prevent contact between the cells and nano-TiO₂)
- Do polymeric coatings that decrease NZVI toxicity also decrease nano-TiO₂ cytotoxicity? What are the reasons for different behaviors of the same coatings?

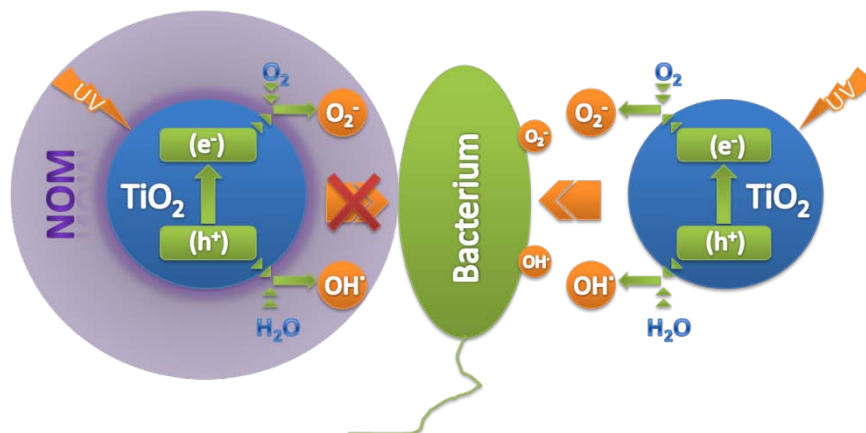


Figure 1.5. Hypotheses for interaction between TiO₂ and bacterial cells and coating effects. Nano-TiO₂ inhibits bacterial growth by generating ROS, which is highly reactive. Coatings that can react with the produced ROS will reduce the cytotoxic effects of nano-TiO₂. Coatings incapable of reacting with ROS may have little impact on nano-TiO₂ cytotoxic activities.

For type III mode of interaction, particles interact with microorganisms with metal ions released from the metal nanoparticle core. In this case, nanoparticles act as toxin sources, delivering toxic metal ions to bacteria. Nanoparticles with type III mode of interaction include AgNP (24), quantum dots (54), nano-ZnO (43), and nano-CuO (43). Figure 1.6 shows the proposed cytotoxic mechanism for AgNP. Particle-cell physical contact is not necessary for mode type III. It should be noted that modes of interaction other than the three generalized cases listed here may be present, but they are out of the scope of this research.

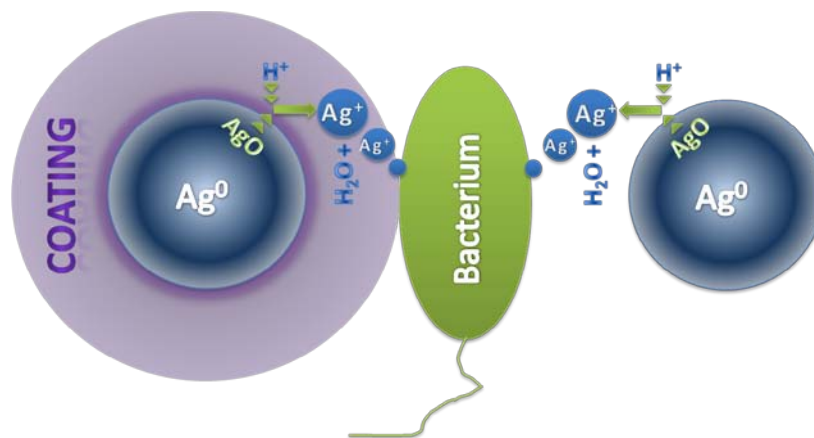


Figure 1.6. Hypotheses for interaction between AgNP and bacterial cells and coating effects. AgNPs inhibit bacterial growth by released Ag ions. Coatings capable of scavenging Ag ions will reduce nanoparticle toxicity. However, this effect may be temporary if the coating becomes saturated with the toxic metal ion.

Based on the hypothesis for type III modes of interaction, we addressed the following questions for AgNP:

- Do NOM and engineered coatings that can scavenge Ag^+ released from AgNPs reduce AgNP toxicity?
- Do polymeric coatings that are incapable of scavenging Ag^+ decrease AgNP toxicity?
- Does the chemical composition of NOM affect their ability to decrease AgNP toxicity?

1.5 Research Approach

1.5.1 Nanoparticles

Three model nanoparticles, NZVI (interaction mode type I), TiO₂ nanoparticles (interaction mode type II), and silver nanoparticles (interaction mode type III), are studied in this research. These three particles are selected in part because of their different modes of interaction with bacteria, in part because they are used in commercial products and based on the literature have potential risks to microorganisms. Silver nanoparticles and TiO₂ nanoparticles are ranked the 1st and 3rd in the numbers of products that use nanotechnology (Figure 1.7). NZVI may be used at a high concentration in groundwater remediation for chlorinated solvent, and potentially affect the local microbial communities.

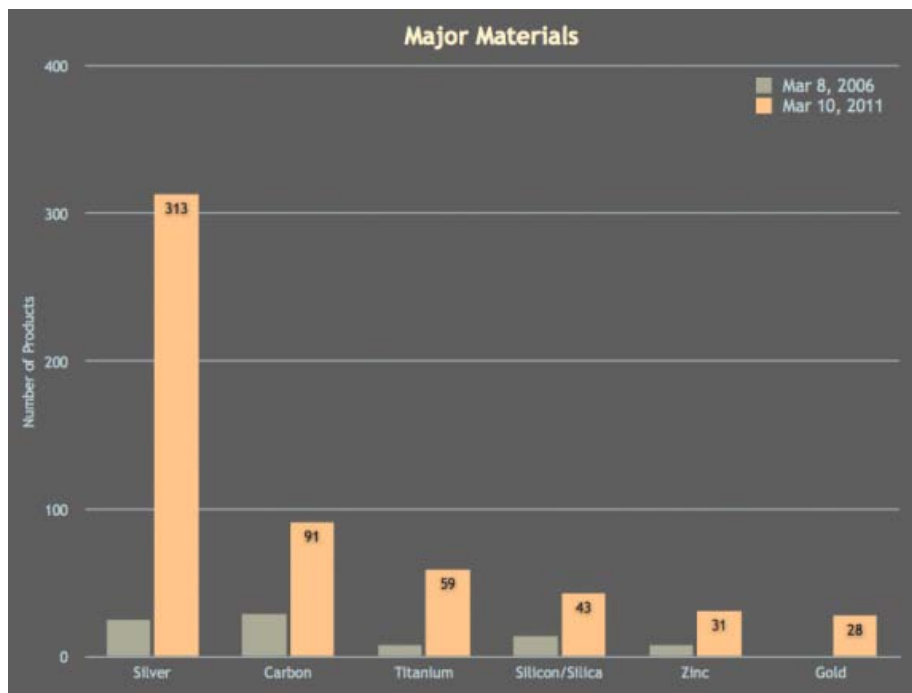


Figure 1.7. Numbers of products associated with specific materials.

(Image source: http://www.nanotechproject.org/inventories/consumer/analysis_draft/)

1.5.2 Nanoparticle Modification

The procedure used to physisorb the polymers to nanoparticles has been previously described (56). Briefly, stock nanoparticle (NZVI, nano-TiO₂, or AgNP) dispersions are ultrasonicated for 20 minutes, and then added to a polymer suspension to coat those particles with a specific polymer. Concentrated polymer suspension was always added to dispersed particles as order of operation was found to affect particle stability against aggregation. After adsorption, the polymer coated nanoparticle suspensions were fractionated by allowing the most unstable particles to settle for 10 minutes. The stable suspension was decanted and used for exposure experiments.

1.5.3 Nanoparticle Characterization

As described earlier, nanoparticle hydrodynamic diameter may affect particle-cell interactions (Table 1.1). Dynamic light scattering was used to monitor the time dependent hydrodynamic diameter of aggregates. Given the polydisperse nature of the nanoparticles used in this study, intensity autocorrelation functions were converted to intensity-weighted particle hydrodynamic diameter distributions using the CONTIN algorithm.

1.5.4 *E. coli* Culture

E. coli (ATCC strain 33876) and *S. oneidensis* (strain MR-1) were used as model bacteria for understanding the particle-cell interactions. *E. coli* is used, since it is the most widely studied prokaryotic model organism, and it is an important species in the fields of biotechnology and microbiology. *S. oneidensis* is a facultative bacterium which can be

found in deep sea anaerobic habitats, and in soil and sedentary habitats (59). *S. oneidensis* is a representative model since they can be found in the soil and may be affected by released nanoparticles.

1.5.5 Coatings

Four model macromolecules, poly(styrene sulfonate) (PSS, average MW=70,000 g/mol), polyaspartate (PAP, average MW=2500 g/mol), humic acid (average MW=1400 to 9200 g/mol), polyvinylpyrrolidone (PVP), and carboxy methyl cellulose (sodium salt) (CMC) were used to coat nanoparticles. PAP was selected, because it is potentially an environmentally benign modifier, with aspartate, one of the 20 natural amino acids, as the monomer unit. Humic acid is ubiquitous in the environment and is expected to be present on all nanoparticles released to the environment. As a result, it is important to understand humic acid effects on nanoparticle-cell interactions so the effect of NOM was studied for all of the nanoparticles studied here. CMC was used, because it is a commonly used modified biopolymer. PVP is representative for neutrally charged polymeric coatings. PSS, with a large molecular weight, was selected since it provides very stable NP suspensions in water. In addition, Ag₂S, an inorganic coating, will be formed on AgNP and has been shown to decrease the dissolution and availability of Ag ion in suspension (60). This Ag₂S coating effect was also investigated.

1.5.6 Transmission Electron Microscopy (TEM)




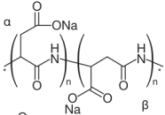
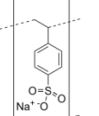
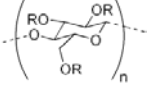
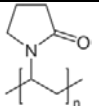
Nanoparticle-microorganism physical association needs to be determined for understanding their interactions. TEM was used to examine such associations. The treated and untreated *E. coli* cells were fixed using 1% formaldehyde and 1% glutaraldehyde in 5mM sodium bicarbonate buffer in an attempt to preserve samples under the same conditions as during exposure and avoid artifacts of drying the samples. A one μL aliquot of the fixed cells was then put on a carbon coated copper grids, air dried, and examined using TEM.

1.5.7 Experimental Design

We investigated the effect of NOM, a naturally existing and environmentally relevant substance, on nanoparticle-microorganism interactions for all three model nanoparticles. We anticipated that NOM can provide electrosteric repulsion to prevent nanoparticle-bacteria interaction and decrease toxicity. Further, we expect that NOM can scavenge ROS formed by nanoparticles, and can complex with Ag ion released from Ag NPs. As such, we expect NOM to decrease NP toxicity across all modes of interaction between bacteria and nanoparticles evaluated here. In addition, based on our hypothesis for nanoparticle modes of interaction, we used engineered polymeric coatings to probe each of these modes of interaction (Table 1.1). PAP and PSS, with different molecular weight and functional groups, were used for NZVI to demonstrate that coatings capable of prevent cell-particle interactions may reduce toxicity of type I nanoparticles. PAP was also studied for nano-TiO₂, since PAP is able to prevent cell-particle interaction but unable to scavenge ROS. We could therefore use PAP to test hypotheses about how

coating properties (e.g. the ability to scavenge ROS) affect their ability to impact the type II mode of interaction. Finally, CMC and PVP were used for AgNP. CMC was used because it is negatively charged at neutral pH and may scavenge positively charged Ag^+ ion. PVP, a neutrally charged polymer, was selected because it is unable to scavenge Ag^+ but able to prevent cell-particle association. Table 1.2 summarizes the model coatings used for each of the three nanoparticles.

Table 1.2. Hypothesis for nanoparticle modes of interaction and model coatings

	NZVI 	Nano-TiO ₂ 	AgNP 
NOM	X	X	X
PAP 	X	X	
PSS 	X		
			X
CMC R = H or CH ₂ CO ₂ H			
PVP 			X

1.6 Research Objectives

The objectives of this study are to assess the effect that organic macromolecular coatings such as synthetic polymers and natural organic matter have on physicochemical

properties of nanoparticles and particle-cell interactions with nanoparticles hypothesized to have type I, II, and III modes of interaction, and investigate the reasons for these effects. Based on the hypotheses, the specific objectives of this research are as follows:

1) To assess the effect that organic macromolecular coatings such as synthetic polymers and natural organic matter have on the cytotoxic properties of NZVI to a gram-negative bacterium, *Escherichia coli*. In addition, to assess how particle aging (partial oxidation) can form oxide coatings on top of NZVI, altering its physicochemical properties. We also investigate this aging effect have on the cytotoxic properties of NZVI.

2) To assess the effect that organic coatings such as synthetic polymers and NOM have on the cytotoxic properties of nano-TiO₂, a nanoparticle hypothesized to have a type II mode of action, to a gram-negative bacterium, *E. coli*; and to investigate how adsorbed coatings affect the cytotoxic properties of nano-TiO₂.

3) To assess the effect that polymers and NOM coatings have on the cytotoxic properties of AgNP to *E. coli*, and to investigate how sulfidation (Ag₂S coating) affects AgNP toxicity.

4) To assess the effect that polymers and NOM coatings have on the cytotoxic properties of NZVI and TiO₂ to a different bacteria, *Shewanella oneidensis*.

1.7 Dissertation Overview

This dissertation is presented in six chapters and four appendices. The body of the dissertation includes Chapter two to Chapter five, which consist of material either published or prepared for publication in the peer-reviewed journals, such as *Environmental Science and Technology*, and *Chemosphere*. Chapter 1 provides an

introduction to the dissertation including a brief background, research approach, and research objectives. A brief description of Chapter two to six and the appendices are presented as follows.

Chapter 2 presents the investigation of the impacts of polymeric and NOM coatings on NZVI cytotoxicity to *E. coli*. This material, written by Zhiqiang Li and co-authored by Karl Greden, Pedro J. J. Alvarez, Kelvin Gregory, and Gregory V. Lowry, was published in *Environmental Science and Technology* in March 2010, under the title of “Adsorbed Polymer and NOM Limits Adhesion and Toxicity of Nano Scale Zero-valent Iron (NZVI) to *E. coli*”.

Chapter 3 presents the investigation of the impacts of polymeric and NOM coatings on nano-TiO₂ cytotoxicity to *E. coli*. This material, written by Zhiqiang Li and co-authored by Gregory V. Lowry and Kelvin Gregory, is in the preparation for publication in *Environmental Science and Technology*, under the title of “Obstruction of Cytotoxicity by Natural Organic Matter Coatings on Titanium Dioxide Nanoparticles”.

Chapter 4 presents the investigation of the impacts of polymeric and NOM coatings on AgNP cytotoxicity to *E. coli*. This material, written by Zhiqiang Li and co-authored by Rui Ma, Gregory V. Lowry and Kelvin Gregory, is in the preparation for publication in *Environmental Science and Technology*.

Chapter 5 presents the investigation of the impacts of polymeric and NOM coatings on NZVI and TiO₂ cytotoxicity to *S. oneidensis*. This material, written by Zhiqiang Li and co-authored by Chanil Jung and Kelvin Gregory, is in the preparation for publication in *Chemosphere*.

Chapter 6 presents the discussions and conclusion of this dissertation.

Appendix A lists notations used in this thesis. Appendices B and C contain supporting information for Chapter 2 and 3, respectively. Appendix D describes detailed experimental methods and protocols.

Appendix E presents a novel smallest of its kind microfluidic microbial fuel cell and its application in self-powered sensing. This material, written by Zhiqiang Li and co-authored by Ying Zhang, Philip R. LeDuc and Kelvin B. Gregory, was published in *Biotechnology and Bioengineering* in April 2011, under the title of “Microbial Electricity Generation via Microfluidic Flow Control”. Appendix F contains supporting information for Appendix D.

1.8 References

- (1) Woodrow Wilson Center: Project on Emerging Nanotechnologies Inventory. http://www.nanotechproject.org/inventories/consumer/analysis_draft/.
- (2) Mueller, N. C.; Nowack, B., Exposure modeling of engineered nanoparticles in the environment. *Environ. Sci. Technol.* **2008**, *42* (12), 4447-4453.
- (3) Kaegi, R.; Ulrich, A.; Sinnert, B.; Vonbank, R.; Wichser, A.; Zuleeg, S.; Simmler, H.; Brunner, S.; Vonmont, H.; Burkhardt, M.; Boller, M., Synthetic TiO₂ nanoparticle emission from exterior facades into the aquatic environment. *Environ. Pollut.* **2008**, *156* (2), 233-239.
- (4) Kiser, M. A.; Westerhoff, P.; Benn, T.; Wang, Y.; Perez-Rivera, J.; Hristovski, K., Titanium Nanomaterial Removal and Release from Wastewater Treatment Plants. *Environ. Sci. Technol.* **2009**, *43* (17), 6757-6763.
- (5) Adams, L. K.; Lyon, D. Y.; Alvarez, P. J. J., Comparative eco-toxicity of nanoscale TiO₂, SiO₂, and ZnO water suspensions. *Water Res.* **2006**, *40* (19), 3527-3532.
- (6) Aruguete, D. M.; Hochella, M. F., Bacteria-nanoparticle interactions and their environmental implications. *Environ. Chem.* **2009**, *7* (1), 3-9.
- (7) Buzea, C.; Pacheco, II; Robbie, K., Nanomaterials and nanoparticles: Sources and toxicity. *Biointerphases* **2007**, *2* (4), MR17-MR71.
- (8) Fabrega, J.; Fawcett, S. R.; Renshaw, J. C.; Lead, J. R., Silver Nanoparticle Impact on Bacterial Growth: Effect of pH, Concentration, and Organic Matter. *Environ. Sci. Technol.* **2009**, *43* (19), 7285-7290.
- (9) Simon-Deckers, A.; Loo, S.; Mayne-L'Hermite, M.; Herlin-Boime, N.; Menguy, N.; Reynaud, C.; Gouget, B.; Carriere, M., Size-, Composition- and Shape-

- Dependent Toxicological Impact of Metal Oxide Nanoparticles and Carbon Nanotubes toward Bacteria. *Environ. Sci. Technol.* **2009**, *43* (21), 8423-8429.
- (10) He, F.; Zhao, D. Y., Manipulating the size and dispersibility of zerovalent iron nanoparticles by use of carboxymethyl cellulose stabilizers. *Environ. Sci. Technol.* **2007**, *41* (17), 6216-6221.
 - (11) Saleh, N.; Sirk, K.; Liu, Y. Q.; Phenrat, T.; Dufour, B.; Matyjaszewski, K.; Tilton, R. D.; Lowry, G. V., Surface modifications enhance nanoiron transport and NAPL targeting in saturated porous media. *Environ. Eng. Sci.* **2007**, *24* (1), 45-57.
 - (12) Chen, K. L.; Elimelech, M., Influence of humic acid on the aggregation kinetics of fullerene (C-60) nanoparticles in monovalent and divalent electrolyte solutions. *J. Colloid Interface Sci.* **2007**, *309* (1), 126-134.
 - (13) Domingos, R. F.; Tufenkji, N.; Wilkinson, K. J., Aggregation of Titanium Dioxide Nanoparticles: Role of a Fulvic Acid. *Environ. Sci. Technol.* **2009**, *43* (5), 1282-1286.
 - (14) Johnson, R. L.; Johnson, G. O.; Nurmi, J. T.; Tratnyek, P. G., Natural Organic Matter Enhanced Mobility of Nano Zerovalent Iron. *Environ. Sci. Technol.* **2009**, *43* (14), 5455-5460.
 - (15) He, F.; Zhao, D. Y., Preparation and characterization of a new class of starch-stabilized bimetallic nanoparticles for degradation of chlorinated hydrocarbons in water. *Environ. Sci. Technol.* **2005**, *39* (9), 3314-3320.
 - (16) Henn, K. W.; Waddill, D. W., Utilization of Nanoscale Zero-Valent Iron for Source Remediation—A Case Study. **2006**, *16* (2), 57-77.
 - (17) Kanel, S. R.; Nepal, D.; Manning, B.; Choi, H., Transport of surface-modified iron nanoparticle in porous media and application to arsenic(III) remediation. *J. Nanopart. Res.* **2007**, *9* (5), 725-735.
 - (18) Liu, Y. Q.; Choi, H.; Dionysiou, D.; Lowry, G. V., Trichloroethene hydrodechlorination in water by highly disordered monometallic nanoiron. *Chem. Mat.* **2005**, *17* (21), 5315-5322.
 - (19) Liu, Y. Q.; Majetich, S. A.; Tilton, R. D.; Sholl, D. S.; Lowry, G. V., TCE dechlorination rates, pathways, and efficiency of nanoscale iron particles with different properties. *Environ. Sci. Technol.* **2005**, *39* (5), 1338-1345.
 - (20) Song, H.; Carraway, E. R., Reduction of chlorinated ethanes by nanosized zero-valent iron: Kinetics, pathways, and effects of reaction conditions. *Environ. Sci. Technol.* **2005**, *39* (16), 6237-6245.
 - (21) Zhang, W. X., Nanoscale iron particles for environmental remediation: An overview. *J. Nanopart. Res.* **2003**, *5* (3-4), 323-332.
 - (22) Auffan, M.; Achouak, W.; Rose, J.; Roncato, M. A.; Chaneac, C.; Waite, D. T.; Masion, A.; Woicik, J. C.; Wiesner, M. R.; Bottero, J. Y., Relation between the redox state of iron-based nanoparticles and their cytotoxicity toward *Escherichia coli*. *Environ. Sci. Technol.* **2008**, *42* (17), 6730-6735.
 - (23) Lee, C.; Kim, J. Y.; Il Lee, W.; Nelson, K. L.; Yoon, J.; Sedlak, D. L., Bactericidal effect of zero-valent iron nanoparticles on *Escherichia coli*. *Environ. Sci. Technol.* **2008**, *42* (13), 4927-4933.

- (24) Lok, C. N.; Ho, C. M.; Chen, R.; He, Q. Y.; Yu, W. Y.; Sun, H. Z.; Tam, P. K. H.; Chiu, J. F.; Che, C. M., Proteomic analysis of the mode of antibacterial action of silver nanoparticles. *J. Proteome Res.* **2006**, *5* (4), 916-924.
- (25) Sondi, I.; Salopek-Sondi, B., Silver nanoparticles as antimicrobial agent: a case study on E-coli as a model for Gram-negative bacteria. *J. Colloid Interface Sci.* **2004**, *275* (1), 177-182.
- (26) Wigginton, N. S.; De Titta, A.; Piccapietra, F.; Dobias, J.; Nesatty, V. J.; Suter, M. J. F.; Bernier-Latmani, R., Binding of Silver Nanoparticles to Bacterial Proteins Depends on Surface Modifications and Inhibits Enzymatic Activity. *Environ. Sci. Technol.* **2010**, *44* (6), 2163-2168.
- (27) Smetana, A. B.; Klabunde, K. J.; Marchin, G. R.; Sorensen, C. M., Biocidal activity of nanocrystalline silver powders and particles. *Langmuir* **2008**, *24* (14), 7457-7464.
- (28) Bothun, G. D., Hydrophobic silver nanoparticles trapped in lipid bilayers: Size distribution, bilayer phase behavior, and optical properties. **2008**, *6*, 13.
- (29) Park, S. H.; Oh, S. G.; Mun, J. Y.; Han, S. S., Effects of silver nanoparticles on the fluidity of bilayer in phospholipid liposome. *Colloid Surf. B-Biointerfaces* **2005**, *44* (2-3), 117-122.
- (30) Choi, O.; Hu, Z. Q., Size dependent and reactive oxygen species related nanosilver toxicity to nitrifying bacteria. *Environ. Sci. Technol.* **2008**, *42* (12), 4583-4588.
- (31) Li, Z.; Greden, K.; Alvarez, P. J. J.; Gregory, K. B.; Lowry, G. V., Adsorbed polymer and NOM limits adhesion and toxicity of nano scale zerovalent iron to E. coli. **2010**, *44* (9), 3462-7.
- (32) Lyon, D. Y.; Fortner, J. D.; Sayes, C. M.; Colvin, V. L.; Hughes, J. B., Bacterial cell association and antimicrobial activity of a C-60 water suspension. *Environ. Toxicol. Chem.* **2005**, *24* (11), 2757-2762.
- (33) Tang, Y. J. J.; Ashcroft, J. M.; Chen, D.; Min, G. W.; Kim, C. H.; Murkhejee, B.; Larabell, C.; Keasling, J. D.; Chen, F. Q. F., Charge-associated effects of fullerene derivatives on microbial structural integrity and central metabolism. *Nano Lett.* **2007**, *7* (3), 754-760.
- (34) Applerot, G.; Lipovsky, A.; Dror, R.; Perkash, N.; Nitzan, Y.; Lubart, R.; Gedanken, A., Enhanced Antibacterial Activity of Nanocrystalline ZnO Due to Increased ROS-Mediated Cell Injury. *Adv. Funct. Mater.* **2009**, *19* (6), 842-852.
- (35) Kamat, J. P.; Devasagayam, T. P. A.; Priyadarsini, K. I.; Mohan, H., Reactive oxygen species mediated membrane damage induced by fullerene derivatives and its possible biological implications. *Toxicology* **2000**, *155* (1-3), 55-61.
- (36) Oberdorster, E., Manufactured nanomaterials (Fullerenes, C-60) induce oxidative stress in the brain of juvenile largemouth bass. *Environ. Health Perspect.* **2004**, *112* (10), 1058-1062.
- (37) Tejral, G.; Panyala, N. R.; Havel, J., Carbon nanotubes: toxicological impact on human health and environment. *J. Appl. Biomed.* **2009**, *7* (1), 1-13.
- (38) Lyon, D. Y.; Brunet, L.; Hinkal, G. W.; Wiesner, M. R.; Alvarez, P. J. J., Antibacterial activity of fullerene water suspensions (nC(60)) is not due to ROS-mediated damage. *Nano Lett.* **2008**, *8* (5), 1539-1543.

- (39) Kovochich, M.; Espinasse, B.; Auffan, M.; Hotze, E. M.; Wessel, L.; Xia, T.; Nel, A. E.; Wiesner, M. R., Comparative Toxicity of C-60 Aggregates toward Mammalian Cells: Role of Tetrahydrofuran (THF) Decomposition. *Environ. Sci. Technol.* **2009**, *43* (16), 6378-6384.
- (40) Maness, P. C.; Smolinski, S.; Blake, D. M.; Huang, Z.; Wolfrum, E. J.; Jacoby, W. A., Bactericidal activity of photocatalytic TiO₂ reaction: Toward an understanding of its killing mechanism. *Appl. Environ. Microbiol.* **1999**, *65* (9), 4094-4098.
- (41) Rincon, A. G.; Pulgarin, C., Effect of pH, inorganic ions, organic matter and H₂O₂ on E-coli K12 photocatalytic inactivation by TiO₂ - Implications in solar water disinfection. *Appl. Catal. B-Environ.* **2004**, *51* (4), 283-302.
- (42) Franklin, N. M.; Rogers, N. J.; Apte, S. C.; Batley, G. E.; Gadd, G. E.; Casey, P. S., Comparative toxicity of nanoparticulate ZnO, bulk ZnO, and ZnCl₂ to a freshwater microalga (*Pseudokirchneriella subcapitata*): The importance of particle solubility. *Environ. Sci. Technol.* **2007**, *41* (24), 8484-8490.
- (43) Heinlaan, M.; Ivask, A.; Blinova, I.; Dubourguier, H. C.; Kahru, A., Toxicity of nanosized and bulk ZnO, CuO and TiO₂ to bacteria *Vibrio fischeri* and crustaceans *Daphnia magna* and *Thamnocephalus platyurus*. *Chemosphere* **2008**, *71* (7), 1308-1316.
- (44) Brunet, L.; Lyon, D. Y.; Hotze, E. M.; Alvarez, P. J. J.; Wiesner, M. R., Comparative Photoactivity and Antibacterial Properties of C-60 Fullerenes and Titanium Dioxide Nanoparticles. *Environ. Sci. Technol.* **2009**, *43* (12), 4355-4360.
- (45) Jones, N.; Ray, B.; Ranjit, K. T.; Manna, A. C., Antibacterial activity of ZnO nanoparticle suspensions on a broad spectrum of microorganisms. *FEMS Microbiol. Lett.* **2008**, *279* (1), 71-76.
- (46) Nyberg, L.; Turco, R. F.; Nies, L., Assessing the impact of nanomaterials on anaerobic microbial communities. *Environ. Sci. Technol.* **2008**, *42* (6), 1938-1943.
- (47) Panacek, A.; Kvitek, L.; Prucek, R.; Kolar, M.; Vecerova, R.; Pizurova, N.; Sharma, V. K.; Nevecna, T.; Zboril, R., Silver colloid nanoparticles: Synthesis, characterization, and their antibacterial activity. *J. Phys. Chem. B* **2006**, *110* (33), 16248-16253.
- (48) Yamamoto, O., Influence of particle size on the antibacterial activity of zinc oxide. *Int. J. Inorg. Mater.* **2001**, *3* (7), 643-646.
- (49) Zhang, L. L.; Jiang, Y. H.; Ding, Y. L.; Povey, M.; York, D., Investigation into the antibacterial behaviour of suspensions of ZnO nanoparticles (ZnO nanofluids). *J. Nanopart. Res.* **2007**, *9* (3), 479-489.
- (50) Zhang, Y. W.; Peng, H. S.; Huang, W.; Zhou, Y. F.; Yan, D. Y., Facile preparation and characterization of highly antimicrobial colloid Ag or Au nanoparticles. *J. Colloid Interface Sci.* **2008**, *325* (2), 371-376.
- (51) Liu, J.; Aruguete, D. A.; Jinschek, J. R.; Rimstidt, J. D.; Hochella, M. F., The non-oxidative dissolution of galena nanocrystals: Insights into mineral dissolution rates as a function of grain size, shape, and aggregation state. *Geochim. Cosmochim. Acta* **2008**, *72* (24), 5984-5996.

- (52) Kloepper, J. A.; Mielke, R. E.; Nadeau, J. L., Uptake of CdSe and CdSe/ZnS quantum dots into bacteria via purine-dependent mechanisms. *Appl. Environ. Microbiol.* **2005**, *71* (5), 2548-2557.
- (53) Li, D.; Lyon, D. Y.; Li, Q.; Alvarez, P. J. J., Effect of soil sorption and aquatic natural organic matter on the antibacterial activity of a fullerene water suspension. *Environ. Toxicol. Chem.* **2008**, *27* (9), 1888-1894.
- (54) Mahendra, S.; Zhu, H. G.; Colvin, V. L.; Alvarez, P. J., Quantum Dot Weathering Results in Microbial Toxicity. *Environ. Sci. Technol.* **2008**, *42* (24), 9424-9430.
- (55) Goodman, C. M.; McCusker, C. D.; Yilmaz, T.; Rotello, V. M., Toxicity of gold nanoparticles functionalized with cationic and anionic side chains. *Bioconjugate Chem.* **2004**, *15* (4), 897-900.
- (56) Phenrat, T.; Saleh, N.; Sirk, K.; Kim, H. J.; Tilton, R. D.; Lowry, G. V., Stabilization of aqueous nanoscale zerovalent iron dispersions by anionic polyelectrolytes: adsorbed anionic polyelectrolyte layer properties and their effect on aggregation and sedimentation. *J. Nanopart. Res.* **2008**, *10* (5), 795-814.
- (57) Hauck, T. S.; Ghazani, A. A.; Chan, W. C. W., Assessing the effect of surface chemistry on gold nanorod uptake, toxicity, and gene expression in mammalian cells. *Small* **2008**, *4* (1), 153-159.
- (58) Fang, J. S.; Lyon, D. Y.; Wiesner, M. R.; Dong, J. P.; Alvarez, P. J. J., Effect of a fullerene water suspension on bacterial phospholipids and membrane phase behavior. *Environ. Sci. Technol.* **2007**, *41* (7), 2636-2642.
- (59) Schaechter, M.; Ingraham, J. L.; Neidhardt, F. C., *Microbe*. 1 ed.; ASM Press: Washington, DC 20036, 2005; p 370.
- (60) Levard, C.; Reinsch, B. C.; Michel, F. M.; Oumahi, C.; Lowry, G. V.; Brown, G. E., Sulfidation Processes of PVP-Coated Silver Nanoparticles in Aqueous Solution: Impact on Dissolution Rate. *Environ. Sci. Technol.* **2011**, *45* (12), 5260-5266.

Chapter 2: ADSORBED POLYMER AND NOM LIMITS ADHESION AND TOXICITY OF NANO SCALE ZERO-VALENT IRON (NZVI) TO *E. COLI*

2.1 Abstract

Nanoscale zero-valent iron (NZVI) is used for groundwater remediation. Freshly synthesized bare, i.e. uncoated NZVI is bactericidal at low mg/L concentration, but the impact of surface modifiers and aging (partial oxidation) on its bactericidal properties have not been determined. Here we assess the effect that adsorbed synthetic polymers and natural organic matter (NOM), and aging (partial oxidation) have on the bactericidal properties of NZVI to the gram-negative bacterium, *Escherichia coli*. Exposure to 100 mg/L of bare NZVI with 28% Fe⁰ content resulted in a 2.2-log inactivation after 10 minutes and a 5.2-log inactivation after 60 minutes. Adsorbed poly(styrene sulfonate) (PSS), poly(aspartate) (PAP), or NOM on NZVI with the same Fe⁰ content significantly decreased its toxicity, causing less than 0.2-log inactivation after 60 minutes. TEM images and heteroaggregation studies indicate that bare NZVI adheres significantly to cells, and that the adsorbed polyelectrolyte or NOM prevents adhesion, thereby decreasing NZVI toxicity. The 1.8-log inactivation observed for bare NZVI with 7% Fe⁰ content was lower than the 5.2-log inactivation using NZVI with 28% Fe⁰ after 1 hr; however, the minimum inhibitory concentration (MIC) after 24 hours was 5 mg/L regardless of Fe⁰ content. The MIC of PSS, PAP, and NOM coated NZVI were much higher; 500 mg/L, 100 g/L, and 100 g/L, respectively. But the MIC was much lower than the typical injection concentration used in remediation (10 g/L). Complete oxidation of

Fe^0 in NZVI under aerobic conditions eliminated its bactericidal effects. This study indicates that polyelectrolyte coatings and NOM will mitigate the toxicity of NZVI for exposure concentrations below 0.1 to 0.5 g/L depending on the coating, and that aged NZVI without Fe^0 is relatively benign to bacteria.

2.2 Introduction

Nanoscale zero-valent iron (NZVI) is a highly redox active material used to treat heavy metal and chlorinated organic solvent contaminants found in groundwater and soil (1-7). NZVI reduces contaminants through the oxidation of the metallic iron core of the particle and subsequent transfer of electrons to the contaminant. The NZVI particles used in aquifer remediation will come in contact with subsurface bacteria, which can be important contributors to the remediation process for halogenated contaminants since they can assist in the degradation of PCE and TCE when zero valent iron is present (8, 9). However, NZVI may adversely affect bacterial populations in the subsurface. Recent studies indicate that NZVI is bactericidal in pure cultures at concentrations as low as a few mg/L (10, 11), while NZVI is typically injected in to the ground to achieve porewater concentrations in the grams per liter range (2). The bactericidal properties of NZVI are therefore important to understand as it may affect the remediation efficiency of NZVI if native bacterial populations are adversely affected. Further, significant toxicity of NZVI to native microbial communities may have other unintended ecological consequences (12).

NZVI is just one of many nanomaterials whose use has become widespread, with many potential applications. Silver (13), magnesium oxide (14), fullerenes (15), copper

(16), titanium oxide (17), cerium oxide (18), and gold (19) have all been shown to display antimicrobial properties. The mechanism by which these nanomaterials cause cell death remains unclear, however, based on a recent summary of the biophysicochemical interactions of ~130 nanoparticles at the nano-bio interface (20), the mechanisms for toxicity may include disruption of the cell membrane structures (21), increased membrane permeability, interruption of energy transduction due to nanoparticle attachment to the membrane (22, 23), DNA and protein damage caused by released ions (e.g. silver (23, 24)), and apoptosis caused by the endogenous generation of reactive oxygen species (ROS) (25). Specific modes of action for the bactericidal properties of NZVI have been postulated to be reductive decomposition of protein functional groups in the cell membrane due to strong reducing conditions at the NZVI surface (11), and oxidative damage from intracellular ROS produced from Fenton's chemistry (10, 11).

Without cellular uptake, the oxidation state of iron atoms in NZVI and Fe-oxide nanoparticles have also been shown to correlate with its cytotoxicity to *E. coli* (10); NZVI (Fe(0)/Fe(II)/Fe(III)) being most toxic, magnetite (mixed Fe(II)/Fe(III) particle) less toxic, and maghemite (all Fe(III)) was non-toxic. NZVI exposed to environmental conditions will be oxidized under both oxic and anoxic conditions (26, 27). Oxidation of NZVI in groundwater can lead to the formation of different oxide layers, such as magnetite, maghemite, and lepidocrocite (27, 28). It is therefore possible that partially oxidized (aged) NZVI particles will be less toxic to *E. coli* than NZVI particles containing a larger amount of Fe⁰ and therefore more redox active.

While NZVI toxicity may be mediated through ROS generation or through release of Fe²⁺ (11), it is reasonable to assume that close proximity of the NZVI to the bacteria

would increase its toxicity potential. Prior reports of NZVI toxicity to *E. coli* have used uncoated NZVI which appears to have attached to the *E. coli* cell wall (10, 11). However, NZVI particles used in remediation are typically coated with polymer to increase its mobility in the subsurface (29, 30), or will become coated with natural organic matter (NOM) (31). Electrostatic repulsions caused by the negatively charged polymer coatings or adsorbed NOM may decrease the physical interaction between NZVI and the bacteria cell wall, and therefore its toxicity. The effect of the NZVI coatings on its bactericidal properties has not been evaluated. The objectives of this study were to assess the effect that organic macromolecular coatings such as synthetic polymers and natural organic matter, and aging (partial oxidation) have on the bactericidal properties of NZVI to a gram-negative bacterium, *Escherichia coli*.

2.3 Materials and Methods

2.3.1 Chemicals and NZVI

Sodium bicarbonate, hydrochloric acid, and agar were from Fisher Scientific (Howell, NJ). Poly(styrene sulfonate) (PSS, average MW=70,000 g/mol) and humic acid (average MW=1400 to 9200 g/mol (32)) were from Aldrich (St. Louis, MO). Miller LB broth was from Acros (Geel, Belgium). Polyaspartate (PA, average MW=2500 g/mol) was from Lanxess (Pittsburgh, PA). All solutions and dilutions were prepared in distilled and deionized water (Barnstead Nanopure). Ultrahigh-purity N₂ was from Butler Gas products (Pittsburgh, PA). The NZVI, Reactive Nanoscale Iron Particles (RNIP 10-DS) and maleic acid co-olefin (average MW =16,000 g/mol) modified RNIP (MRNIP2), was

supplied by Toda Kogyo Corp. (Onoda, Japan). RNIP are redox reactive $\text{Fe}^0/\text{Fe}_3\text{O}_4$ core-shell NZVI particles. RNIP physical and chemical properties have been described previously (5). The Fe^0 content of the RNIP was determined by acid digestion and measurement of the H_2 formed, as previously described (4). The RNIP had been stored anaerobically in an aqueous slurry (pH=12) for several months before and during the experimental program and had a Fe^0 content ranging from 20 to 28 wt % over the course of the study period.

2.3.2 NZVI Preparation

The procedure used to physisorb the polymers to the NZVI has been previously described (33). Briefly, a stock NZVI dispersion is diluted to a concentration of 120 g/L and ultrasonicated for 20 minutes. This dispersion is further diluted in a deoxygenated polymer solution to provide a final solution (30 mL) containing NZVI and polymer at a concentration of 3g/L and 1 g/L, respectively, in a 70 mL bottle. Concentrated polymer suspension was always added to dispersed particles as order of operation was found to affect particle stability against aggregation. The 70 mL reactor was then rotated end-over-end for 24 hrs to reach adsorption equilibrium. This same method was also used to coat the particles with humic acid, with initial humic acid concentrations of 10 and 80 mg/L. After adsorption, the polymer coated NZVI suspensions were fractionated by allowing the most unstable particles to settle for 10 minutes. The stable suspension was decanted and used for exposure experiments after measuring the Fe^0 content by acid digestion. To evaluate the effect of Fe^0 content on toxicity to *E. coli*, the NZVI (28 wt % Fe^0) was aged in water to partially or fully oxidize the Fe^0 in the particle core. Two types

of aged particles were used: anaerobically aged particles that contained 7 wt % Fe^0 and aerobically aged particles that contained no measureable Fe^0 as determined by acid digestion. Anaerobically aged particles were NZVI that had been aging in water in an anaerobic glovebox for 18 months. Aerobically aged particles were oxidized in O_2 -saturated water for 24 hours. After aging, polymer or NOM was physisorbed to the particles as described above.

2.3.3 *E. coli* Culture

E. coli (ATCC strain 33876) was inoculated in 60 mL of LB Miller broth medium and grown at 37 °C for 12 h. The bacteria were harvested by centrifugation at 5000g for 10 minutes. The supernatant was decanted, the cells were resuspended in 5 mM sodium bicarbonate (pH=8.2 \pm 0.1), then centrifuged again at 5000g for 10 minutes. This washing step was repeated. The *E. coli* stock was prepared by resuspending the bacteria pellets in 15 ml of 5 mM sodium bicarbonate. The stock concentration of *E. coli* was determined to be in the range of 1×10^9 to 2×10^9 colony forming units (CFU) /mL by the spread plate method using LB agar plates incubated at 37 °C for 12 hours.

2.3.4 Exposure Experiments and Minimal Inhibitory Concentration (MIC) Determination

The *E. coli* stock suspension was diluted 1000 fold in 5 mM bicarbonate solution in 20 mL culture tubes to reach final bacterial concentration of 10^6 CFU/mL. A suspension containing either bare, polymer-, or NOM-modified NZVI was added to the

tubes to provide an initial NZVI concentration of 100 mg/L as determined by atomic absorption spectrometry (AAS). The culture tubes were placed on an orbital shaker at 350 rpm and 37 °C. Samples were taken at 0, 5, 15, 30, 45, and 60 minutes and serially diluted. The cells were plated in triplicate on LB agar plates, incubated for 12 h at 37 °C, and the colonies were counted.

Exposure under anaerobic conditions and aerobic conditions were conducted. For exposure under anaerobic conditions, the cell suspensions and the buffer solution were sparged with nitrogen gas for 30 minutes prior to adding NZVI and were capped to exclude oxygen. For aerobic exposure, the cell suspensions were not sparged and the tubes were left open to the atmosphere to maintain oxygen saturation. Bacterial controls were performed side by side with the inoculation experiments. The controls consisted of cells (10^6 CFU/mL) in 5 mM sodium bicarbonate solution under both aerobic and anaerobic conditions to mirror the inoculation experiments.

The minimal inhibitory concentration (MIC) is defined as the lowest concentration of an agent that inhibits the visible growth of a microbe in an overnight culture (34). To measure the MIC of bare and coated NZVI 5 mL of the bacterial suspension was mixed with 5 mL of an NZVI suspension that ranged in concentration from 0.001 to 1 g/L in culture tubes. The MIC of free PSS in solution (a synthetic polymer that may have some toxicity) was also measured, with PSS concentrations ranging from 0.1 to 2 g/L. A 6.5 mL aliquot of the cell/NZVI or polymer suspension was added to 6.5 mL of LB Miller broth and incubated at 37 °C for 12 h. The tube with the lowest concentration of NZVI to remain unclouded was recorded as the MIC (35).

2.3.5 Measuring the Dispersed Iron Concentration in Culture Tubes

The uncoated NZVI used in this study aggregates rapidly (36). The coated NZVI will also agglomerate to some degree and partially sediment from solution despite the coating applied (33). NZVI aggregation was monitored by measuring the concentration of suspended particles over time during quiescent settling in 5 mM bicarbonate solution using UV-vis ($\lambda=508$ nm) as previously described (33). Attachment of NZVI to the *E. coli* could prevent NZVI aggregation and keep it suspended in solution. The UV-vis method did not work with cells present due to scattering interference from the cells, so to monitor heteroaggregation between NZVI and the cells the mass of bare or modified NZVI that remained in suspension after mixing with the cells was measured. A 5 mL aliquot was removed from the supernatant and acid digested in concentrated HCl to dissolve the suspended NZVI. The samples were then analyzed by AAS to determine the amount of iron that remained in suspension. Control samples without *E. coli* were measured in the same way to determine the amount of NZVI that remained in suspension due to sorption to the cell membrane.

2.3.6 Transmission Electron Microscopy (TEM)

The treated and untreated *E. coli* cells were fixed using 1% formaldehyde and 1% glutaraldehyde in 5mM sodium bicarbonate buffer for 24 hours at 4 °C, and washed three times with 5mM sodium bicarbonate buffer. A one μ L aliquot of the fixed cells was then put on a carbon coated copper grids for TEM examination. Cells were exposed to 10 mg/l of bare or coated (MRNIP2) NZVI.

2.4 Results and Discussion

2.4.1 NZVI Cytotoxicity Assessment

Exposure to 100 ppm of uncoated NZVI having 20% Fe^0 under anaerobic conditions resulted in a 2.2-log reduction in viable *E. coli* cells after 10 min., and up to a 5.2-log reduction in viable *E. coli* cells after 1 hour (Figure 2.1a). This is consistent with previous reports of NZVI toxicity; 3.4- and 4.5-log reductions in viable *E. coli* cells were observed after 10 minutes and 1 hour exposure to 9 ppm NZVI, respectively. However, the NZVI used previously appears to exert toxicity towards *E. coli* more quickly than RNIP (3.4-log inactivation after 10 min. (11) vs. 2.5-log inactivation after 10 min in this study). One explanation for the apparent increase in toxicity is that the NZVI used in previous studies was produced by borohydride reduction of dissolved iron (Fe(B)) (11), whereas the NZVI used here (RNIP) was made from reduction of Fe-oxides by H_2 gas. The most relevant differences between Fe(B) and RNIP are their Fe^0 content, Fe(B) is upwards of 98 wt % Fe^0 compared to 20-28 wt % Fe^0 for RNIP, and the amount of Fe(II) released during reaction, Fe(B) undergoes oxidative dissolution with dissolved Fe(II) accounting for as much as 40% of the NZVI at pH=8 whereas the Fe_3O_4 shell of RNIP limits Fe(II) solubility at pH=8 (5). Both Fe^0 content and the presence of Fe(II) have been positively correlated with NZVI toxicity to *E. coli*. (10, 11). Further, Fe(B) has been shown to generate ROS such as hydroxyl radicals that may be toxic to *E. coli*. (37). Thus Fe(B) has more Fe^0 , produces more Fe(II) , and can produce ROS which may inactivate the cells faster than RNIP (11). The primary particle size and N_2 -BET specific surface area of Fe(B) and RNIP are similar so these properties are not likely to be responsible for the differential toxicity observed. Despite the physicochemical

differences between RNIP and Fe(B); however, the total inactivation of *E. coli* after 1 hour was similar in both cases suggesting that the mode of action of toxicity is related to the presence of Fe^0 and the particle's overall redox activity rather than external factors such as Fe(II), size, or surface area. It also suggests that physical proximity of the NZVI to the cell is needed to exert toxicity; i.e., not through a soluble carrier like Fe(II).

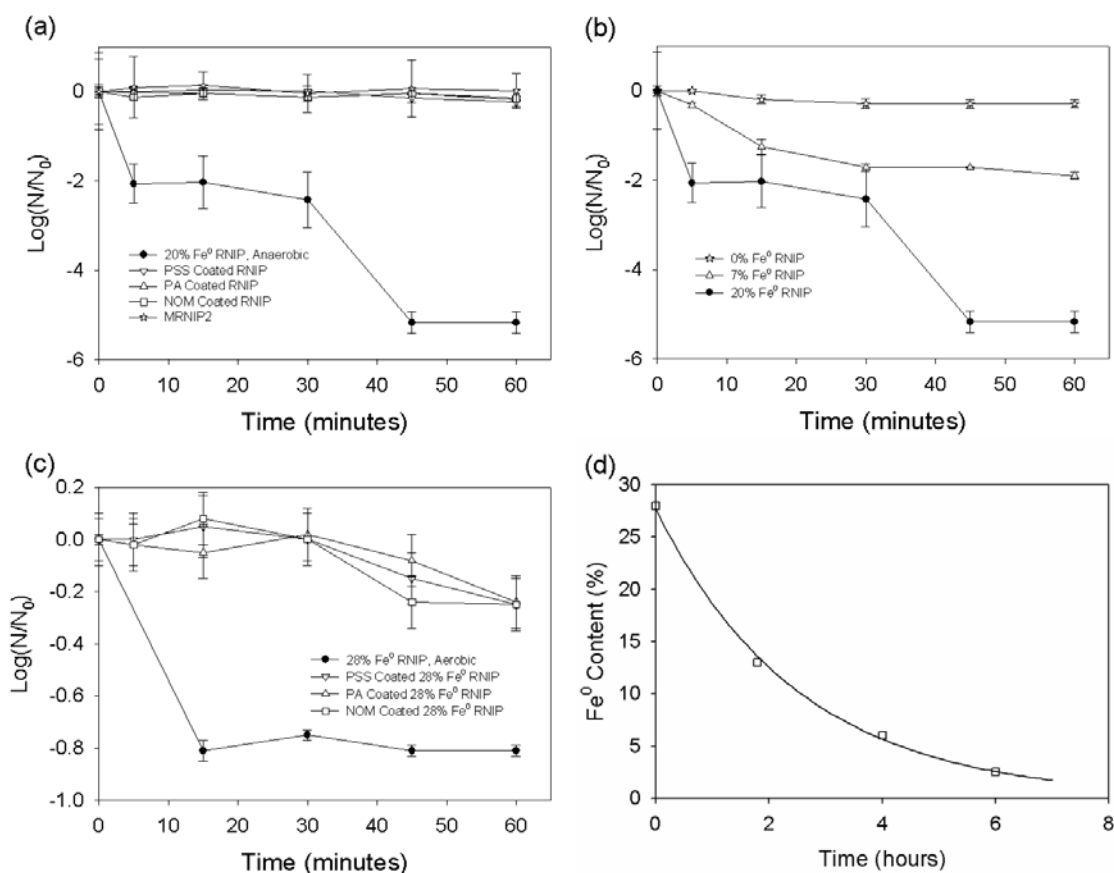


Figure 2.1. (a) Exposure of *E. coli* to bare NZVI and coated NZVI under anaerobic conditions; (b) Exposure of *E. coli* to aged NZVI, containing 0%, 7%, and 20% Fe^0 under anaerobic conditions; (c) Exposure of *E. coli* to NZVI and coated NZVI under aerobic conditions; and (d) Fe^0 content in NZVI as a function of exposure time to air-saturated water (NZVI concentration was approximately 1g/L). Oxygen was continuously bubbled through the vessel during aging.

2.4.2 Effect of Coatings

Exposure of the same NZVI particles coated with PSS, PA, maleic acid co-olefin or NOM resulted in less than a 0.2-log reduction in viable *E. coli* cells, while a 5.2-log reduction was observed for bare NZVI. All of these coatings reduced the cytotoxicity of NZVI to *E. coli*; however, the mechanism by which coatings inhibit toxicity is not clear. One explanation is that coatings prevent the physical contact between NZVI and cells. The cellular uptake and toxicity mechanisms proposed by Lee et al.; ROS produced from intracellular oxygen and reductive decomposition of functional groups in the proteins and lipopolysaccharides of the outer membranes (11), would require close contact between NZVI and cells. Additionally, previous studies have shown that contact between cells and nanoparticles is needed to cause cell death for other nanoparticles: Quantum dots that have their coatings weathered show an increase in toxicity (38); adsorbed natural organic matter reduces the toxicity of fullerenes by reducing direct contact with cells (39); and carbon nanotubes that have physicochemical properties that enhance cell-nanotube contact have a higher toxicity (40). TEM images of *E. coli* exposed to 10 mg/L bare and coated NZVI appear to support the hypothesis that the NZVI surface coatings prevent contact between the NZVI and the cells (Figure 2.2). Figure 2.2a shows that bare NZVI readily attaches to the cell membrane. Bare Fe(B) used in previous studies also showed adhesion of the NZVI to the cell walls (10, 11). However, the coated particles do not appear to attach to *E. coli* (Figure 2.2b). This observation was true for all *E. coli* observed on the grids (>20).

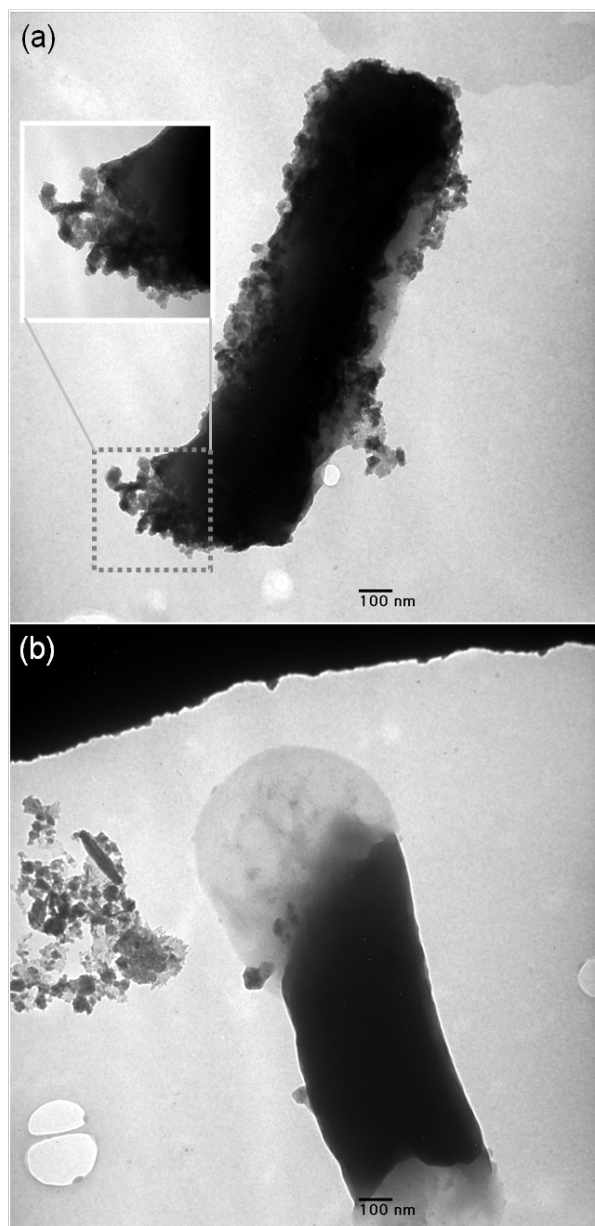


Figure 2.2. TEM images of *E. coli* incubated with (a) 10 mg/L of bare NZVI (20% Fe⁰) and (b) 10 mg/L of MRNIP2 (coated with olefin maleic acid, MW=16, 000 g/mol) for 1 h. The globular material on the cells was observed for all cells that had been exposed to MRNIP2. The chemical composition of the material is not known, but it did not appear to affect cell viability.

To further investigate attachment of bare and coated NZVI to *E. coli* cells, the aggregation and sedimentation of bare and coated NZVI was measured in the absence and in the presence of *E. coli* (10^6 CFU/mL). Despite the polymer and NOM coatings on NZVI, in all cases a fraction of the NZVI (100 mg/L) was not stable in 5 mM NaHCO₃ buffer and sedimented rapidly from solution (Figure A1.1, Supporting Information). In particular, bare NZVI rapidly aggregates and sediments from solution, as has been previously reported (36). After each 60 min exposure period, the particles were allowed to settle quiescently and a 5 mL sample of the supernatant was removed and analyzed for total iron content. The iron suspended in the presence of cells was compared with the iron suspended in identical reactors but without the cells. The percent increase (+) or decrease (-) in suspended iron due to the presence of cells under both anaerobic and aerobic exposures are provided in Table 2.1. For bare NZVI under either aerobic or anaerobic conditions, the presence of *E. coli* resulted in 50 to 250 % more NZVI remaining in suspension compared to the absence of cells. The increase in suspended NZVI in the presence of cells under aerobic conditions compared to anaerobic conditions is unclear. The amount of polymer and NOM coated NZVI remaining in suspension did not change or was slightly lower in the presence of cells than without. This indicates that bare NZVI is physically interacting with and attaching to the cells, whereas NZVI with physisorbed synthetic polymer or NOM are not physically attaching to *E. coli*. This observation is consistent with the TEM micrographs (Figure 2.2), which also indicate adhesion of bare NZVI to cells and limited adhesion of coated NZVI to cells.

Table 2.1. MIC and the change in suspended iron after contact with bacteria cells

Iron	MIC (mg/L)	% Change* of iron remaining in suspension after contact with <i>E. coli</i>	
		Anaerobic	Aerobic
28% Fe ⁰ NZVI	5	50	250
7% Fe ⁰ NZVI	5	80	170
PSS NZVI	516	-20	No change
PA NZVI	140	No change	-10
NOM NZVI	100	-20	No change
PSS Polymer	<2 g/L	No change	No change

*All values are $\pm 5\%$

The polyelectrolyte and NOM coatings on NZVI can decrease adhesion by several different methods: electrostatic, steric, and electrosteric repulsion (Figure 2.3). Low MW adsorbed polyelectrolytes that do not extend or form brushes provide electrostatic repulsions. Large uncharged polymers can afford steric repulsions by inhibiting close contact between the particles and the cells. Large MW polyelectrolytes afford both an electrostatic and steric repulsion, known as electrosteric repulsion, that is stronger than either electrostatic repulsion or steric repulsion (33), and its repulsive force is less sensitive to changes in ionic strength or pH than electrostatic repulsions that would occur using bare (uncoated) particles. NOM adsorbed to the particles decreased NZVI toxicity similarly as the polyelectrolytes tested here. NOM is probably acting as a polyelectrolyte to provide electrosteric repulsions between the particles and the cells. Polyelectrolytes such as poly(maleic acid) have been used as NOM analogs because they have the same types of functional groups and behave similarly to NOM in natural waters (41).

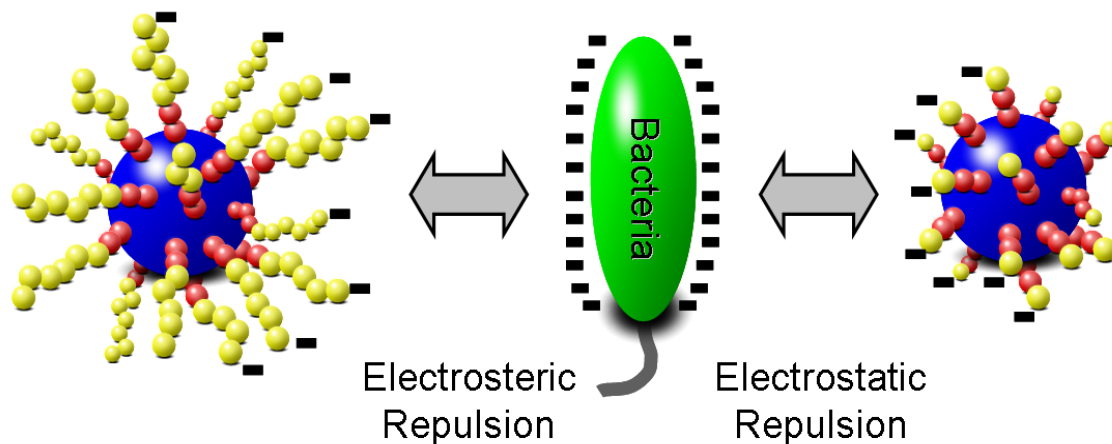


Figure 2.3. The surface coatings on NZVI may prevent physical interaction with *E. coli*. Higher MW polyelectrolyte coatings provide electrosteric repulsive forces while low MW surfactants and polyelectrolytes provide predominantly electrostatic repulsive forces that are more prone to charge screening with increasing ionic strength. Uncharged polymers provide steric repulsions (not shown). Natural organic matter can act as a polyelectrolyte or surfactant, providing electrostatic or electrosteric repulsive forces.

2.4.3 Effect of Fe⁰ Content

Auffan *et al.* showed that iron nanoparticles containing either Fe(II) or Fe⁰ are more cytotoxic to *E. coli* than particles with only Fe(III) (10). To determine if toxicity was a function of the iron zero content, *E. coli* toxicity from exposure to NZVI with 7% Fe⁰ were compared to those with 20% Fe⁰ (Figure 2.1b). The Fe⁰/Fe₃O₄ core shell structure of NZVI is preserved during anaerobic oxidation by water so the more oxidized particles are identical except with a thicker magnetite layer and less Fe⁰ (5). The other type of particle that was tested was aged aerobically and contained no Fe⁰. In the presence of dissolved oxygen (8.9 mg/L) the Fe⁰ content of the particles is very rapidly consumed (Figure 2.1d), and the oxide that is formed is likely a combination of magnetite, maghemite, and possibly lepidocrocite (26-28). Particles with no Fe⁰ remaining had little to no effect to *E. coli* cells (less than 0.2-log reduction in cells), while

particles containing 7% Fe^0 caused a 2-log reduction in cells (Figure 2.1b). This is less than the 5.2-log reduction caused by particles with 20% Fe^0 . This indicates that percentage of Fe^0 is related to NZVI cytotoxicity, consistent with previous reports (10). These results suggest that as NZVI ages anaerobically, its toxicity to bacteria will decrease. When aged anaerobically, the half life time of Fe^0 in this particular type of NZVI ranges from several weeks to several months depending on the pH of the groundwater and the contaminant loading (42) so time scales for this toxicity reduction should be months to just a few years after injection without dissolved oxygen present. With dissolved oxygen present, the Fe^0 lifetime is very short (~ 2 hours) (Figure 2.1d), and NZVI should rapidly oxidize to become non-toxic.

2.4.4 Effect of Aerobic and Anaerobic Conditions

NZVI (28% Fe^0 content) was less toxic to *E. coli* exposed under aerobic conditions (0.8-log inactivation) compared to exposure under anaerobic conditions (5.2-log inactivation) (Figure 2.1c). NZVI particles are quickly oxidized under aerobic (Figure 2.1d). The reason for the decreased toxicity is, however, probably not the loss of Fe^0 in the particles during exposure under aerobic conditions. The toxic effects on *E. coli* also appear to be mitigated after 15 minutes of exposure (Figure 2.1c) whereas the Fe^0 content is not depleted significantly during this time (Figure 2.1d). The lower observed toxicity during exposure under aerobic conditions could be a result of the formation of a different type of Fe-oxide at the particle surface, such as maghemite (26, 28), when aged aerobically compared to aging under anaerobic conditions. This different Fe-oxide may decrease adhesion to the cells, inhibit electron transfer due to the formation of Fe-oxides

on the particle surface that are less conductive than magnetite, or lower the amount of Fe(II) adsorbed to or within in the surface oxide (26) and therefore its toxicity to *E. coli*. It is also possible that under aerobic conditions, *E. coli* express enzymes that destroy ROS such as superoxide dismutase. These hypotheses remain to be evaluated. Finally, it may be possible that under aerobic conditions, the smallest NZVI particles and the ones present in the greatest number are fully oxidized, rendering them non toxic to *E. coli*. It has been previously shown that the smallest size fraction of NZVI in a polydisperse dispersion of RNIP contained only 4 wt% Fe⁰, whereas the larger size fraction contained 63% Fe⁰ (43).

2.4.5 Minimum Inhibitory Concentrations (MIC)

The minimum inhibitory concentrations were measured for bare and coated NZVI to confirm the plate count studies and to further distinguish differences in the antimicrobial properties of the various coating types (Table 2.1). The MIC for bare NZVI was 5 mg/L using either 7 or 28 % Fe⁰ content. Thus, after 24 hours, NZVI with Fe⁰ remaining in the particles will exhibit some toxicity. This MIC is significantly higher than those measure for silver nanoparticles (13 µg/L (44)), and slightly higher than those measured for bare and poly(vinylpyrrolidone) nC₆₀ fullerene aggregates (45), indicating that NZVI toxicity potential is lower than for these other manufactured nanomaterials.

The measured MIC's for the NOM-, PSS-, and PAP-coated NZVI are 20 to 100 times greater (i.e. less toxic) than for uncoated particles. The longer term (24 hr) MIC results further confirm the short term (1 h) plate count results, which showed that coated NZVI was non-toxic or considerably less toxic than the bare NZVI. No inhibition was

observed for just the PSS polymer solution in the concentration range that was used. The order of toxicity measured by the MIC test was PSS<PAP<NOM. This follows the order of the ability of the surface coating to stabilize the particles against aggregation at short times (< 20 minutes) (Figure A1.1, Supporting Information) as previously reported (33). The adsorbed mass and adsorbed layer thickness of PSS, PAP, and NOM on NZVI have been reported (33, 46). The adsorbed mass was similar for NOM (0.4 to 2.2 mg/m²) and PSS and PAP (1.9 to 2.2 mg/m²), but the adsorbed layer conformation and thickness were different. The thicker polymer brush afforded by PSS (67 ±7 nm) does a better job of preventing aggregation than do adsorbed PAP (40 ±12 nm) or NOM (4 ±3 nm) which adsorb with a flatter conformation on the NZVI surface. The same forces that prevent aggregation will also prevent adhesion to bacteria, so the order of toxicity measured by the MIC test is consistent with the hypothesis that surface coatings that best prevent adhesion of NZVI to the cells have the lowest toxicity.

All of the MIC values were less than 10 g/L, a typical concentration that NZVI is injected into groundwater (2). This suggests that inhibition of microbial activities may occur in the vicinity of the injection point, even for coated NZVI. Adsorbed NOM significantly decreases the measured NZVI toxicity to *E. coli*. NOM is ubiquitous in the environment and all NPs will ultimately become coated with NOM. While fullerenes (nC₆₀) have been shown to be highly toxic to bacteria in the absence of environmental media, fullerene had no effect on a soil microbial community, even at concentrations as high as 10,000 ppm (47). This study indicates that one reason for the lack of ecological effects may be adsorbed NOM derived from soil. Similarly, adsorbed NOM completely eliminated nC₆₀ antimicrobial activity (39), and decreased the antimicrobial activity of

PVP-coated Ag nanoparticles to *P. fluorescens* (48). The results presented here are consistent with these observations, and indicate that the most likely reason for the decreased toxicity in the presence of NOM or adsorbed polyelectrolyte is that the electrosteric repulsions afforded by the adsorbed polyelectrolyte are limiting adhesion to the bacteria. This suggests that the bactericidal effects of manufactured nanoparticles can, at least in part, be mitigated through the proper selection of surface coatings. However, in the case of NZVI, the adsorbed coatings decrease reactivity with the target contaminant (49). Thus, decreasing toxicity through surface modification will likely involve trade-offs with performance.

2.5 Acknowledgements

This research was funded by the National Science Foundation (BES-0608646 and EF-0830093) and the U.S. EPA R833326.

2.6 References

- (1) He, F.; Zhao, D. Y., Preparation and characterization of a new class of starch-stabilized bimetallic nanoparticles for degradation of chlorinated hydrocarbons in water. *Environ. Sci. Technol.* **2005**, *39* (9), 3314-3320.
- (2) Henn, K. W.; Waddill, D. W., Utilization of nanoscale zero-valent iron for source remediation—a case study. **2006**, *16* (2), 57-77.
- (3) Kanel, S. R.; Nepal, D.; Manning, B.; Choi, H., Transport of surface-modified iron nanoparticle in porous media and application to arsenic(III) remediation. *J. Nanopart. Res.* **2007**, *9* (5), 725-735.
- (4) Liu, Y. Q.; Choi, H.; Dionysiou, D.; Lowry, G. V., Trichloroethene hydrodechlorination in water by highly disordered monometallic nanoiron. *Chem. Mat.* **2005**, *17* (21), 5315-5322.
- (5) Liu, Y. Q.; Majetich, S. A.; Tilton, R. D.; Sholl, D. S.; Lowry, G. V., TCE dechlorination rates, pathways, and efficiency of nanoscale iron particles with different properties. *Environ. Sci. Technol.* **2005**, *39* (5), 1338-1345.

- (6) Song, H.; Carraway, E. R., Reduction of chlorinated ethanes by nanosized zero-valent iron: Kinetics, pathways, and effects of reaction conditions. *Environ. Sci. Technol.* **2005**, *39* (16), 6237-6245.
- (7) Zhang, W. X., Nanoscale iron particles for environmental remediation: An overview. *J. Nanopart. Res.* **2003**, *5* (3-4), 323-332.
- (8) Lampron, K. J.; Chiu, P. C.; Cha, D. K., Reductive dehalogenation of chlorinated ethenes with elemental iron: The role of microorganisms. **2001**, *35* (13), 3077-3084.
- (9) Weathers, L. J.; Parkin, G. F.; Alvarez, P. J., Utilization of cathodic hydrogen as electron donor for chloroform cometabolism by a mixed, methanogenic culture. *Environ. Sci. Technol.* **1997**, *31* (3), 880-885.
- (10) Auffan, M.; Achouak, W.; Rose, J.; Roncato, M. A.; Chaneac, C.; Waite, D. T.; Masion, A.; Woicik, J. C.; Wiesner, M. R.; Bottero, J. Y., Relation between the redox state of iron-based nanoparticles and their cytotoxicity toward *Escherichia coli*. *Environ. Sci. Technol.* **2008**, *42* (17), 6730-6735.
- (11) Lee, C.; Kim, J. Y.; Il Lee, W.; Nelson, K. L.; Yoon, J.; Sedlak, D. L., Bactericidal effect of zero-valent iron nanoparticles on *Escherichia coli*. *Environ. Sci. Technol.* **2008**, *42* (13), 4927-4933.
- (12) Wiesner, M. R.; Lowry, G. V.; Jones, K. L.; Hochella, M. F.; Di Giulio, R. T.; Casman, E.; Bernhardt, E. S., Decreasing uncertainties in assessing environmental exposure, risk, and ecological implications of nanomaterials. *Environ. Sci. Technol.* **2009**, *43* (17), 6458-6462.
- (13) Morones, J. R.; Elechiguerra, J. L.; Camacho, A.; Holt, K.; Kouri, J. B.; Ramirez, J. T.; Yacaman, M. J., The bactericidal effect of silver nanoparticles. *Nanotechnology* **2005**, *16* (10), 2346-2353.
- (14) Stoimenov, P. K.; Klinger, R. L.; Marchin, G. L.; Klabunde, K. J., Metal oxide nanoparticles as bactericidal agents. *Langmuir* **2002**, *18* (17), 6679-6686.
- (15) Lyon, D. Y.; Alvarez, P. J. J., Fullerene water suspension (nC(60)) exerts antibacterial effects via ROS-independent protein oxidation. *Environ. Sci. Technol.* **2008**, *42* (21), 8127-8132.
- (16) Hsiao, M. T.; Chen, S. F.; Shieh, D. B.; Yeh, C. S., One-pot synthesis of hollow Au₃Cu₁ spherical-like and biomineral botallackite Cu₂(OH)₃Cl flowerlike architectures exhibiting antimicrobial activity. *J. Phys. Chem. B* **2006**, *110* (1), 205-210.
- (17) Armelao, L.; Barreca, D.; Bottaro, G.; Gasparotto, A.; Maccato, C.; Maragno, C.; Tondello, E.; Stangar, U. L.; Bergant, M.; Mahne, D., Photocatalytic and antibacterial activity of TiO₂ and Au/TiO₂ nanosystems. *Nanotechnology* **2007**, *18* (37), 7.
- (18) Thill, A.; Zeyons, O.; Spalla, O.; Chauvat, F.; Rose, J.; Auffan, M.; Flank, A. M., Cytotoxicity of CeO₂ nanoparticles for *Escherichia coli*. Physico-chemical insight of the cytotoxicity mechanism. *Environ. Sci. Technol.* **2006**, *40* (19), 6151-6156.
- (19) Zhang, Y. W.; Peng, H. S.; Huang, W.; Zhou, Y. F.; Yan, D. Y., Facile preparation and characterization of highly antimicrobial colloid Ag or Au nanoparticles. *J. Colloid Interface Sci.* **2008**, *325* (2), 371-376.

- (20) Nel, A. E.; Madler, L.; Velegol, D.; Xia, T.; Hoek, E. M. V.; Somasundaran, P.; Klaessig, F.; Castranova, V.; Thompson, M., Understanding biophysicochemical interactions at the nano-bio interface. *Nat. Mater.* **2009**, *8* (7), 543-557.
- (21) Fang, J. S.; Lyon, D. Y.; Wiesner, M. R.; Dong, J. P.; Alvarez, P. J. J., Effect of a fullerene water suspension on bacterial phospholipids and membrane phase behavior. *Environ. Sci. Technol.* **2007**, *41* (7), 2636-2642.
- (22) Lyon, D. Y.; Brunet, L.; Hinkal, G. W.; Wiesner, M. R.; Alvarez, P. J. J., Antibacterial activity of fullerene water suspensions (nC(60)) is not due to ROS-mediated damage. *Nano Lett.* **2008**, *8* (5), 1539-1543.
- (23) Panacek, A.; Kvitek, L.; Prucek, R.; Kolar, M.; Vecerova, R.; Pizurova, N.; Sharma, V. K.; Nevecna, T.; Zboril, R., Silver colloid nanoparticles: Synthesis, characterization, and their antibacterial activity. *J. Phys. Chem. B* **2006**, *110* (33), 16248-16253.
- (24) Gogoi, S. K.; Gopinath, P.; Paul, A.; Ramesh, A.; Ghosh, S. S.; Chattopadhyay, A., Green fluorescent protein-expressing *Escherichia coli* as a model system for investigating the antimicrobial activities of silver nanoparticles. *Langmuir* **2006**, *22* (22), 9322-9328.
- (25) Hsin, Y. H.; Chena, C. F.; Huang, S.; Shih, T. S.; Lai, P. S.; Chueh, P. J., The apoptotic effect of nanosilver is mediated by a ROS- and JNK-dependent mechanism involving the mitochondrial pathway in NIH3T3 cells. *Toxicol. Lett.* **2008**, *179* (3), 130-139.
- (26) Reinsch, B. C.; Forsberg, B.; Penn, R. L.; Kim, C. S.; Lowry, G. V., Chemical transformations during aging of zero-valent iron nanoparticles in the presence of common groundwater dissolved constituents. *Environ. Sci. Technol.* **2009** (submitted).
- (27) Zhang, T. C.; Huang, Y. H., Profiling iron corrosion coating on iron grains in a zerovalent iron system under the influence of dissolved oxygen. *Water Res.* **2006**, *40* (12), 2311-2320.
- (28) Kohn, T.; Livi, K. J. T.; Roberts, A. L.; Vikesland, P. J., Longevity of granular iron in groundwater treatment processes: Corrosion product development. *Environ. Sci. Technol.* **2005**, *39* (8), 2867-2879.
- (29) He, F.; Zhao, D. Y., Manipulating the size and dispersibility of zerovalent iron nanoparticles by use of carboxymethyl cellulose stabilizers. *Environ. Sci. Technol.* **2007**, *41* (17), 6216-6221.
- (30) Saleh, N.; Kim, H. J.; Phenrat, T.; Matyjaszewski, K.; Tilton, R. D.; Lowry, G. V., Ionic strength and composition affect the mobility of surface-modified Fe⁰ nanoparticles in water-saturated sand columns. *Environ. Sci. Technol.* **2008**, *42* (9), 3349-3355.
- (31) Johnson, R. L.; Johnson, G. O.; Nurmi, J. T.; Tratnyek, P. G., Natural organic matter enhanced mobility of nano zerovalent iron. *Environ. Sci. Technol.* **2009**, *43* (14), 5455-5460.
- (32) Pitois, A.; Abrahamsen, L. G.; Ivanov, P. I.; Bryan, N. D., Humic acid sorption onto a quartz sand surface: A kinetic study and insight into fractionation. *J. Colloid Interface Sci.* **2008**, *325* (1), 93-100.
- (33) Phenrat, T.; Saleh, N.; Sirk, K.; Kim, H. J.; Tilton, R. D.; Lowry, G. V., Stabilization of aqueous nanoscale zerovalent iron dispersions by anionic

- polyelectrolytes: Adsorbed anionic polyelectrolyte layer properties and their effect on aggregation and sedimentation. *J. Nanopart. Res.* **2008**, *10* (5), 795-814.
- (34) Andrews, J. M., Determination of minimum inhibitory concentrations. *J. Antimicrob. Chemother.* **2001**, *48*, 5-16.
 - (35) Malcher, M.; Volodkin, D.; Heurtault, B.; Andre, P.; Schaaf, P.; Mohwald, H.; Voegel, J. C.; Sokolowski, A.; Ball, V.; Boulmedais, F.; Frisch, B., Embedded silver ions-containing liposomes in polyelectrolyte multilayers: Cargos films for antibacterial agents. *Langmuir* **2008**, *24* (18), 10209-10215.
 - (36) Phenrat, T.; Saleh, N.; Sirk, K.; Tilton, R. D.; Lowry, G. V., Aggregation and sedimentation of aqueous nanoscale zerovalent iron dispersions. *Environ. Sci. Technol.* **2007**, *41* (1), 284-290.
 - (37) Joo, S. H.; Feitz, A. J.; Sedlak, D. L.; Waite, T. D., Quantification of the oxidizing capacity of nanoparticulate zero-valent iron. *Environ. Sci. Technol.* **2005**, *39* (5), 1263-1268.
 - (38) Mahendra, S.; Zhu, H. G.; Colvin, V. L.; Alvarez, P. J., Quantum dot weathering results in microbial toxicity. *Environ. Sci. Technol.* **2008**, *42* (24), 9424-9430.
 - (39) Li, D.; Lyon, D. Y.; Li, Q.; Alvarez, P. J. J., Effect of soil sorption and aquatic natural organic matter on the antibacterial activity of a fullerene water suspension. *Environ. Toxicol. Chem.* **2008**, *27* (9), 1888-1894.
 - (40) Kang, S.; Mauter, M. S.; Elimelech, M., Physicochemical determinants of multiwalled carbon nanotube bacterial cytotoxicity. *Environ. Sci. Technol.* **2008**, *42* (19), 7528-7534.
 - (41) Wang, L. L.; Chin, Y. P.; Traina, S. J., Adsorption of (poly)maleic acid and an aquatic fulvic acid by goethite. *Geochim. Cosmochim. Acta* **1997**, *61* (24), 5313-5324.
 - (42) Liu, Y. Q.; Lowry, G. V., Effect of particle age (Fe^0 content) and solution pH on NZVI reactivity: H_2 evolution and TCE dechlorination. *Environ. Sci. Technol.* **2006**, *40* (19), 6085-6090.
 - (43) Phenrat, T.; Kim, H.-J.; Fagerlund, F.; Illangasekare, T.; Tilton, R. D.; Lowry, G. V., Particle size distribution, concentration, and magnetic attraction affect transport of polymer-modified Fe^0 nanoparticles in sand columns. *Environ. Sci. Technol.* **2009**, *43* (13), 5079-5085.
 - (44) Martinez-Castanon, G. A.; Nino-Martinez, N.; Martinez-Gutierrez, F.; Martinez-Mendoza, J. R.; Ruiz, F., Synthesis and antibacterial activity of silver nanoparticles with different sizes. *J. Nanopart. Res.* **2008**, *10* (8), 1343-1348.
 - (45) Lyon, D. Y.; Adams, L. K.; Falkner, J. C.; Alvarez, P. J. J., Antibacterial activity of fullerene water suspensions: Effects of preparation method and particle size. *Environ. Sci. Technol.* **2006**, *40* (14), 4360-4366.
 - (46) Phenrat, T.; Song, J. E.; Cisneros, C. M.; Schoenfelder, D. P.; Tilton, R. D.; Lowry, G. V., Attachment and deposition of nanoparticles coated with organic macromolecules: Mechanistic insights from an empirical model. *Environ. Sci. Technol.* **2009 (submitted)**.
 - (47) Tong, Z. H.; Bischoff, M.; Nies, L.; Applegate, B.; Turco, R. F., Impact of fullerene (C60) on a soil microbial community. *Environ. Sci. Technol.* **2007**, *41* (8), 2985-2991.

- (48) Fabrega, J.; Fawcett, S. R.; Renshaw, J. C.; Lead, J. R., Silver nanoparticle impact on bacterial growth: Effect of pH, concentration, and organic matter. *Environ. Sci. Technol.* **2009**, *43* (19), 7285–7290.
- (49) Phenrat, T.; Liu, Y. Q.; Tilton, R. D.; Lowry, G. V., Adsorbed polyelectrolyte coatings decrease Fe⁰ nanoparticle reactivity with TCE in water: Conceptual model and mechanisms. *Environ. Sci. Technol.* **2009**, *43* (5), 1507-1514.

Chapter 3: OBSTRUCTION OF CYTOTOXICITY BY NATURAL ORGANIC MATTER COATINGS ON TITANIUM DIOXIDE NANOPARTICLES

3.1 Abstract

Nanosized TiO₂ is used in a variety of industries and is predicted to enter the environment in concentrations that may be harmful. TiO₂ nanoparticles are known to be toxic due to photocatalytically generated reactive oxygen species (ROS). However, the impact of polymeric or natural organic matter (NOM) coatings on nano-TiO₂ toxicity has not been evaluated. Here we quantify the effect that organic coatings have on the toxicity of nano-TiO₂ to a gram-negative bacterium, *Escherichia coli* (*E. coli*), and examine the mechanisms by which adsorbed coatings affect the cytotoxicity. Exposure of cells to 100 mg/L bare nano-TiO₂ and UV irradiation resulted in 5-log inhibition after 3 hours. Adsorbed NOM decreased nano-TiO₂ toxicity, resulting in less than 0.3-log inhibition over the same period. Surprisingly, adsorbed polyaspartate (PAP) coatings had no impact on the toxicity of nano-TiO₂. Results show that NOM coatings interfere with ROS as toxic agents produced by nano-TiO₂ more than PAP coatings. These findings demonstrate that the potential for detrimental impacts of nanoparticles is lessened by NOM when reactive oxygen species are the toxic agents and highlight the importance of understanding the mechanisms by which natural and engineered coatings impact cytotoxicity to better predict their potential for adverse environmental impacts.

3.2 Introduction

Engineered nanoparticles including nanoscale zero valent iron (NZVI) (1-3), nano-TiO₂ (4-5), silver nanoparticles (AgNP) (6-8), fullerenes (9-10), and carbon nanotubes (CNT) (11) may be toxic to bacteria in pure and mixed cultures. However, adsorbed polymeric coatings and natural organic matter (NOM) may reduce antibacterial activities of nanoparticles (3,12-14). For example, adsorbed polyelectrolyte or NOM on NZVI prevents toxicity by limiting the physical interaction between the cell and particle through electrosteric and electrostatic repulsions (3,15-16). Coatings that prevent contact between NPs and cells or that sequester or prevent release of toxic metals from the NPs can decrease or eliminate the toxicity of quantum dots (13). As a result, the use of polymeric coatings on engineered nanoparticles has been proposed as a means to reduce their potential for detrimental environmental impacts (17).

Nano-TiO₂ is one of the most widely used nanomaterials, with an estimated worldwide production of 5000 t/year (18). Nano-TiO₂ can be used in a variety of products, including paints, pigments, ceramics, and sunscreens (18). Previous studies suggested using TiO₂ in photocatalytic disinfection (19-20) and wastewater treatment (21). Based on the current production volume and assumed paths of particle release, a recent risk assessment study suggested that nano-TiO₂ may pose a risk to aquatic organisms (18). In addition, the concentration of nano-TiO₂ in sediments (U.S.) is predicted to triple between 2008 and 2012 from 0.2 to 0.6 mg/kg (22), suggesting that a need exists to better define the fate, transport and potential cytotoxicity nano-TiO₂ in the environment.

Nano-TiO₂ may express toxicity through photocatalytic and non-photocatalytic mechanisms. Reactive oxygen species (ROS) generated from photocatalyzed reactions of TiO₂ in water is the primary route for cytotoxicity towards bacteria. ROS evolved from TiO₂ oxidize membrane phospholipids and inhibit cellular respiratory processes (5). However, during disinfection with TiO₂, the photocatalyzed toxicity is reduced by aqueous constituents commonly found in natural systems such as sulfate, nitrate, and organic matter (20). Recent studies with nano-TiO₂ show that dark interactions between the nanoparticles and cells also inhibit cell growth (4). These studies suggest that the mechanisms and effectors of cytotoxicity of nano-TiO₂ are more complicated than previously suspected. Here we describe the effect of polymeric and NOM coatings on the toxicity of nano-TiO₂ to *E. coli*. We demonstrate the importance of coating type and explore the mechanism by which coatings affect toxicity of nano-TiO₂.

3.3 Materials and Methods

3.3.1 Chemicals and TiO₂ Nanoparticles

Sodium bicarbonate, Miller LB broth, agar, and hydrogen peroxide (30%, certified ACS) were from Fisher Scientific (Howell, NJ). Polyaspartate (PAP, average MW=2500 g/mol) was from Lanxess (Pittsburgh, PA). All solutions and dilutions were prepared in distilled and deionized water (Barnstead Nanopure). Humic acid (average MW=1400 to 9200 g/mol), superoxide dismutase (SOD) from bovine erythrocytes (2,000-7,500 units/mg protein), catalase from bovine liver (2,000-5,000 units/mg protein), D-mannitol, *p*-chlorobenzoic acid (*p*CBA) 99%, and acetonitrile (HPLC grade,

$\geq 99.9\%$) were from Sigma-Aldrich (St. Louis, MO). The hydrogen peroxide test kit (HACH[®], model HYP-1) was from Hach Company (Loveland, CO). TiO₂ nanoparticles (P25) were provided by Degussa. The properties of these particles including crystallite size ($\sim 30\text{nm}$), aggregate size distribution (800-2000nm), and chemical composition (70 wt% anatase and 30 wt% rutile) have been reported previously (23).

3.3.2 TiO₂ Nanoparticle Dispersion Preparation

A TiO₂ stock aqueous dispersion (30 g/L) was prepared by dispersing a weighed mass of TiO₂ P-25 powder in water using an ultrasonic probe (Sonifier[®] 450) for 30 minutes at power level 3. After cooling down to room temperature this dispersion was diluted to 3 g/L using a solution of PAP or NOM to obtain a dispersion with 3 g/L TiO₂ and 1 g/L of coating. Concentrated polymer suspension was always added to dispersed particles, since adding particles to polymer will result in less stable coated TiO₂ nanoparticles. This solution was mixed using an end-to-end rotator for 24 hours to achieve adsorption equilibrium. After adsorption, the TiO₂ nanoparticles were washed by centrifuging at 6000 rpm for 30 minutes and resuspended in DI water. This was repeated two more times to remove excess free polymer in solution. Finally, washed TiO₂ nanoparticle was resuspended in 5 mM sodium bicarbonate buffer solution. The TiO₂ concentration was verified using UV-vis spectroscopy ($\lambda=800\text{nm}$) after washing. The instrument was calibrated using nano-TiO₂ standards with concentrations of 10, 50, 100, 200, and 500 mg/L ($R^2=0.995$). Coated and bare nanoparticles were characterized by dynamic light scattering (DLS) to determine their size distribution in the exposure media.

Before use the TiO₂ suspensions were ultrasonicated at power level 3 for 5 minutes to break aggregates formed during storage.

3.3.3 *E. coli* Culture Preparation

Bacteria culture was prepared by inoculating 25 mL of LB Miller broth medium with *E. coli* (ATCC strain 33876) and incubated at 37 °C for 12 h. The culture was then washed 3 times by centrifugation at 6000g and resuspended in 5 mM sodium bicarbonate (pH=7±0.1). The *E. coli* stock was prepared by resuspending the bacterial pellets in 10 ml of 5 mM sodium bicarbonate (pH=7). The concentration of *E. coli* in the stock solution was between 1×10^9 to 2×10^9 colony forming units (CFU)/mL.

3.3.4 UV Irradiation and Intensity Measurements

For UV irradiated experiments, a 20 watt long-wave UV bench lamp (BlackRay[®]) was used. This UV source provided irradiation in the UVA region, with a peak wavelength of 365 nm. This wavelength had negligible growth inhibition effect on *E. coli* as determined in a UV only control experiment. UV light intensity on the culture tubes was 6 W/m², measured using a UV AB digital light meter (General[®] UV513AB). All irradiated experiments were performed in a chamber with UV-absorbing insulation, eliminating effects from reflected UV irradiation.

3.3.5 Exposure Experiments

Before the exposure test, test tubes and buffer solution were autoclaved to sterilize them. The *E. coli* stock suspension was diluted 1000 fold aseptically in 5 mM bicarbonate solution (pH=7) in 20 mL culture tubes to reach a final bacterial concentration of 10^6 CFU/mL. A suspension containing either bare, polymer-, or NOM-modified TiO₂ was added to the tubes to provide a TiO₂ concentration of 100 mg/L as determined by UV-vis spectroscopy. The culture tubes were placed horizontally on a roller mixer at 30 °C. Samples were taken at 0, 30, 60, 90, 120, and 180 minutes and serially diluted. The cells were plated in triplicate on LB agar plates, incubated for 24 h at 37 °C, and the colonies were counted.

3.3.6 Reactive Oxygen Species Scavenging Experiments

Toxicity from ROS was determined by performing exposure tests with the addition of specific ROS scavengers. Three ROS scavengers were used: 1) catalase, an enzyme that scavenges hydrogen peroxide by converting it to water and oxygen (24), 2) superoxide dismutase (SOD), an enzyme that selectively scavenges superoxide by catalyzing its dismutation into oxygen and hydrogen peroxide (25) and, 3) mannitol, an efficient hydroxyl radical scavenger (24). Superoxide dismutase (SOD) was added to a concentration of 20-75 units/mL, based on manufacturer's estimate. Final catalase concentration was 20-50 units/mL, based on manufacturer's estimate. Hydroxyl radicals were scavenged by addition of 0.1 or 1 mM of mannitol (24). All scavenger solutions were filter sterilized using a 0.2µm filter and added to the culture tubes using aseptic techniques.

3.3.7 Hydroxyl Radical Measurement

Hydroxyl radical ($\cdot\text{OH}$) was quantified using *p*CBA as a probe compound (19). The steady state concentration of $\cdot\text{OH}$ was determined from the *p*CBA degradation rate using equations 1 through 3 as previously described (19). The second order rate constant for the reaction between $\cdot\text{OH}$ and *p*CBA ($k_{\text{OH},p\text{CBA}} = 5 \times 10^9 \text{ M}^{-1} \text{ s}^{-1}$) has been reported (26). A plot of the $\ln([p\text{CBA}]/[p\text{CBA}]_0)$ yields k_{exp} , the pseudo first order rate constant (eqn 2). The steady state $\cdot\text{OH}$ concentration was determined from k_{exp} using eqn 3.

$$-\frac{d[p\text{CBA}]}{dt} = k_{\text{OH},p\text{CBA}}[\cdot\text{OH}]_s[p\text{CBA}] = k_{\text{exp}}[p\text{CBA}] \quad (1)$$

$$-\ln \frac{[p\text{CBA}]}{[p\text{CBA}]_0} = k_{\text{exp}} t \quad (2)$$

$$[\cdot\text{OH}]_s = \frac{k_{\text{exp}}}{k_{\text{OH},p\text{CBA}}} \quad (3)$$

*p*CBA was added in reactors whose $\cdot\text{OH}$ concentrations needed to be determined at an initial concentration of 3 mg/L. Samples were taken at 0, 30, 60, and 180 minutes, followed by immediate addition of 10 μL (less than 1% of the sample volume) of 1 M mannitol to quench the reaction between *p*CBA and $\cdot\text{OH}$. Nano- TiO_2 was removed from samples by centrifuging at 13,000 g for 2 minutes. The *p*CBA concentration was determined using high-performance liquid chromatography (Agilent Technologies) equipped with a C18 reverse-phase column. The mobile phase contains 35% acetonitrile and 65% water. Signals were analyzed with a UV detector at wavelength of 230 nm. The instrument was calibrated using *p*CBA standards with concentration of 0.3, 0.75, 1.5, 2.25, and 3 mg/L ($R^2 = 0.99$).

3.3.8 NOM and Hydroxyl Radicals Reaction Constant

The rate constant for the reaction between NOM and $\cdot\text{OH}$ were determined using methods described elsewhere (27-28). In brief, six different ozone doses (10, 20, 30, 40, 50 and 60 μM) were added to pH 7.5 buffered solutions containing 10 mg/L NOM and 3 μM *p*CBA. *p*CBA concentration was measured 24 hours after complete ozone decomposition. The rate constant between NOM and $\cdot\text{OH}$ was determined using $k_{\text{OH,NOM}} = \Omega\eta k_{\text{OH,pCBA}}$, where Ω , the oxidation-competition value, is defined as the concentration of O_3 consumed, after depletion of the $\cdot\text{OH}$ probe begins, that resulted in a one-natural-log (37%) reduction in the original *p*CBA concentration. Ω was estimated by log-linear regressions. The term $k_{\text{OH,NOM}}$ is the first-order rate constant for $\cdot\text{OH}$ with NOM, and η (0.4-1.0) is the stoichiometric yield of $\cdot\text{OH}$ from ozone after its decomposition. A value of 0.67 was chosen for η . As described by Westerhoff et al (28), this value is representative of the base-catalyzed $\cdot\text{OH}$ yield. Dissolved ozone was measured spectrophotometrically at 254 nm (29).

3.4 Results and Discussion

3.4.1 Growth Inhibition by Nano-TiO₂

Nano-TiO₂ is slightly inhibitory to cell growth without UV illumination (4,11). In dark experiments we observed less than 1-log inhibition for 1000 mg/L bare nano-TiO₂ after 3 hours (Figure 3.1). This cell concentration remained unchanged after 9 hours of exposure.

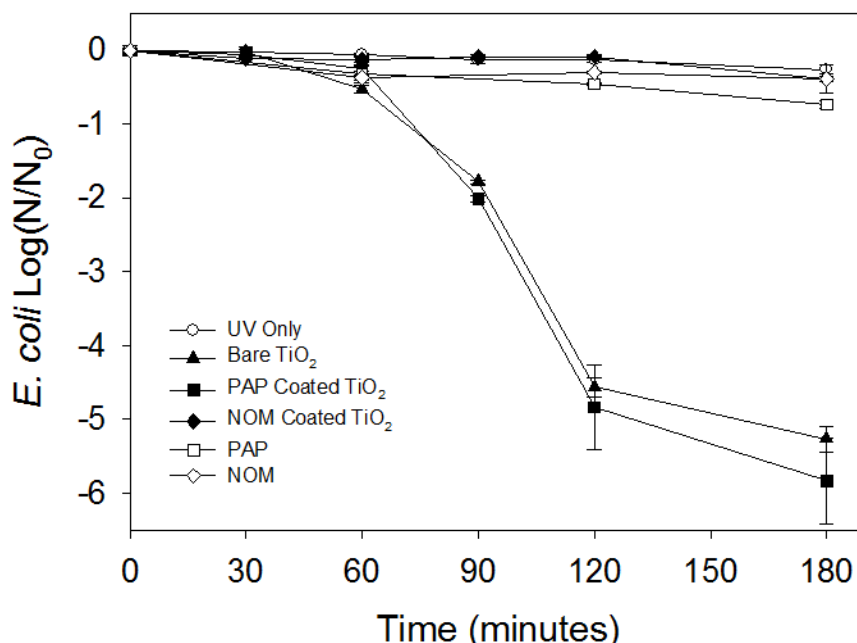


Figure 3.1. Exposure of *E. coli* to bare, PAP coated, and NOM coated nano-TiO₂ under UV irradiation, control experiment without nano-TiO₂ under UV irradiation, and control experiment with 100 mg/L PAP, and 100 mg/L NOM without UV irradiation. Less than 1-log inhibition was observed in the absence of illumination with 1000 mg/L bare nano-TiO₂ over 3 hours.

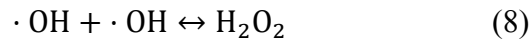
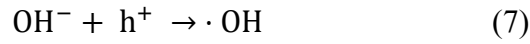
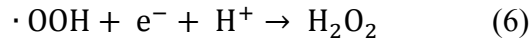
As expected, nano-TiO₂ displayed much higher toxicity to *E. coli* under UV irradiation. Figure 3.1 shows the cytotoxic properties of bare and coated nano-TiO₂ irradiated with UV. Control experiments show that bacteria growth was not significantly inhibited (<0.5 log) by UV irradiation alone, or by 100 mg/L PAP or 100 mg/L NOM (in the absence of TiO₂) after 3 hours. These free coating concentrations are conservatively representative of the highest concentration of PAP or NOM which could occur if all of it were to desorb from the coated particles. These findings show that the toxicity of UV light or coatings alone is negligible and that the observed growth inhibition for bare and coated nano-TiO₂ with UV irradiation can be attributed to the TiO₂ nanoparticles. Bare nano-TiO₂ at 100 mg/L resulted in 4.6-log inhibition after 2 hours and 5-log inhibition

after 3 hours (Figure 3.1), similar to a previous report by Cho et al (19). PAP coated nano-TiO₂ at 100 mg/L showed similar growth inhibition of *E. coli* as the bare nanoparticles, resulting in 5.5-log inhibition over 3 hours (Figure 3.1). However, in sharp contrast to the PAP coating, adsorbed NOM decreased growth inhibition of nano-TiO₂; after 3 hours, less than 0.5-log inhibition was observed (Figure 3.1). Unlike PAP coatings on NZVI which greatly reduced its toxicity, PAP does not similarly impact the toxicity of nano-TiO₂. It is likely that the physical contact necessary for the toxicity of NZVI is less important for nano-TiO₂, as is implied if the principal mechanism of toxicity is cell wall oxidation by ROS. ROS such as H₂O₂ may persist in solution and interact with cells independently of the particles. The contrary effects on growth inhibition between the PAP and NOM coated particles suggest that they do not merely prevent cell-particle contact as was the case for NZVI, but may also interfere with the primary mechanisms of toxicity and therefore impact the production of ROS or their reaction with cells.

3.4.2 Reactive Oxygen Species

The differential impact of the individual coatings on the growth inhibition of *E. coli* was explored by investigating the production and toxicity of ROS by nano-TiO₂ using selective scavenging compounds. Hydroxyl radical ($\cdot\text{OH}$), superoxide (O_2^-), and hydrogen peroxide (H_2O_2) are the reactive oxygen species commonly found in nano-TiO₂ catalyzed reactions (19). Equations 4-8 summarize the photocatalytic reactions involved in ROS generation. Mannitol, superoxide dismutase (SOD), or catalase was added in PAP coated nano-TiO₂ to scavenge $\cdot\text{OH}$, O_2^- , and H_2O_2 respectively. Figure 3.2a shows growth inhibition by PAP coated nano-TiO₂ with and without scavengers. The addition of

20-75 units/mL of SOD resulted in more than 3.5-log inhibition of growth over 3 hours, similar to the bare and PAP coated nano-TiO₂ without SOD shown in Figure 3.1. This implies that superoxide is not a significant contributor to the observed toxicity. However, toxicity was significantly reduced with addition of mannitol or catalase over 3 hours. 0.1 mM mannitol reduced inhibition to 2-log units after 3 hours while 1 mM mannitol reduced it to 0.5-log units (Figure 3.2a). Similarly, 20-50 units/mL catalase reduced toxicity of PAP coated nano-TiO₂ to less than 1.4-log inhibition after 3 hours (Figure 3.2a). The significant reduction in toxicity with mannitol and catalase indicate that photocatalytically produced $\cdot\text{OH}$ and/or H₂O₂ from nano-TiO₂ were primarily responsible for *E. coli* growth inhibition.



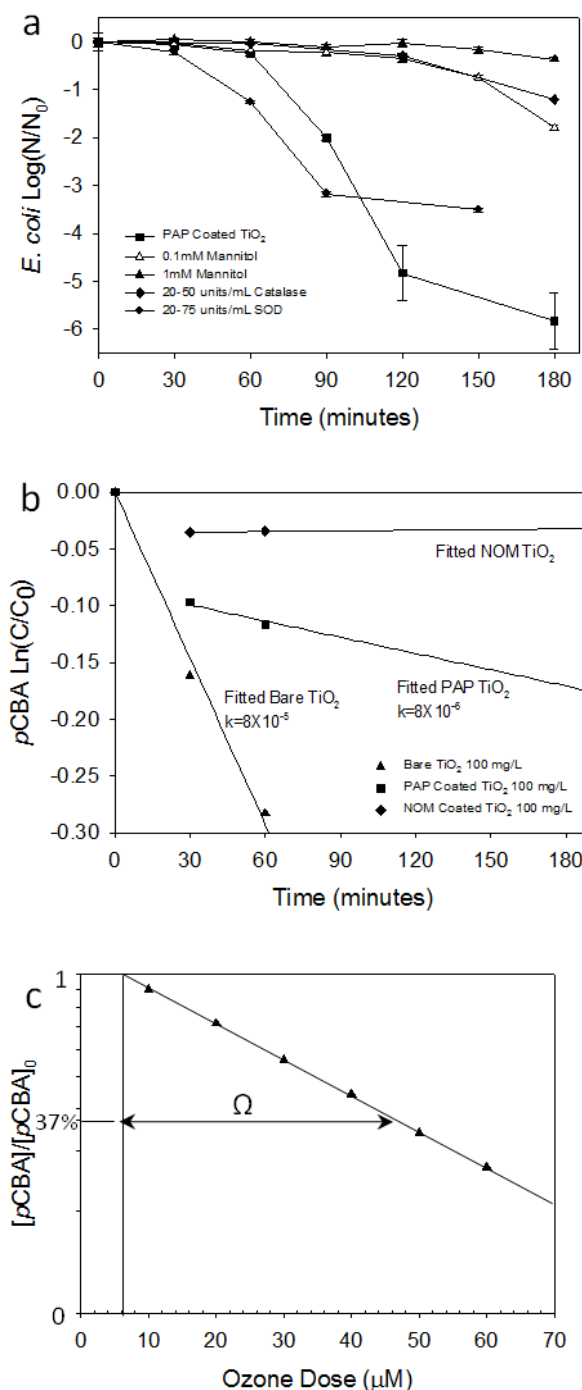


Figure 3.2. (a) Exposure of *E. coli* to 100 mg/L PAP coated nano-TiO₂ with ROS scavengers: 0.1 and 1.0 mM mannitol, 20-50 units/mL catalase, and 20-75 units/mL superoxide dismutase; (b) *pCBA* degradation by 100 mg/L bare, PAP coated, and NOM coated nano-TiO₂ under UV irradiation; (c) first-order fits of *pCBA* degradation as a function of O₃ dose and Ω for NOM (10 mg/L).

3.4.3 Hydroxyl Radical

Hydroxyl radical concentration was determined from *p*CBA degradation measurements. Figure 3.2b shows the normalized *p*CBA degradation data and fitted curves for bare and coated nano-TiO₂. Table 3.1 lists the fitted k_{exp} and estimated $\cdot\text{OH}$ concentrations. The estimated hydroxyl radical concentration for bare nano-TiO₂ was 1.63×10^{-14} mol/L. Cho et al reported a higher $\cdot\text{OH}$ concentration, 2×10^{-12} mol/L, using 100 mg/L nano-TiO₂ (19), but this discrepancy may be attributed to differing experimental conditions (i.e. light intensity, TiO₂ concentration, particle characteristics, and pH). Hydroxyl radical concentration for PAP coated nano-TiO₂ was 1.59×10^{-15} mol/L, 10 times lower than that for bare nano-TiO₂. This suggests that PAP may decrease TiO₂ $\cdot\text{OH}$ production. *p*CBA degradation was not observed for NOM coated nano-TiO₂ (*p*CBA concentration change was less than 0.3%, within the range of measurement errors), suggesting that the NOM coating decreases $\cdot\text{OH}$ concentration. Although the reason for this decrease of $\cdot\text{OH}$ concentration is still unclear, two explanations may be proposed: 1) coatings decrease the light intensity reaching the TiO₂ nanoparticle surface and decrease the photocatalytic reaction rate; and/or 2) coatings may react with $\cdot\text{OH}$ and lower its steady state concentration to below a threshold value where *E. coli* can survive.

Scavenging of $\cdot\text{OH}$ by the organic coating molecules was investigated using the oxidation-competition method (27-28). Figure 3.2c demonstrates the determination of Ω . The reaction rate constants between NOM and $\cdot\text{OH}$ are listed in Table 3.2. The rate constant normalized by the concentration of organic carbon, $K_{\text{OH},\text{DOC}}$, is 3.3×10^8 l (mol C)⁻¹ s⁻¹, consistent to a previously reported value of 3.6×10^8 l (mol C)⁻¹ s⁻¹ (28). This suggests that NOM is able to scavenge $\cdot\text{OH}$ consistent with other studies (28).

Westerhoff et al (28) found that the rate constant between NOM and $\cdot\text{OH}$ is positively correlated with aromatic carbon content, and inversely correlated with aliphatic carbon content. This may be used to explain our toxicity observations. PAP, containing no aromatic content, may not be able to scavenge $\cdot\text{OH}$ as efficiently as NOM, which contains higher aromatic content. Hydroxyl radical is an important toxic agent produced by TiO_2 -NP. NOM reduces its toxicity, at least in part, by scavenging $\cdot\text{OH}$.

Table 3.1. Growth inhibition test and ROS concentrations

	^a Growth Inhibition $\log(\text{N}/\text{N}_0)$ after 3 hours	^b $[\cdot\text{OH}]$ (mol/L)	k_{exp} (s^{-1})
Bare TiO_2	-5.26 ± 0.17	1.6×10^{-14}	8.1×10^{-5}
PAP TiO_2	-5.83 ± 0.58	1.6×10^{-15}	7.9×10^{-6}
NOM TiO_2	-0.38 ± 0.18	^c N/D	-3.1×10^{-7}

^a Growth inhibition was tested by expose 10^6 CFU/ml *E. coli* to 100 mg/L bare, PAP coated, and NOM coated nano- TiO_2 , and to 5mM H_2O_2 , with or without 100 mg/L PAP and 100 mg/L NOM with UV irradiation.

^b $\cdot\text{OH}$ concentration was determined by fitting the *p*CBA degradation data.

^c $\cdot\text{OH}$ concentration was none-detectable (N/D). Less than 0.3% *p*CBA concentration change was observed, within the range of measurement errors.

Table 3.2. Reaction rate constants between NOM and hydroxyl radical

Calculated $\Omega(\mu\text{M of O}_3)$	$K_{\text{OH,NOM}} (\text{s}^{-1})$	$K_{\text{OH,DOC}}$ ($10^8 \text{ l (mol C)}^{-1} \text{ s}^{-1}$)	Reference
41	1.37×10^5	^a 3.3	This work
25	-	3.6	Westerhoff et al, 1999

^a Organic carbon concentration was calculated using carbon content of 51% for NOM.

3.4.4 Hydrogen Peroxide

H_2O_2 is also produced by nano- TiO_2 via photocatalytic reactions (eq. 6 and 8). *E. coli* exposure tests were performed using H_2O_2 to understand its contribution to nano- TiO_2 toxicity. No significant inhibition was observed for 1 mmol/L H_2O_2 (data not

shown). H_2O_2 concentration was measured using the hydrogen peroxide test kit (HACH[®], model HYP-1). No significant change in H_2O_2 concentration change was observed over the course of these exposure tests. These findings indicate that H_2O_2 is not the direct cause for growth inhibition by nano- TiO_2 . However, toxicity from H_2O_2 cannot be ruled out since H_2O_2 scavenger, 20-50 units/mL catalase, reduced PAP coated nano- TiO_2 toxicity (Figure 3.2a). The role of H_2O_2 in TiO_2 toxicity to bacteria has been discussed by Kikuchi et al (24).

3.4.5 Coating Effects

An NOM coating significantly reduced nano- TiO_2 toxicity to *E. coli* whereas PAP coatings did not. An analogous, negative effect on photocatalytic disinfection of *E. coli* with TiO_2 occurs in presence of natural organic substances (20). Similarly decreased photocatalytic degradation of aqueous pollutants was observed with the presence of NOM (21) and was attributed to attenuation of radiation, competition for reactive sites, and deactivation of the catalytic surface. The OH^\bullet formed directly from TiO_2 or from H_2O_2 decomposition (eqn 8) may be the cytotoxic agent for nano- TiO_2 . It is likely that aromatic groups on NOM may scavenge OH^\bullet and decreases nano- TiO_2 cytotoxicity (Figure 3.3). Contrary to our previous reports on cytotoxicity of NZVI, experiments with nano- TiO_2 show that the type of coating and not merely the existence is an important determinate for cytotoxic behavior for nanoparticles. Our findings suggest that the reactivity of functional groups of the coatings will be a key consideration for the design of nanomaterials with reduced cellular and environmental toxicity. Our findings further suggest that the toxic properties of nano- TiO_2 may be mitigated by NOM after their release to the environment. The proposed mechanisms of toxicity reduction for nano-

TiO₂ may be extended to other nanoparticles that exert toxicity via the production of ROS. For example, NOM plays an important role in reducing toxicity of fullerene in a number of studies (14,30). Finally, different coatings affected TiO₂ toxicity differently than for NZVI (3). These data suggest that only ROS scavenging coatings (e.g. NOM) may reduce the toxicity nanoparticles like TiO₂ that produce ROS. These results underscore the importance of understanding the toxic pathways and coating reactivity to best predict the effect of coatings on nanoparticle toxicity.

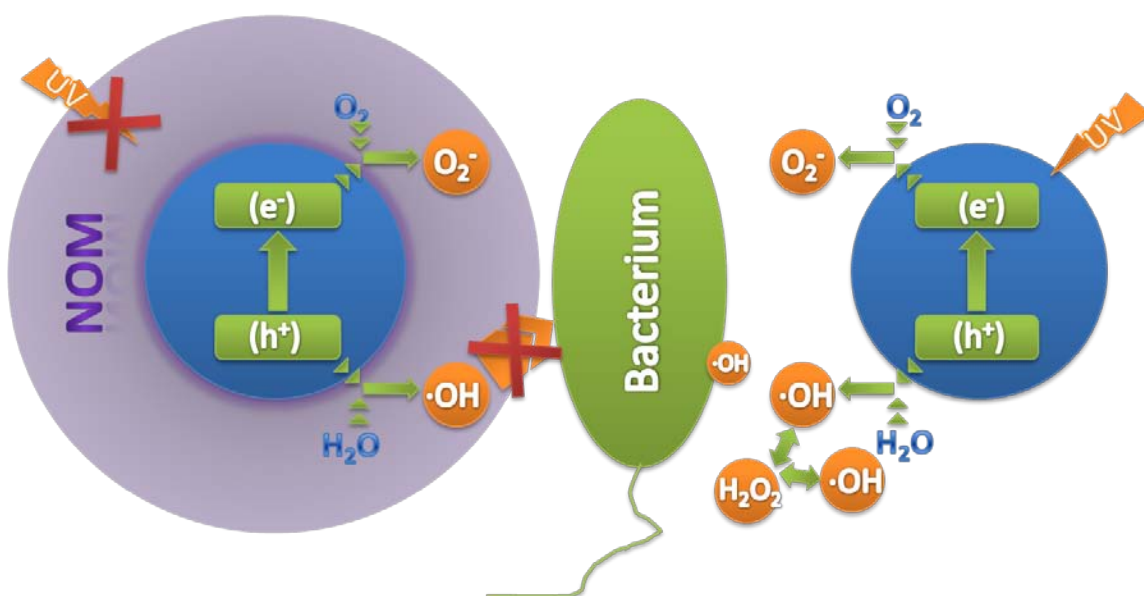


Figure 3.3. Nano-TiO₂ inhibits bacterial growth by generating hydroxyl radical. Natural organic matter may react with •OH or decrease light intensity reached at the particles and reduces cytotoxic effects of nano-TiO₂.

3.5 Supporting Information Available

Inhibition data for bare nano-TiO₂ without UV irradiation. Inhibition data for 2.5, 5, 7.5, and 10mM H₂O₂ with 1000 mg/L PAP and 1000 mg/L NOM. This information is available free of charge via the Internet at <http://pubs.acs.org/>.

3.6 Literature Cited

- (1) Auffan, M.; Achouak, W.; Rose, J.; Roncato, M. A.; Chaneac, C.; Waite, D. T.; Masion, A.; Woicik, J. C.; Wiesner, M. R.; Bottero, J. Y., Relation between the redox state of iron-based nanoparticles and their cytotoxicity toward *Escherichia coli*. *Environ. Sci. Technol.* **2008**, *42* (17), 6730-6735.
- (2) Lee, C.; Kim, J. Y.; Il Lee, W.; Nelson, K. L.; Yoon, J.; Sedlak, D. L., Bactericidal effect of zero-valent iron nanoparticles on *Escherichia coli*. *Environ. Sci. Technol.* **2008**, *42* (13), 4927-4933.
- (3) Li, Z.; Greden, K.; Alvarez, P. J. J.; Gregory, K. B.; Lowry, G. V., Adsorbed polymer and NOM limits adhesion and toxicity of nano scale zerovalent iron to *E. coli*. **2010**, *44* (9), 3462-7.
- (4) Adams, L. K.; Lyon, D. Y.; Alvarez, P. J. J., Comparative eco-toxicity of nanoscale TiO₂, SiO₂, and ZnO water suspensions. *Water Res.* **2006**, *40* (19), 3527-3532.
- (5) Maness, P. C.; Smolinski, S.; Blake, D. M.; Huang, Z.; Wolfrum, E. J.; Jacoby, W. A., Bactericidal activity of photocatalytic TiO₂ reaction: Toward an understanding of its killing mechanism. *Appl. Environ. Microbiol.* **1999**, *65* (9), 4094-4098.
- (6) Choi, O.; Hu, Z. Q., Size dependent and reactive oxygen species related nanosilver toxicity to nitrifying bacteria. *Environ. Sci. Technol.* **2008**, *42* (12), 4583-4588.
- (7) Fabrega, J.; Fawcett, S. R.; Renshaw, J. C.; Lead, J. R., Silver Nanoparticle Impact on Bacterial Growth: Effect of pH, Concentration, and Organic Matter. *Environ. Sci. Technol.* **2009**, *43* (19), 7285-7290.
- (8) Morones, J. R.; Elechiguerra, J. L.; Camacho, A.; Holt, K.; Kouri, J. B.; Ramirez, J. T.; Yacaman, M. J., The bactericidal effect of silver nanoparticles. *Nanotechnology* **2005**, *16* (10), 2346-2353.
- (9) Fang, J. S.; Lyon, D. Y.; Wiesner, M. R.; Dong, J. P.; Alvarez, P. J. J., Effect of a fullerene water suspension on bacterial phospholipids and membrane phase behavior. *Environ. Sci. Technol.* **2007**, *41* (7), 2636-2642.
- (10) Lyon, D. Y.; Brunet, L.; Hinkal, G. W.; Wiesner, M. R.; Alvarez, P. J. J., Antibacterial activity of fullerene water suspensions (nC(60)) is not due to ROS-mediated damage. *Nano Lett.* **2008**, *8* (5), 1539-1543.

- (11) Simon-Deckers, A.; Loo, S.; Mayne-L'Hermite, M.; Herlin-Boime, N.; Menguy, N.; Reynaud, C.; Gouget, B.; Carriere, M., Size-, Composition- and Shape-Dependent Toxicological Impact of Metal Oxide Nanoparticles and Carbon Nanotubes toward Bacteria. *Environ. Sci. Technol.* **2009**, *43* (21), 8423-8429.
- (12) Li, D.; Lyon, D. Y.; Li, Q.; Alvarez, P. J. J., Effect of soil sorption and aquatic natural organic matter on the antibacterial activity of a fullerene water suspension. *Environ. Toxicol. Chem.* **2008**, *27* (9), 1888-1894.
- (13) Mahendra, S.; Zhu, H. G.; Colvin, V. L.; Alvarez, P. J., Quantum Dot Weathering Results in Microbial Toxicity. *Environ. Sci. Technol.* **2008**, *42* (24), 9424-9430.
- (14) Tong, Z. H.; Bischoff, M.; Nies, L.; Applegate, B.; Turco, R. F., Impact of fullerene (C-60) on a soil microbial community. *Environ. Sci. Technol.* **2007**, *41* (8), 2985-2991.
- (15) Chen, J.; Xiu, Z.; Lowry, G. V.; Alvarez, P. J. J., Effect of natural organic matter on toxicity and reactivity of nano-scale zerovalent iron. *Water Research* **2010**, in press.
- (16) Xiu, Z. M.; Gregory, K. B.; Lowry, G. V.; Alvarez, P. J. J., Effect of Bare and Coated Nanoscale Zerovalent Iron on tceA and vcrA Gene Expression in Dehalococcoides spp. *Environ. Sci. Technol.* **2010**, *44* (19), 7647-7651.
- (17) Wiesner, M. R.; Lowry, G. V.; Jones, K. L.; Hochella, M. F.; Di Giulio, R. T.; Casman, E.; Bernhardt, E. S., Decreasing Uncertainties in Assessing Environmental Exposure, Risk, and Ecological Implications of Nanomaterials. *Environ. Sci. Technol.* **2009**, *43* (17), 6458-6462.
- (18) Mueller, N. C.; Nowack, B., Exposure modeling of engineered nanoparticles in the environment. *Environ. Sci. Technol.* **2008**, *42* (12), 4447-4453.
- (19) Cho, M.; Chung, H.; Choi, W.; Yoon, J., Linear correlation between inactivation of E-coli and OH radical concentration in TiO₂ photocatalytic disinfection. *Water Res.* **2004**, *38* (4), 1069-1077.
- (20) Rincon, A. G.; Pulgarin, C., Effect of pH, inorganic ions, organic matter and H₂O₂ on E-coli K12 photocatalytic inactivation by TiO₂ - Implications in solar water disinfection. *Appl. Catal. B-Environ.* **2004**, *51* (4), 283-302.
- (21) Doll, T. E.; Frimmel, F. H., Photocatalytic degradation of carbamazepine, clofibric acid and iomeprol with P25 and Hombikat UV100 in the presence of natural organic matter (NOM) and other organic water constituents. *Water Res.* **2005**, *39* (2-3), 403-411.
- (22) Gottschalk, F.; Sonderer, T.; Scholz, R. W.; Nowack, B., Modeled Environmental Concentrations of Engineered Nanomaterials (TiO₂, ZnO, Ag, CNT, Fullerenes) for Different Regions. *Environ. Sci. Technol.* **2009**, *43* (24), 9216-9222.
- (23) Long, T. C.; Saleh, N.; Tilton, R. D.; Lowry, G. V.; Veronesi, B., Titanium dioxide (P25) produces reactive oxygen species in immortalized brain microglia (BV2): Implications for nanoparticle neurotoxicity. *Environ. Sci. Technol.* **2006**, *40* (14), 4346-4352.
- (24) Kikuchi, Y.; Sunada, K.; Iyoda, T.; Hashimoto, K.; Fujishima, A., Photocatalytic bactericidal effect of TiO₂ thin films: Dynamic view of the active oxygen species responsible for the effect. *J. Photochem. Photobiol. A-Chem.* **1997**, *106* (1-3), 51-56.

- (25) Suthanthiran, M.; Solomon, S. D.; Williams, P. S.; Rubin, A. L.; Novogrodsky, A.; Stenzel, K. H., Hydroxyl Radical Scavengers Inhibit Human Natural-Killer Cell-Activity. *Nature* **1984**, 307 (5948), 276-278.
- (26) Elovitz, M. S.; von Gunten, U.; Kaiser, H. P., Hydroxyl radical/ozone ratios during ozonation processes. II. The effect of temperature, pH, alkalinity, and DOM properties. *Ozone-Sci. Eng.* **2000**, 22 (2), 123-150.
- (27) Haag, W. R.; Yao, C. C. D. In *Ozonation of U.S. drinking water sources: HO concentrations and oxidation-competition values*, Ozone in Water and Wastewater, San Francisco, CA, San Francisco, CA, 1993; pp S-17-119-125.
- (28) Westerhoff, P.; Aiken, G.; Amy, G.; Debroux, J., Relationships between the structure of natural organic matter and its reactivity towards molecular ozone and hydroxyl radicals. *Water Res.* **1999**, 33 (10), 2265-2276.
- (29) Langlais, B.; Reckhow, D. A.; Brink, D. R., *Ozone in Water Treatment: Applications and Engineering*. Lewis Publishers: 1991.
- (30) Xie, B.; Xu, Z. H.; Guo, W. H.; Li, Q. L., Impact of natural organic matter on the physicochemical properties of aqueous C-60 nanoparticles. *Environ. Sci. Technol.* **2008**, 42 (8), 2853-2859.

Chapter 4: OBSTRUCTION OF CYTOTOXICITY BY DISSOLVED NATURAL ORGANIC MATTER ON SILVER NANOPARTICLES

4.1 Abstract

Silver nanoparticles (AgNP) are used in a variety of industrial and commercial products and are predicted to enter the environment in concentrations that may be harmful. AgNPs are known to be toxic, primarily due to released Ag^+ . However, the impact of adsorbed polymeric coatings or natural organic matter (NOM) on AgNP toxicity is not well understood. Here we quantify the effect that organic coatings have on the toxicity of AgNP to a gram-negative bacterium, *Escherichia coli* (*E. coli*), and determine the mechanisms by which NOM in solution affects the toxicity. Exposure of cells to 1 mg/L of uncoated AgNPs resulted in 6-log inhibition after 3 hours. Dissolved coal-derived humic acid at 100 mg/L decreased AgNP toxicity, resulting in less than 1-log inhibition over the same period. However, dissolved polyvinylpyrrolidone (PVP) and carboxy methyl cellulose (CMC) had no impact on the toxicity of AgNP. Results show that NOM scavenges Ag^+ ion released by AgNP more than CMC and PVP, resulting in the lower observed toxicity. A correlation between sulfur content in the NOM and AgNP toxicity is observed. Humic acid containing higher sulfur content resulted in less toxicity. This suggests that Ag^+ scavenging by NOM is causing the decrease in toxicity. These findings suggest that the potential for detrimental impacts of nanoparticles that interact with bacteria through the release of toxic metal ions can be decreased by NOM or other polymeric coatings that scavenge those toxic metal ions.

4.2 Introduction

Engineered nanoparticles including nanoscale zero valent iron (NZVI) (1-3), nano-TiO₂ (4-5), silver nanoparticles (AgNP) (6-8), fullerenes (9-10), and carbon nanotubes (CNT) (11) have been shown to be toxic to bacteria in pure and mixed cultures. However, adsorbed polymeric coatings and natural organic matter (NOM) can reduce antibacterial activities of nanoparticles (3-12-14). For example, adsorbed polyelectrolyte or NOM on NZVI prevents toxicity by limiting the physical interaction between the cell and particle through electrosteric and electrostatic repulsions (3-15-16). Coatings that prevent contact between NPs and cells or that sequester or prevent release of toxic metals from the NPs can decrease or eliminate toxicity as has been observed for quantum dots (13). As a result, the use of polymeric coatings on engineered nanoparticles has been proposed as a means to reduce their potential for detrimental environmental impacts (17). However, limited understanding of the mechanisms by which the coatings decrease toxicity of the nanoparticles makes it difficult to select or to design coatings that will be useful for that purpose.

Silver nanoparticles are one of the most widely used nanomaterials because of their antimicrobial properties. AgNPs have been incorporated in many products, such as antibacterial washing machines, toothpaste, cookware, and socks (18). AgNPs are also used in medical applications to reduce infection, and inhibit bacterial colonization on catheters. The primary cytotoxic agent is believed to be the released Ag⁺ ions, which may damage protein and DNA (19-21). A proteomic analysis of the interactions between *E. coli* and Ag⁺ or AgNP shows similar protein expression profiles (19). Both Ag⁺ and AgNPs damaged the outer membrane, reduced the plasma membrane potential, and

caused ATP depletion. In addition, Ag^+ has been suggested to be the active toxic agent for AgNPs because AgNP toxicity was eliminated by adding NaCl and forming $\text{AgCl}_{(s)}$ to eliminate free Ag^+ (22).

Other cytotoxic mechanisms were also proposed. AgNPs may be embedded into the lipid bilayer (23-24), causing cell membrane leakage by changing bilayer fluidity. In addition, reactive oxygen species (ROS) generated by AgNPs may also account for its toxicity. Intracellular ROS concentrations were reported to increase in the presence of Ag^+ and AgNPs for nitrifying bacteria (6). The toxicity was correlated with the amounts of intracellular ROS.

The effect of coatings on AgNP cytotoxic properties is not well understood. We hypothesize that coatings that prevent the release of Ag^+ ions from the particles, or that can bind released Ag^+ ions may decrease the toxicity of those particles. Further, we hypothesize that if the AgNP releases enough Ag^+ ions to saturate the binding capacity of the coating it will no longer prevent toxicity. Here we describe the effect of adsorbed polymers and NOM on the toxicity of AgNP to *E. coli*. We systematically investigated the effect of coatings on AgNP interactions with and toxicity to *E. coli* to determine the reasons for the decreased toxicity of Ag NPs in the presence of polymers and NOM, and demonstrate the importance of the chemical compositions of NOM on its effect on AgNP toxicity to *E. coli*.

4.3 Materials and Methods

4.3.1 Chemicals and Silver Nanoparticles

Sodium bicarbonate, Miller LB broth, agar, and hydrogen peroxide (30%, certified ACS) were from Fisher Scientific (Howell, NJ). Polyaspartate (PAP, average MW=2500 g/mol) was from Lanxess (Pittsburgh, PA). All solutions and dilutions were prepared in distilled and deionized water (Barnstead Nanopure). A commercially available humic acid derived from brown coal (CD-HA) was from Sigma Aldrich (St. Louis, MO). Elliott Soil standard humic acid (ES-HA), with lower sulfur content, was purchased from International Humic Substances Society (IHSS). An anthropogenic surface water humic acid (Anth-SW-HA), with higher sulfur content, was kindly provided by Dr. Anett Georgi. Silver nitrate was from Sigma-Aldrich (St. Louis, MO).

4.3.2 Silver Nanoparticle Synthesis and Dispersion Preparation

20 g of PVP (MW 55,000) was dissolved in 50 mL of ethylene glycol. The solution was transferred to a round-bottom flask equipped with a condenser, 1.5 g of silver nitrate was added, and the mixture was stirred at room temperature. Once the silver nitrate was dissolved, the solution was heated in an oil bath to 120°C for 24 h. The PVP-stabilized silver nanoparticles were then removed from heat, diluted 1:10 with water, and centrifuged at 27,000 x g for 1 h. The precipitate was resuspended in water and centrifuged twice more before finally resuspending in water.

An AgNP stock aqueous dispersion (30g/L) was sonicated using an ultrasonic probe (Sonifier[®] 450) for 10 minutes at power level 3 (~10W). After cooling to room

temperature this dispersion was diluted to 3 g/L using a solution of CMC or NOM to obtain a dispersion with 3 g/L of PVP-coated AgNPs and 1 g/L of excess polymer or NOM. It is expected that CMC or NOM will adsorb onto the particles to some extent, possibly displacing PVP on AgNP to obtain CMC or NOM coated AgNPs. However, the presence of adsorbed materials or displacement of PVP was never confirmed experimentally. Concentrated polymer suspension was always added to dispersed particles, since adding particles to polymer will result in less stable coated AgNPs. This solution was mixed using an end-to-end rotator for 24 hours to achieve adsorption equilibrium. After adsorption, the AgNPs were washed by centrifuging at 11,000xg for 60 minutes and resuspended in DI water. This was repeated two more times to remove excess free polymer in solution. Finally, washed AgNP was resuspended in 5 mM sodium bicarbonate buffer solution by shaking. The AgNP concentration was verified using Atomic Absorption Spectroscopy after washing and acid digestion. The instrument was calibrated using AgNO₃ standards in 5% HNO₃ with concentrations of 10, 50, 100, 200, and 500 µg/L ($R^2=0.995$). Samples were digested in 5% HNO₃ before analysis. Coated nanoparticles at 15 mg/L were characterized by dynamic light scattering (DLS) to determine their size distribution in the exposure media (5 mM sodium bicarbonate buffer solution at pH 7). Before use the AgNP suspensions were ultrasonicated at power level 3 (~10W) for 5 minutes to break aggregates formed during storage.

4.3.3 *E. coli* Culture Preparation

Bacteria culture was prepared by inoculating 25 mL of LB Miller broth medium with *E. coli* (ATCC strain 33876) and incubated at 37 °C for 12 h. The culture was then

washed 3 times by centrifugation at 6000xg and resuspended in 5 mM sodium bicarbonate (pH=7±0.1). The *E. coli* stock was prepared by resuspending the bacteria pellets in 10 ml of 5 mM sodium bicarbonate (pH=7). The concentration of *E. coli* in the stock solution was between 1×10^9 to 2×10^9 colony forming units (CFU)/mL by the spread plate method using LB agar plates incubated at 37 °C for 12 hours.

4.3.4 Exposure Experiments

Before the exposure test, test tubes and buffer solution were sterilized by autoclave. The *E. coli* stock suspension was diluted 1000 fold aseptically in 5 mM bicarbonate solution (pH=7) in 20 mL culture tubes to reach a final bacterial concentration of 10^6 CFU/mL. A suspension containing either polymer-, or NOM-modified AgNP was added to the tubes to provide an AgNP concentration of 0.1, and 1 mg/L as determined by AAS before the addition. Ag ion present initially should have been low due to the washing process prior to use, but was not measured directly. NOMs with different levels of sulfur content (CD-HA, ES-HA, and Anth-SW-HA) were used. The culture tubes were placed horizontally on a roller mixer at 30 °C. Samples were taken at 0, 30, 60, 90, 120, and 180 minutes and serially diluted. The cells were plated in triplicate on LB agar plates, incubated for 24 h at 37 °C, and the colonies were counted.

4.4 Results and Discussions

4.4.1 Growth Inhibition by AgNP

Figure 4.1 shows the cytotoxic properties of PVP-coated AgNPs in the absence and presence of humic acid CD-HA. PVP-AgNP displayed high toxicity to *E. coli*, with a 6 log inhibition after 90 minutes. This suggests that particle-cell association is not required for AgNPs to exert toxicity. AgNP modified by CD-HA at 1 mg/L showed 6-log inhibition after 90 minutes, same as the PVP-AgNP. However, AgNP cytotoxicity was significantly reduced by addition of 100 mg/L dissolved CD-HA. A 1-log inhibition was observed for 1 mg/L AgNP with 100 mg/L dissolved CD-HA after 3 hours. NOM coatings do not have impact on AgNP toxicity, while dissolved NOM reduced its cytotoxicity. One explanation may be that NOM was not displacing PVP from the particle surface, and there was not enough NOM on the surface or in solution to scavenge Ag ions released from the particles during exposure. This result is different from the coating effects on NZVI and nano-TiO₂, whose toxicity was significantly reduced by adsorbed NOM (3). The difference may be the lack of adsorbed NOM on Ag NPs compared to NZVI and TiO₂ particles since bare nanoparticles were used for NOM adsorption in those cases. Another difference may be because of the way in which the coating affects the NP-bacteria interaction. For Ag NPs Ag⁺ is likely the toxic agent, since ROS photocatalytically generated by AgNPs is ruled out by performing the experiment in dark. The release of Ag ion and subsequent toxicity does not require direct contact with the bacteria so coatings that worked to decrease toxicity of NZVI (which required direct contact) were not effective on Ag NPs. Because ROS did not cause the observed toxicity, NOM cannot prevent toxicity as it did for TiO₂. It is likely that the

mass of NOM in the system (adsorbed or in solution) had insufficient binding capacity to complex with the Ag ion released, This is confirmed by experiments with a much higher NOM concentration in solution (100 mg/L) that was capable of scavenging Ag ions and decreasing toxicity to *E. coli*.

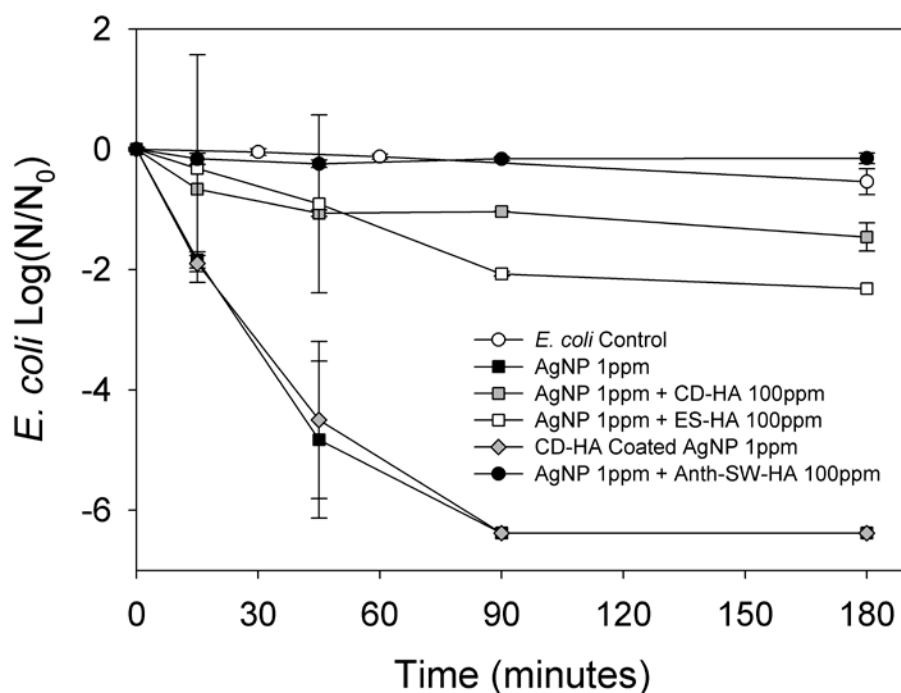


Figure 4.1. Exposure of *E. coli* to 1 mg/L AgNP, 1 mg/L AgNP with 100 mg/L dissolved CD-HA, 100 mg/L dissolved ES-HA, and 100 mg/L dissolved Anth-SW-HA, 1 mg/L CD-HA coated AgNP, and *E. coli* control experiment.

4.4.2 Silver Ions

Because Ag^+ ion is likely the toxic species, we evaluated the ability of different coatings having different affinity for Ag^+ ion to prevent this toxicity. Figure 4.2 shows the toxicity of Ag^+ and the effect of NOM in solution on its toxicity. As expected, Ag^+

displayed high toxicity to *E. coli*. Ag^+ at 0.2 mg/L caused 5.5-log inhibition after 90 minutes, which is similar to that observed using 1 mg/L PVP-coated AgNPs. This Ag^+ concentration was used because 20% dissolution for AgNP was observed at equilibrium within these solution conditions (25). An Ag^+ concentration dependency was observed for Ag^+ toxicity: 0.02 mg/L Ag^+ resulted in 1.5-log inhibition after 3 hours. Dissolved CD-HA reduced Ag^+ cytotoxicity from 5.5 to 3.5-log inhibition after 3 hours. Interestingly, NOM was found to be more effective at reducing the toxicity of AgNPs than Ag^+ . This may be because the initial Ag^+ concentration for AgNPs is lower than 0.2 mg/L, the equilibrium concentration.

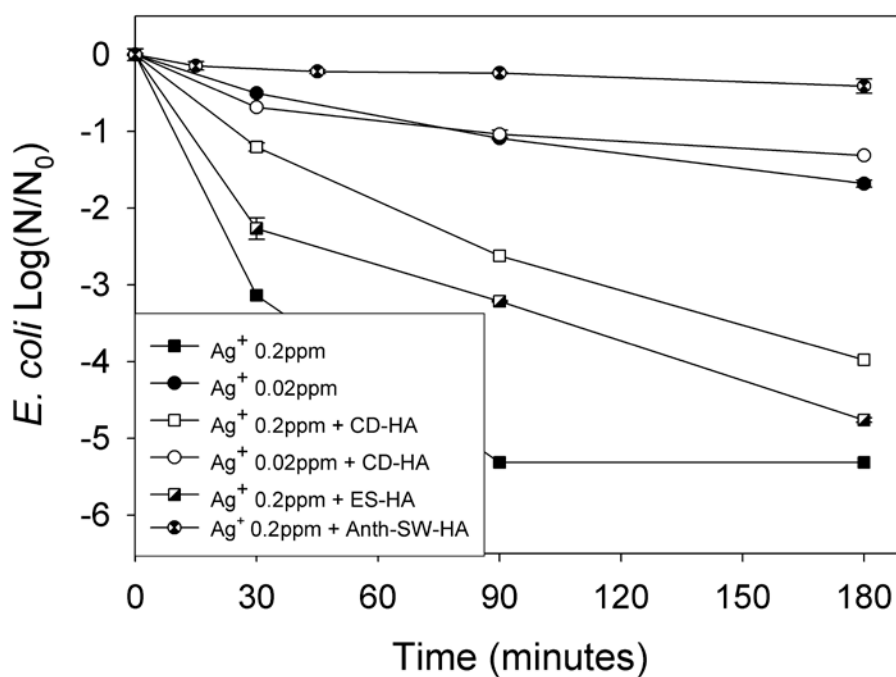


Figure 4.2. Exposure of *E. coli* to 0.2 mg/L Ag^+ , 0.2 mg/L Ag^+ with 100 mg/L dissolved CD-HA, 0.2 mg/L Ag^+ with 100 mg/L dissolved ES-HA, and 0.2 mg/L Ag^+ with 100 mg/L Anth-SW-HA.

In addition, effects of dissolved CMC and PVP on Ag^+ cytotoxicity were evaluated. Figure 4.3 shows the toxicity of Ag^+ and Ag^+ in the presence of 100 mg/L CMC or PVP. Both CMC and PVP do not decrease the toxicity of Ag^+ , causing 6.2-log inhibition after 3 hours, compared to 5.5-log inhibition by Ag^+ . This higher toxicity of Ag^+ with dissolved CMC and PVP may be an artifact that the initial *E. coli* concentrations for the CMC and PVP experiments were higher than the Ag^+ exposure experiment.

To explain the dissolved NOM effects on AgNP and Ag^+ toxicity, we measured the dissolved Ag^+ concentration in the presence of CD-HA and CMC, AgNPs with CD-HA, and AgNPs over 3 hours. It is shown in Figure 4.4 that Ag^+ concentration remained unchanged at 0.2 mg/L over 3 hours for CMC treated Ag^+ . However, the Ag^+ concentration was significantly reduced by CD-HA for both AgNPs and Ag^+ . In addition, Ag^+ increased from 0.02 mg/L to 0.04 mg/L over three hours for AgNPs. This result supports our hypothesis that initial Ag^+ concentration for AgNP is lower than 0.2 mg/L, which caused different effects of NOM for AgNPs compared to Ag^+ . The Ag^+ concentration correlates with the toxicity data very well, suggesting that Ag^+ is indeed the toxic agent.

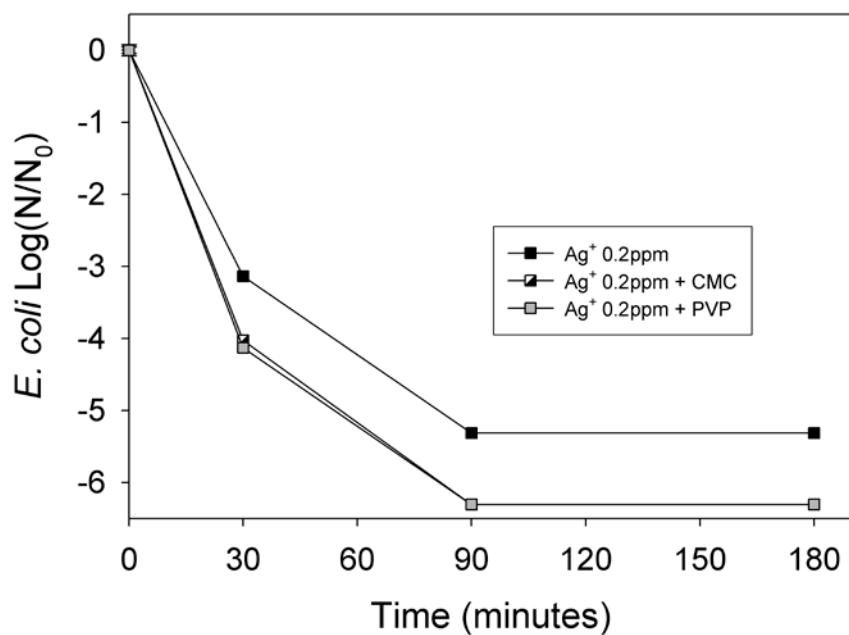


Figure 4.3. Exposure of *E. coli* to 0.2 mg/L Ag^+ , 0.2 mg/L Ag^+ with 100 mg/L dissolved CMC, and 0.2 mg/L Ag^+ with 100 mg/L PVP.

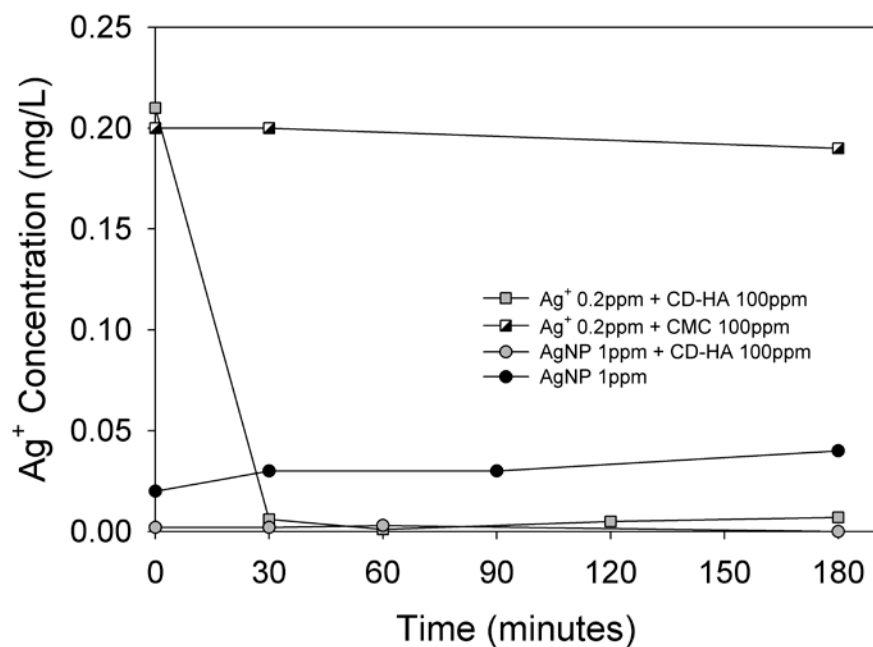


Figure 4.4. Ag^+ concentration change over three hours for 0.2 mg/L Ag^+ with 100 mg/L CD-HA, 0.2 mg/L Ag^+ with 100 mg/L CMC, 1 mg/L AgNP with 100 mg/L CD-HA, and 1 mg/L AgNP .

4.4.3 Dissolved Humic Acid Effects

It is still unclear how NOM sequesters Ag^+ and reduces AgNP toxicity. However, we may rule out the possibility of negatively charged carboxyl group, since Ag^+ was not scavenged by CMC, which contains multiple carboxylic acid groups and is negatively charged at neutral pH (pK_a of 4.3). To better understand how NOM was decreasing toxicity of Ag NPs and Ag ions we investigated the effect of two other humic substances on the toxicity of Ag NPs to *E. coli*, ES-HA and Anth-SW-HA, which have a lower and higher sulfur content respectively (Table 4.1). Figure 4.1 and Figure 4.2 shows that ES-HA decreases the toxicity of AgNP and Ag^+ less than for CD-HA, and Anth-SW-HA decreases the toxicity of AgNP and Ag^+ toxicity more than for CD-HA. We observed 2.1-log and 4.7-log inhibition for ES-HA treated AgNP and Ag^+ after 3 hours, compared to 1.5-log and 3.9-log inhibition for CD-HA treated AgNP and Ag^+ . However, we observed only 0.1-log and 0.2-log inhibition for Anth-SW-HA treated AgNP and Ag^+ after 3 hours. The difference in the ability to decrease the toxicity of Ag ion and Ag NPs to *E. coli* correlates with the reduced sulfur content of the HA. Table 4.1 summarizes the elemental composition for ES-HA, CD-HA, and Anth-SW-HA. CD-HA contains approximately 6 times more sulfur than ES-HA, 4 times less sulfur than Anth-SW-HA. Previous studies have shown that strong binding of mercury by dissolved organic matter (DOM) is attributed to coordination of mercury at reduced sulfur sites within the organic matter (26). It could be a similar case for the Ag^+ binding to DOM since both are class B metals and react very strongly with reduced sulfur. Figure 4.5 summarizes the proposed mechanism by which NOM affects AgNP toxicity to *E. coli*. In addition, inorganic sulfide also plays an important role in AgNP toxicity (27). Inorganic sulfide may also

scavenge Ag^+ to form Ag_2S , which has very low solubility and therefore decreases the amount of dissolved Ag in solution compared to unsulfidized particles. As a result, both inorganic and organic sulfide may significantly reduce AgNP cytotoxicity. However, further investigation is needed to understand how the sulfur oxidation state in the NOM (e.g. ratio of reduced to oxidized sulfur) may affect AgNP toxicity.

Table 4.1. Humic substances elemental compositions

Sample Origin	Name	%Ash	%C	%H	%O	%N	%S
Elliott Soil Humic	ES-HA	0.88	58.13	3.68	34.08	4.14	0.44
Coal derived	CD-HA	9.2	55.1	4.78	27.2	1.34	2.42
Anthropogenic surface water HA	Anth-SW-HA	5.6	52.3	4.01	26.3	2.46	9.3

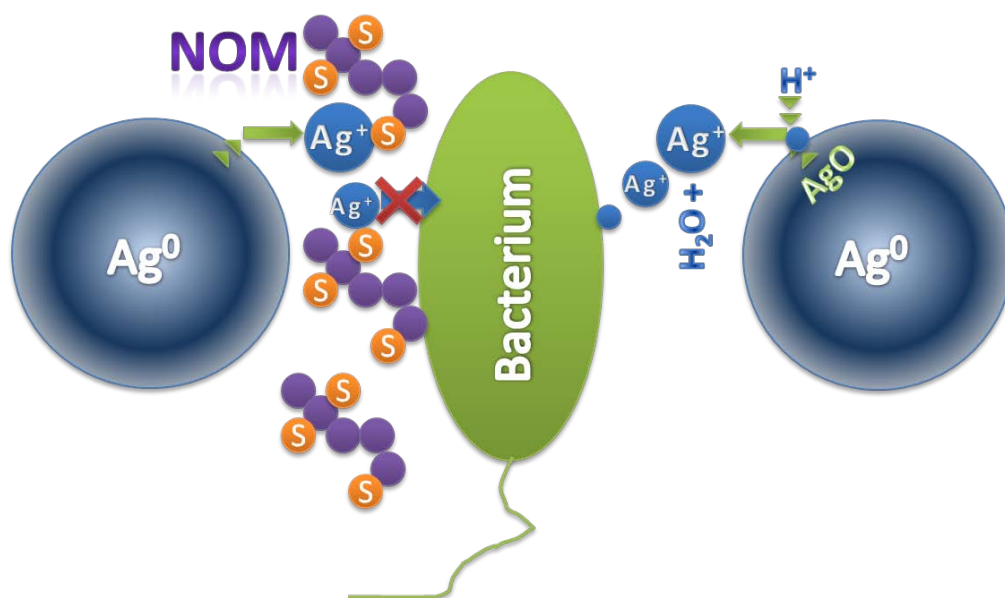


Figure 4.5. AgNP inhibits bacterial growth by releasing Ag^+ . Natural organic matter may react with Ag^+ and reduces cytotoxic effects of AgNP.

4.5 References

- (1) Auffan, M.; Achouak, W.; Rose, J.; Roncato, M. A.; Chaneac, C.; Waite, D. T.; Masion, A.; Woicik, J. C.; Wiesner, M. R.; Bottero, J. Y., Relation between the redox state of iron-based nanoparticles and their cytotoxicity toward *Escherichia coli*. *Environmental Science & Technology* **2008**, *42* (17), 6730-6735.
- (2) Lee, C.; Kim, J. Y.; Il Lee, W.; Nelson, K. L.; Yoon, J.; Sedlak, D. L., Bactericidal effect of zero-valent iron nanoparticles on *Escherichia coli*. *Environmental Science & Technology* **2008**, *42* (13), 4927-4933.
- (3) Li, Z.; Greden, K.; Alvarez, P. J. J.; Gregory, K. B.; Lowry, G. V., Adsorbed polymer and NOM limits adhesion and toxicity of nano scale zerovalent iron to *E. coli*. *Environ Sci Technol* **2010**, *44* (9), 3462-7.
- (4) Adams, L. K.; Lyon, D. Y.; Alvarez, P. J. J., Comparative eco-toxicity of nanoscale TiO₂, SiO₂, and ZnO water suspensions. *Water Research* **2006**, *40* (19), 3527-3532.
- (5) Maness, P. C.; Smolinski, S.; Blake, D. M.; Huang, Z.; Wolfrum, E. J.; Jacoby, W. A., Bactericidal activity of photocatalytic TiO₂ reaction: Toward an understanding of its killing mechanism. *Applied and Environmental Microbiology* **1999**, *65* (9), 4094-4098.
- (6) Choi, O.; Hu, Z. Q., Size dependent and reactive oxygen species related nanosilver toxicity to nitrifying bacteria. *Environmental Science & Technology* **2008**, *42* (12), 4583-4588.
- (7) Fabrega, J.; Fawcett, S. R.; Renshaw, J. C.; Lead, J. R., Silver Nanoparticle Impact on Bacterial Growth: Effect of pH, Concentration, and Organic Matter. *Environmental Science & Technology* **2009**, *43* (19), 7285-7290.
- (8) Morones, J. R.; Elechiguerra, J. L.; Camacho, A.; Holt, K.; Kouri, J. B.; Ramirez, J. T.; Yacaman, M. J., The bactericidal effect of silver nanoparticles. *Nanotechnology* **2005**, *16* (10), 2346-2353.
- (9) Fang, J. S.; Lyon, D. Y.; Wiesner, M. R.; Dong, J. P.; Alvarez, P. J. J., Effect of a fullerene water suspension on bacterial phospholipids and membrane phase behavior. *Environmental Science & Technology* **2007**, *41* (7), 2636-2642.
- (10) Lyon, D. Y.; Brunet, L.; Hinkal, G. W.; Wiesner, M. R.; Alvarez, P. J. J., Antibacterial activity of fullerene water suspensions (nC(60)) is not due to ROS-mediated damage. *Nano Lett.* **2008**, *8* (5), 1539-1543.
- (11) Simon-Deckers, A.; Loo, S.; Mayne-L'Hermite, M.; Herlin-Boime, N.; Menguy, N.; Reynaud, C.; Gouget, B.; Carriere, M., Size-, Composition- and Shape-Dependent Toxicological Impact of Metal Oxide Nanoparticles and Carbon Nanotubes toward Bacteria. *Environmental Science & Technology* **2009**, *43* (21), 8423-8429.
- (12) Li, D.; Lyon, D. Y.; Li, Q.; Alvarez, P. J. J., Effect of soil sorption and aquatic natural organic matter on the antibacterial activity of a fullerene water suspension. *Environ. Toxicol. Chem.* **2008**, *27* (9), 1888-1894.
- (13) Mahendra, S.; Zhu, H. G.; Colvin, V. L.; Alvarez, P. J., Quantum Dot Weathering Results in Microbial Toxicity. *Environmental Science & Technology* **2008**, *42* (24), 9424-9430.

- (14) Tong, Z. H.; Bischoff, M.; Nies, L.; Applegate, B.; Turco, R. F., Impact of fullerene (C-60) on a soil microbial community. *Environmental Science & Technology* **2007**, *41* (8), 2985-2991.
- (15) Chen, J.; Xiu, Z.; Lowry, G. V.; Alvarez, P. J. J., Effect of natural organic matter on toxicity and reactivity of nano-scale zerovalent iron. *Water Research* **2010**, in press.
- (16) Xiu, Z. M.; Gregory, K. B.; Lowry, G. V.; Alvarez, P. J. J., Effect of Bare and Coated Nanoscale Zerovalent Iron on tceA and vcrA Gene Expression in Dehalococcoides spp. *Environmental Science & Technology* **2010**, *44* (19), 7647-7651.
- (17) Wiesner, M. R.; Lowry, G. V.; Jones, K. L.; Hochella, M. F.; Di Giulio, R. T.; Casman, E.; Bernhardt, E. S., Decreasing Uncertainties in Assessing Environmental Exposure, Risk, and Ecological Implications of Nanomaterials. *Environmental Science & Technology* **2009**, *43* (17), 6458-6462.
- (18) Aruguete, D. M.; Hochella, M. F., Bacteria-nanoparticle interactions and their environmental implications. *Environ. Chem.* **2009**, *7* (1), 3-9.
- (19) Lok, C. N.; Ho, C. M.; Chen, R.; He, Q. Y.; Yu, W. Y.; Sun, H. Z.; Tam, P. K. H.; Chiu, J. F.; Che, C. M., Proteomic analysis of the mode of antibacterial action of silver nanoparticles. *J. Proteome Res.* **2006**, *5* (4), 916-924.
- (20) Sondi, I.; Salopek-Sondi, B., Silver nanoparticles as antimicrobial agent: a case study on E-coli as a model for Gram-negative bacteria. *J. Colloid Interface Sci.* **2004**, *275* (1), 177-182.
- (21) Wigginton, N. S.; De Titta, A.; Piccapietra, F.; Dobias, J.; Nesatty, V. J.; Suter, M. J. F.; Bernier-Latmani, R., Binding of Silver Nanoparticles to Bacterial Proteins Depends on Surface Modifications and Inhibits Enzymatic Activity. *Environmental Science & Technology* **2010**, *44* (6), 2163-2168.
- (22) Smetana, A. B.; Klabunde, K. J.; Marchin, G. R.; Sorensen, C. M., Biocidal activity of nanocrystalline silver powders and particles. *Langmuir* **2008**, *24* (14), 7457-7464.
- (23) Bothun, G. D., Hydrophobic silver nanoparticles trapped in lipid bilayers: Size distribution, bilayer phase behavior, and optical properties. *J Nanobiotechnology* **2008**, *6*, 13.
- (24) Park, S. H.; Oh, S. G.; Mun, J. Y.; Han, S. S., Effects of silver nanoparticles on the fluidity of bilayer in phospholipid liposome. *Colloid Surf. B-Biointerfaces* **2005**, *44* (2-3), 117-122.
- (25) Ma, R.; Levard, C.; Marinakos, S.; Cheng, Y.; Liu, J.; Michel, F.M.; Brown, G.E.; Lowry, G.V., Size controlled dissolution of organic coated silver nanoparticles. *Environ Sci Technol* **2011**, in revision.
- (26) Ravichandran, M., Interactions between mercury and dissolved organic matter - a review. *Chemosphere* **2004**, *55* (3), 319-331.
- (27) Choi, O.; Cleuenger, T. E.; Deng, B. L.; Surampalli, R. Y.; Ross, L.; Hu, Z. Q., Role of sulfide and ligand strength in controlling nanosilver toxicity. *Water Research* **2009**, *43* (7), 1879-1886.

**Chapter 5: NATURAL ORGANIC MATTER COATINGS ELIMINATE
CYTOTOXICITY OF NANOSCALE ZERO-VALENT IRON AND TITANIUM
DIOXIDE NANOPARTICLES TO *SHEWANELLA ONEIDENSIS***

5.1 Abstract

NZVI and nano-TiO₂ are manufacturing materials that may be released in the environment. These nanomaterials are known to be harmful to both *Prokaryotes* and *Eukaryotes*. Prokaryote studies have largely focused on cytotoxicity towards well-studied laboratory strains of *Escherichia coli* (*E. coli*), an enteric bacterium. Little is known about the cytotoxicity of nanoparticles towards environmentally relevant species. Here we quantify the effect that organic, polymer coatings have on the cytotoxicity of NZVI and nano-TiO₂ towards *Shewanellaceae*, a family of dissimilatory iron reducing bacteria broadly distributed in terrestrial environments and examine the mechanisms by which adsorbed coatings affect their interaction. Exposure of *S. oneidensis* to 100 mg/L of bare NZVI with 28% Fe⁰ content resulted in a 3-log inactivation after 60 minutes. Adsorbed maleic acid co-olefin or NOM greatly decreased cytotoxicity, resulting in less than 0.1-log inactivation after 120 minutes. Exposure of cells to 100 mg/L bare nano-TiO₂ and UV irradiation resulted in 3-log inhibition after 3 hours. Adsorbed NOM decreased nano-TiO₂ toxicity, resulting in less than 0.6-log inhibition over the same period. Adsorbed polyaspartate (PAP) coating had no impact on the toxicity of nano-TiO₂. These findings show that the cytotoxic effects of nanoparticles are lessened by the presence of organic polymer coatings and that the type of coating is important for TiO₂. The overall results

were similar to previous studies with *E. coli*, suggesting that cytotoxicity studies with this well-studied laboratory bacterium may be sufficient for predicting the effects on other gram-negative species.

5.2 Introduction

Nanoparticles may have adverse effects towards microbes. Nanoscale zero valent iron (NZVI) (1-3), nano-TiO₂ (4-5), silver nanoparticles (AgNP) (6-8), fullerenes (9-10), and carbon nanotubes (CNT) (11) are cytotoxic to bacteria. A recent study suggested that nano-Ag, nano-TiO₂, and nano-ZnO may pose risks to aquatic organisms (12). However, adsorbed polymeric coatings and natural organic matter (NOM) may reduce antibacterial activities of nanoparticles (3,13-15). For example, adsorbed polyelectrolyte or NOM on NZVI prevents its toxicity towards *E. coli* by limiting the physical interaction between the cell and particle through electrosteric and electrostatic repulsions (3,16-17). NOM on nano-TiO₂ may reduce its toxicity to *E. coli* by scavenging reactive oxygen species (ROS) (Chapter 3). Coatings that prevent contact between NPs and cells or that sequester or prevent release of toxic species from the NPs can decrease or eliminate toxicity of nanoparticles (14). As a result, the use of polymeric coatings on engineered nanoparticles has been proposed as a means to reduce their potential for detrimental environmental impacts (18).

The nanoscale zero-valent iron (NZVI) particles used in aquifer remediation will come in contact with subsurface bacteria. Recent studies indicate that NZVI is bactericidal in pure cultures at concentrations as low as a few mg/L (1-2), while NZVI is typically injected into the ground to achieve porewater concentrations in the grams per

liter range (19). The bactericidal properties of NZVI are therefore important to understand as it may affect the remediation efficiency of NZVI if native bacterial populations are adversely affected. Barnes et al. shows that NZVI may inhibit biological TCE and sulfate reduction (20).

Nano-TiO₂ is one of the most widely used nanomaterials (21). Based on the current production volume and assumed paths of particle release, a recent risk assessment study suggested that nano-TiO₂ may pose a risk to aquatic organisms (21). In addition, the concentration of nano-TiO₂ in sediments (U.S.) is predicted to triple between 2008 and 2012 from 0.2 to 0.6 mg/kg (12). Both of NZVI and nano-TiO₂ may pose a risk to the soil microbial communities, but little is known about the cytotoxic effects of nano-TiO₂ on terrestrial bacteria.

Shewanella oneidensis (*S. oneidensis*) is a Gram-negative, facultative anaerobe that is best known for dissimilatory iron reducing metabolism and is common a variety of terrestrial and marine habitats (22). *S. oneidensis* has been widely studied for its tolerance of metal concentrations and ability to mediate bioreduction of metals such as uranium and chromium during bioremediation. However, the interactions between *Shewanella* and nanoparticles are not well defined. Recent studies revealed that *S. oneidensis* can mediate the formation of As-S nanotubes (23) and Ag-nanoparticles (24). The cytotoxicity and the effect of organic coatings are unclear. Here we describe the effect of polymeric and NOM coatings on the toxicity of NZVI and nano-TiO₂ to *S. oneidensis*. We demonstrate the importance of coating type and examine the mechanisms by which coatings affect toxicity of nanoparticles.

5.3 Materials and Methods

5.3.1 Chemicals and Nanoparticles

Sodium bicarbonate, Miller LB broth, agar, and hydrogen peroxide (30%, certified ACS) were from Fisher Scientific (Howell, NJ). Polyaspartate (PAP, average MW=2500 g/mol) was from Lanxess (Pittsburgh, PA). All solutions and dilutions were prepared in distilled and deionized water (Barnstead Nanopure). Humic acid (average MW=1400 to 9200 g/mol) was from Sigma-Aldrich (St. Louis, MO). Ultrahigh-purity N₂ was from Butler Gas products (Pittsburgh, PA). The NZVI, Reactive Nanoscale Iron Particles (RNIP 10-DS) and maleic acid co-olefin (average MW =16,000 g/mol) modified RNIP (MRNIP2), was supplied by Toda Kogyo Corp. (Onoda, Japan). RNIP are redox reactive Fe⁰/Fe₃O₄ core-shell NZVI particles. RNIP physical and chemical properties have been described previously (5). The Fe⁰ content of the RNIP was determined by acid digestion and measurement of the H₂ formed, as previously described (4). The RNIP had been stored anaerobically in an aqueous slurry (pH=12) for several months before and during the experimental program and had a Fe⁰ content ranging from 20 to 28 wt % over the course of the study period. TiO₂ nanoparticles (P25) were provided by Degussa. The properties of these particles including crystallite size (~30nm), aggregate size distribution (800-2000nm), and chemical composition (70 wt% anatase and 30 wt% rutile) have been reported previously (25).

5.3.2 NZVI Preparation

The procedure used to physisorb the polymers to the NZVI has been previously described (26). Briefly, a stock NZVI dispersion is diluted to a concentration of 120 g/L and ultrasonicated for 20 minutes. This dispersion is further diluted in a deoxygenated polymer solution to provide a final solution (30 mL) containing NZVI and polymer at a concentration of 3g/L and 1 g/L, respectively, in a 70 mL bottle, which was rotated end-over-end for 24 hrs to reach adsorption equilibrium. This same method was also used to coat the particles with humic acid. After adsorption, the polymer coated NZVI suspensions were fractionated by allowing the most unstable particles to settle for 10 minutes. The stable suspension was decanted and used for exposure experiments after measuring the Fe^0 content by acid digestion.

5.3.3 TiO_2 Nanoparticle Dispersion Preparation

A TiO_2 stock aqueous dispersion (30g/L) was prepared by dispersing a weighed mass of TiO_2 P-25 powder in water using an ultrasonic probe (Sonifier[®] 450) for 30 minutes at power level 3. After cooling down to room temperature this dispersion was diluted to 3 g/L using a solution of PAP or NOM to obtain a dispersion with 3 g/L TiO_2 and 1 g/L of coating. This solution was mixed using an end-to-end rotator for 24 hours to achieve adsorption equilibrium. After adsorption, the TiO_2 nanoparticles were washed by centrifuging at 6000 rpm for 30 minutes and resuspended in DI water. This was repeated two more times to remove excess free polymer in solution. Finally, washed TiO_2 nanoparticle was resuspended in 5 mM sodium bicarbonate buffer solution. The TiO_2 concentration was verified using UV-vis spectroscopy ($\lambda=800\text{nm}$) after washing. The

instrument was calibrated using nano-TiO₂ standards with concentrations of 10, 50, 100, 200, and 500 mg/L ($R^2=0.995$). Coated and bare nanoparticles were characterized by dynamic light scattering (DLS) to determine their size distribution in the exposure media. Before use the TiO₂ suspensions were ultrasonicated at power level 3 for 5 minutes to break aggregates formed during storage.

5.3.4 *S. oneidensis* Culture Preparation

Shewanella oneidensis MR-1 (ATCC 700550) was cultured in liquid LB (Luria-Bertani) medium with 20 mM lactate as electron donor under aerobic conditions at 30°C for 12 hr. The bacteria were harvested by centrifugation at 5,000 g for 30 min. After decanting the supernatant, 5 mM sodium bicarbonate (pH=7.0) was added to resuspend the bacteria and then centrifuged again at 5,000 g. This process was repeated 3 times to achieve completed harvesting of bacteria. To get a *S. oneidensis* stock for experiments, its pellets were resuspended with 15 mL of 5 mM sodium bicarbonate. Through the spread plate (LB and Agar) method at 30°C for 24 h, 6.0×10^8 to 9.4×10^8 colony forming units (CFU) was determined as the stock concentration of *S. oneidensis*.

5.3.5 UV Irradiation and Intensity Measurements

For UV irradiated experiments, a 20 watt long-wave UV bench lamp (BlackRay[®]) was used. This UV source provided irradiation in the UVA region, with a peak wavelength of 365 nm. This wavelength had negligible growth inhibition effect on *S. oneidensis* as determined in a UV only control experiment. UV light intensity on the

culture tubes was 6 W/m², measured using a UV AB digital light meter (General[®] UV513AB). All irradiated experiments were performed in a chamber with UV-absorbing insulation, eliminating effects from reflected UV irradiation.

5.3.6 Exposure Experiments

Before the exposure test, test tubes and buffer solution were autoclaved to sterilize them. The *S. oneidensis* stock suspension was diluted aseptically in 5 mM bicarbonate solution (pH=7) in 20 mL culture tubes to reach a final bacterial concentration of 10⁶ CFU/mL. A suspension containing either bare, polymer-, or NOM-modified NZVI or TiO₂ was added to the tubes. The culture tubes were placed horizontally on a roller mixer at 30 °C. Samples were taken over 2 or 3 hours period and serially diluted. The cells were plated in triplicate on LB agar plates, incubated for 24 h at 30 °C, and the colonies were counted.

5.3.7 Hydroxyl Radical Measurement

Hydroxyl radical ($\cdot\text{OH}$) was quantified using *p*CBA as a probe compound (27). The steady state concentration of $\cdot\text{OH}$ was determined from the *p*CBA degradation rate using equations 1 through 3 as previously described (27). The second order rate constant for the reaction between $\cdot\text{OH}$ and *p*CBA ($k_{\text{OH},p\text{CBA}} = 5 \times 10^9 \text{ M}^{-1} \text{ s}^{-1}$) has been reported (28). A plot of the $\ln([p\text{CBA}]/[p\text{CBA}]_0)$ yields k_{exp} , the pseudo first order rate constant (eqn 2). The steady state $\cdot\text{OH}$ concentration was determined from k_{exp} using eqn 3.

$$-\frac{d[p\text{CBA}]}{dt} = k_{\text{OH},p\text{CBA}}[\cdot\text{OH}]_s[p\text{CBA}] = k_{\text{exp}}[p\text{CBA}] \quad (1)$$

$$-\ln \frac{[pCBA]}{[pCBA]_0} = k_{exp} t \quad (2)$$

$$[\cdot OH]_s = \frac{k_{exp}}{k_{OH,pCBA}} \quad (3)$$

*p*CBA was added in reactors whose $\cdot OH$ concentrations needed to be determined at an initial concentration of 3 mg/L. Samples were taken at 0, 30, 60, and 180 minutes, followed by immediate addition of 10 μ L (less than 1% of the sample volume) of 1 M mannitol to quench the reaction between *p*CBA and $\cdot OH$. Nano-TiO₂ was removed from samples by centrifuging at 13,000 g for 2 minutes. The *p*CBA concentration was determined using high-performance liquid chromatography (Agilent Technologies) equipped with a C18 reverse-phase column. The mobile phase contains 35% acetonitrile and 65% water. Signals were analyzed with a UV detector at wavelength of 230 nm. The instrument was calibrated using *p*CBA standards with concentration of 0.3, 0.75, 1.5, 2.25, and 3 mg/L ($R^2 = 0.99$).

5.3.8 NOM and Hydroxyl Radicals Reaction Constant

The rate constant for the reaction between NOM and $\cdot OH$ were determined using methods described elsewhere (29-30). In brief, six different ozone doses (10, 20, 30, 40, 50 and 60 μ M) were added to pH 7.5 buffered solutions containing 10 mg/L NOM and 3 μ M *p*CBA. *p*CBA concentration was measured 24 hours after complete ozone decomposition. The rate constant between NOM and $\cdot OH$ was determined using $k_{OH,NOM} = \Omega \eta k_{OH,pCBA}$, where Ω , the oxidation-competition value, is defined as the concentration of O₃ consumed, after depletion of the $\cdot OH$ probe begins, that resulted in a one-natural-log (37%) reduction in the original *p*CBA concentration. Ω was estimated by

log-linear regressions. The term $k_{\text{OH},\text{NOM}}$ is the first-order rate constant for $\cdot\text{OH}$ with NOM, and η (0.4-1.0) is the stoichiometric yield of $\cdot\text{OH}$ from ozone after its decomposition. A value of 0.67 was chosen for η . As described by Westerhoff et al (30), this value is representative of the base-catalyzed $\cdot\text{OH}$ yield. Dissolved ozone was measured spectrophotometrically at 254 nm (31).

5.4 Results and Discussion

5.4.1 Growth Inhibition by NZVI

Exposure of *S. oneidensis* to 100 ppm of uncoated NZVI having 28% Fe^0 under anaerobic conditions resulted in a 3-log reduction in viable cells after 60 min., and leveled off at 3.2-log inactivation at 2 hours (Figure 5.1a). This trend is similar with previous reports of NZVI toxicity to *E. coli*; 3.4- and 4.5-log reductions in viable *E. coli* cells were observed after 10 minutes and 1 hour exposure to 100 ppm NZVI, respectively. However, the NZVI appears to exert less inactivation towards *S. oneidensis* than to *E. coli* (3.2-log inactivation after 120 min. in this study vs. 5.2-log inactivation after 60 min. (3)).

Exposure of the same NZVI particles coated with maleic acid co-olefin or NOM resulted in less than a 0.1-log reduction in viable *S. oneidensis* cells, while a 3-log reduction was observed for bare NZVI. All of these coatings reduced the cytotoxicity of NZVI to *S. oneidensis* as they did in previous studies with *E. coli* (3). It is likely that contact between cells and NZVI is needed before inactivation of the cell can take place (3). Related studies show that the weathering of quantum dot coatings may increase

toxicity (14), adsorbed natural organic matter reduces the toxicity of fullerenes by reducing direct contact with cells (13), and carbon nanotubes may be engineered with surface modifications that enhance cell-nanotube contact and result in higher toxicity (25).

5.4.2 Growth Inhibition by Nano-TiO₂

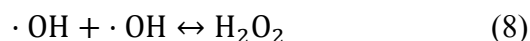
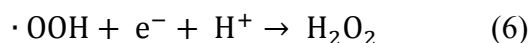
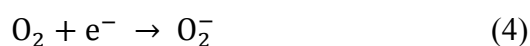


Figure 5.2.a shows the cytotoxic properties of bare, nano-TiO₂ at concentrations of 25-500 ppm irradiated with UV against *S. oneidensis*. The toxicity of UV light alone was negligible. The observed growth inhibition for bare and coated nano-TiO₂ with UV irradiation can be attributed to the TiO₂ nanoparticles. Bare nano-TiO₂ at 100 mg/L resulted in 2.8-log inhibition after 2 hours and 3-log inhibition after 3 hours (Figure 5.2.a), similar to *E. coli* (27). PAP coated nano-TiO₂ at 100 mg/L showed a delayed growth inhibition of *S. oneidensis* as the bare nanoparticles, resulting in 1.2-log inhibition at 2 hours and 3.2-log inhibition over 3 hours (Figure 5.2.b). However, in sharp contrast to the PAP coating, adsorbed NOM decreased growth inhibition of nano-TiO₂; after 3 hours, less than 0.5-log inhibition was observed (Figure 5.2.b). Unlike PAP coatings on NZVI which greatly reduced its toxicity, PAP does not similarly impact the toxicity of nano-TiO₂. It is likely that the physical contact necessary for the toxicity of NZVI is less

important for nano-TiO₂, as is implied if the principal mechanism of toxicity is cell wall oxidation by ROS. ROS such as H₂O₂ may persist in solution and interact with cells independently of the particles. Equations 1-5 summarize the photocatalytic reactions involved in ROS generation for nano-TiO₂. The contrary effects on growth inhibition between the PAP and NOM coated particles suggest that they do not merely prevent cell-particle contact as was the case for NZVI, but may also interfere with the primary mechanisms of toxicity and therefore impact the production of ROS or their reaction with cells (Chapter 3).

5.4.3 Coating Effects

The polyelectrolyte and NOM coatings on NZVI can decrease adhesion by several different methods: electrostatic, steric, and electrosteric repulsion (3). Low molecular weight (MW) adsorbed polyelectrolytes that do not extend or form brushes provide electrostatic repulsions. Large uncharged polymers can afford steric repulsions by inhibiting close contact between the particles and the cells. Large MW polyelectrolytes afford both an electrostatic and steric repulsion, known as electrosteric repulsion, that is stronger than either electrostatic repulsion or steric repulsion (26), and its repulsive force is less sensitive to changes in ionic strength or pH than electrostatic repulsions that would occur using bare (uncoated) particles. NOM adsorbed to the particles decreased NZVI toxicity similarly as the polyelectrolytes tested here. NOM is probably acting as a polyelectrolyte to provide electrosteric repulsions between the particles and the cells. Polyelectrolytes such as poly(maleic acid) have been used as

NOM analogs because they have the same types of functional groups and behave similarly to NOM in natural waters (32).

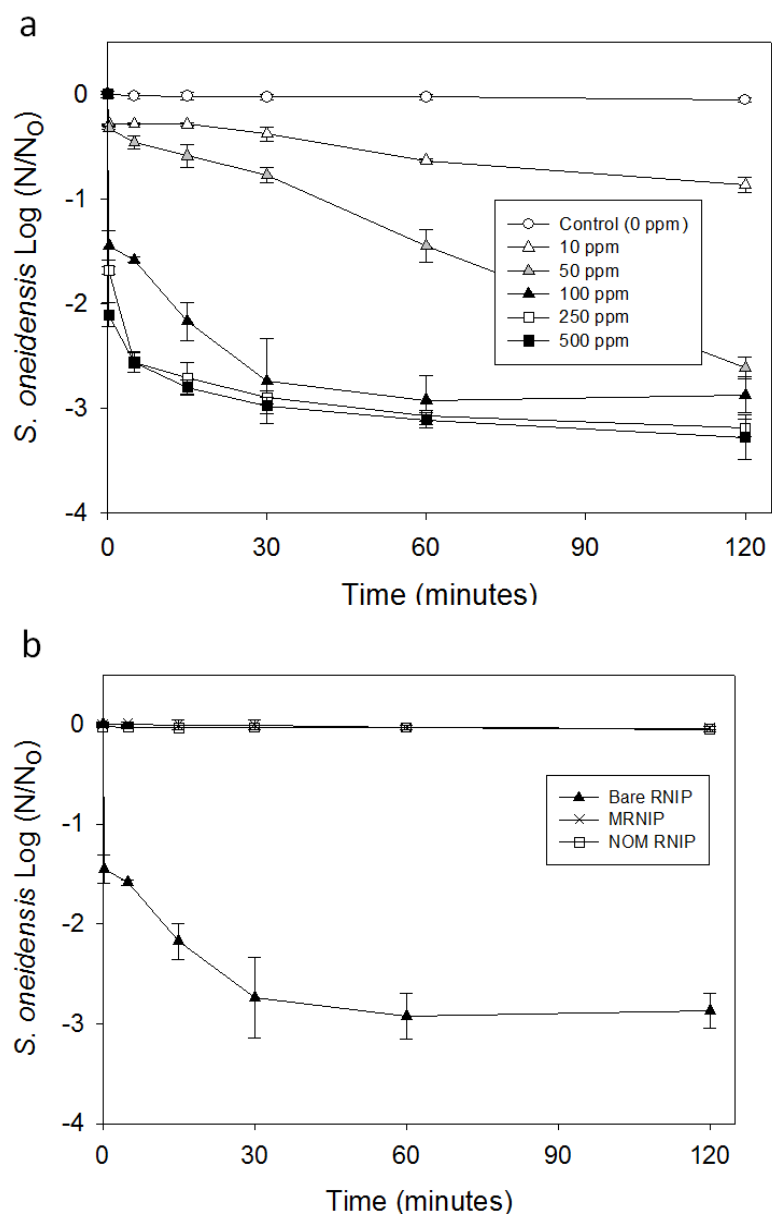


Figure 5.1. (a) Exposure of *S. oneidensis* to 10, 50, 100, 250, and 500 mg/L bare RNIP under anaerobic condition; (b) Exposure of *S. oneidensis* to 100 mg/L bare, maleic acid co-olefin coated, and NOM coated nano-TiO₂ under anaerobic condition.

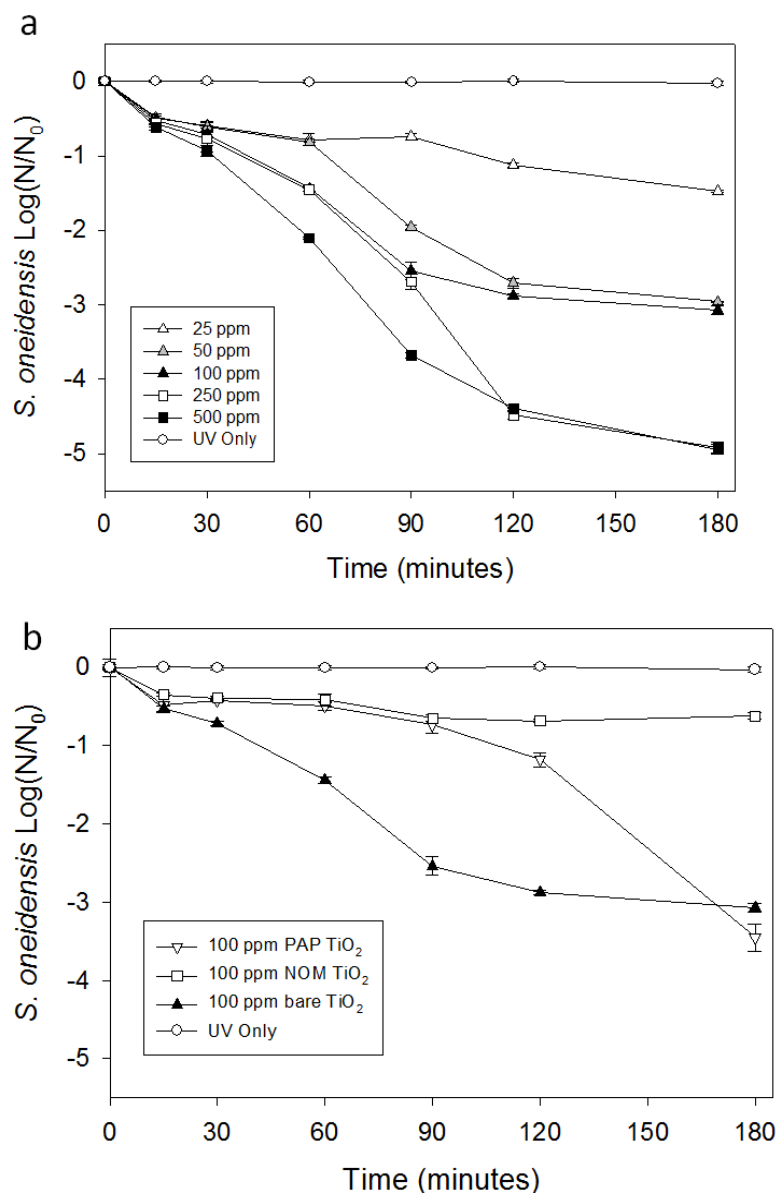


Figure 5.2. (a) Exposure of *S. oneidensis* to 25, 50, 100, 250, and 500 mg/L bare nano-TiO₂ under UV irradiation; (b) Exposure of *S. oneidensis* to 100 mg/L bare, PAP coated, and NOM coated nano-TiO₂ under UV irradiation. Less than 1-log inhibition was observed in the absence of illumination with 1000 mg/L bare nano-TiO₂ over 3 hours.

The NOM coating significantly reduced nano-TiO₂ toxicity to *S. oneidensis* whereas PAP coatings did not. An analogous, negative effect on photocatalytic disinfection of *E. coli* with TiO₂ occurs in presence of natural organic substances (20).

Similarly decreased photocatalytic degradation of aqueous pollutants was observed with the presence of NOM (21) and was attributed to radiation attenuation, competition for reactive sites, and deactivation of the catalytic surface. The $\cdot\text{OH}$ radical formed directly from TiO_2 or from H_2O_2 decomposition (eqn 8) may be the cytotoxic agent for nano- TiO_2 .

Scavenging of $\cdot\text{OH}$ by the organic coating molecules was investigated using the oxidation-competition method (29-30). The reaction rate constants between NOM and $\cdot\text{OH}$ are listed in Table 5.1. The rate constant normalized by the concentration of organic carbon, $K_{\text{OH},\text{DOC}}$, is $3.3 \times 10^8 \text{ l (mol C)}^{-1} \text{ s}^{-1}$, consistent to a previously reported value of $3.6 \times 10^8 \text{ l (mol C)}^{-1} \text{ s}^{-1}$ (30). This suggests that NOM is able to scavenge $\cdot\text{OH}$, consistent with other studies (30). Westerhoff et al (30) found that the rate constant between NOM and $\cdot\text{OH}$ is positively correlated with aromatic carbon content, and inversely correlated with aliphatic carbon content. This may be used to explain our toxicity observations. PAP, containing no aromatic content, may not be able to scavenge $\cdot\text{OH}$ as efficiently as NOM, which contains higher aromatic content. Hydroxyl radical is an important toxic agent produced by TiO_2 -NP. NOM reduces its toxicity, at least in part, by scavenging $\cdot\text{OH}$. Figure 5.3 summarizes the proposed mechanisms by which the coatings on TiO_2 affect their toxicity to *S. oneidensis*. Our findings suggest that the toxic properties of nano- TiO_2 may be mitigated by NOM after being released to the environment. This is consistent with previous report for nano- TiO_2 toxicity (Chapter 3). In addition, NOM plays an important role in reducing toxicity of fullerene in a number of studies (15,33). Finally, different coatings affected TiO_2 toxicity differently than for NZVI (3). These data suggest that only ROS scavenging coatings (e.g. NOM) may reduce the toxicity

nanoparticles like TiO₂ that produce ROS. These results underscore the importance of understanding the toxic pathways to predict the effect of coatings on nanoparticle toxicity to bacteria.

5.5 Conclusions

Bare NZVI is cytotoxic to *S. oneidensis*, resulted in a 3-log inactivation after 60 minutes. Adsorbed maleic acid co-olefin or NOM on NZVI with the same Fe⁰ content significantly decreased its toxicity, causing less than 0.1-log inactivation after 120 minutes. Exposure of cells to 100 mg/L bare nano-TiO₂ and UV irradiation resulted in 3-log inhibition after 3 hours. Adsorbed NOM decreased nano-TiO₂ toxicity, resulting in less than 0.6-log inhibition over the same period. Surprisingly, adsorbed polyaspartate (PAP) coatings had no impact on the toxicity of nano-TiO₂. These findings demonstrate that the potential for detrimental impacts of nanoparticles to *S. oneidensis* may be lessened by coatings.

Table 5.1. Reaction rate constants between NOM and hydroxyl radical

Calculated $\Omega(\mu\text{M of O}_3)$	$K_{\text{OH,NOM}} (\text{s}^{-1})$	$K_{\text{OH,DOC}}$ ($10^8 \text{ l (mol C)}^{-1} \text{ s}^{-1}$)	Reference
41	1.37×10^5	^a 3.3	This work
25	-	3.6	Westerhoff et al, 1999

^aOrganic carbon concentration was calculated using carbon content of 51% for NOM.

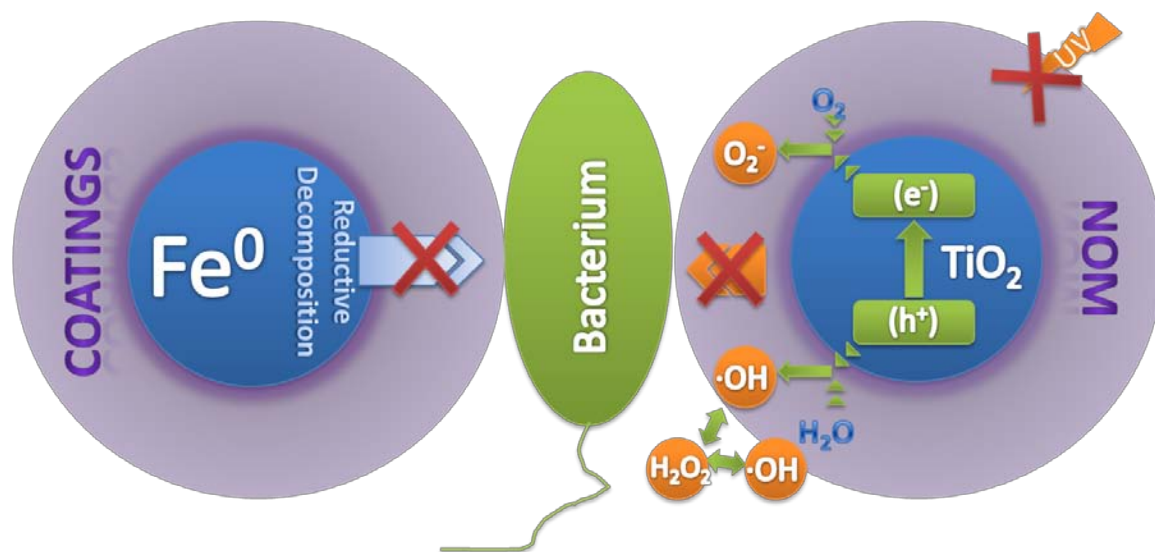


Figure 5.3. (left) The surface coatings on NZVI may prevent physical interaction with *S. oneidensis*, and reduce its cytotoxicity. (right) Nano-TiO₂ inhibits bacterial growth by generating ·OH (hydroxyl radical). Natural organic matter may react with ·OH or decrease light intensity reached at the particles and reduces cytotoxic effects of nano-TiO₂.

5.6 References

- (1) Auffan, M.; Achouak, W.; Rose, J.; Roncato, M. A.; Chaneac, C.; Waite, D. T.; Masion, A.; Woicik, J. C.; Wiesner, M. R.; Bottero, J. Y., Relation between the redox state of iron-based nanoparticles and their cytotoxicity toward *Escherichia coli*. *Environ. Sci. Technol.* **2008**, *42* (17), 6730-6735.
- (2) Lee, C.; Kim, J. Y.; Il Lee, W.; Nelson, K. L.; Yoon, J.; Sedlak, D. L., Bactericidal effect of zero-valent iron nanoparticles on *Escherichia coli*. *Environ. Sci. Technol.* **2008**, *42* (13), 4927-4933.
- (3) Li, Z.; Greden, K.; Alvarez, P. J. J.; Gregory, K. B.; Lowry, G. V., Adsorbed polymer and NOM limits adhesion and toxicity of nano scale zerovalent iron to *E. coli*. **2010**, *44* (9), 3462-7.
- (4) Adams, L. K.; Lyon, D. Y.; Alvarez, P. J. J., Comparative eco-toxicity of nanoscale TiO₂, SiO₂, and ZnO water suspensions. *Water Res.* **2006**, *40* (19), 3527-3532.
- (5) Maness, P. C.; Smolinski, S.; Blake, D. M.; Huang, Z.; Wolfrum, E. J.; Jacoby, W. A., Bactericidal activity of photocatalytic TiO₂ reaction: Toward an understanding of its killing mechanism. *Appl. Environ. Microbiol.* **1999**, *65* (9), 4094-4098.

- (6) Choi, O.; Hu, Z. Q., Size dependent and reactive oxygen species related nanosilver toxicity to nitrifying bacteria. *Environ. Sci. Technol.* **2008**, *42* (12), 4583-4588.
- (7) Fabrega, J.; Fawcett, S. R.; Renshaw, J. C.; Lead, J. R., Silver Nanoparticle Impact on Bacterial Growth: Effect of pH, Concentration, and Organic Matter. *Environ. Sci. Technol.* **2009**, *43* (19), 7285-7290.
- (8) Morones, J. R.; Elechiguerra, J. L.; Camacho, A.; Holt, K.; Kouri, J. B.; Ramirez, J. T.; Yacaman, M. J., The bactericidal effect of silver nanoparticles. *Nanotechnology* **2005**, *16* (10), 2346-2353.
- (9) Fang, J. S.; Lyon, D. Y.; Wiesner, M. R.; Dong, J. P.; Alvarez, P. J. J., Effect of a fullerene water suspension on bacterial phospholipids and membrane phase behavior. *Environ. Sci. Technol.* **2007**, *41* (7), 2636-2642.
- (10) Lyon, D. Y.; Brunet, L.; Hinkal, G. W.; Wiesner, M. R.; Alvarez, P. J. J., Antibacterial activity of fullerene water suspensions (nC(60)) is not due to ROS-mediated damage. *Nano Lett.* **2008**, *8* (5), 1539-1543.
- (11) Simon-Deckers, A.; Loo, S.; Mayne-L'Hermite, M.; Herlin-Boime, N.; Menguy, N.; Reynaud, C.; Gouget, B.; Carriere, M., Size-, Composition- and Shape-Dependent Toxicological Impact of Metal Oxide Nanoparticles and Carbon Nanotubes toward Bacteria. *Environ. Sci. Technol.* **2009**, *43* (21), 8423-8429.
- (12) Gottschalk, F.; Sonderer, T.; Scholz, R. W.; Nowack, B., Modeled Environmental Concentrations of Engineered Nanomaterials (TiO₂, ZnO, Ag, CNT, Fullerenes) for Different Regions. *Environ. Sci. Technol.* **2009**, *43* (24), 9216-9222.
- (13) Li, D.; Lyon, D. Y.; Li, Q.; Alvarez, P. J. J., Effect of soil sorption and aquatic natural organic matter on the antibacterial activity of a fullerene water suspension. *Environ. Toxicol. Chem.* **2008**, *27* (9), 1888-1894.
- (14) Mahendra, S.; Zhu, H. G.; Colvin, V. L.; Alvarez, P. J., Quantum Dot Weathering Results in Microbial Toxicity. *Environ. Sci. Technol.* **2008**, *42* (24), 9424-9430.
- (15) Tong, Z. H.; Bischoff, M.; Nies, L.; Applegate, B.; Turco, R. F., Impact of fullerene (C-60) on a soil microbial community. *Environ. Sci. Technol.* **2007**, *41* (8), 2985-2991.
- (16) Chen, J.; Xiu, Z.; Lowry, G. V.; Alvarez, P. J. J., Effect of natural organic matter on toxicity and reactivity of nano-scale zerovalent iron. *Water Research* **2010**, in press.
- (17) Xiu, Z. M.; Gregory, K. B.; Lowry, G. V.; Alvarez, P. J. J., Effect of Bare and Coated Nanoscale Zerovalent Iron on tceA and vcrA Gene Expression in Dehalococcoides spp. *Environ. Sci. Technol.* **2010**, *44* (19), 7647-7651.
- (18) Wiesner, M. R.; Lowry, G. V.; Jones, K. L.; Hochella, M. F.; Di Giulio, R. T.; Casman, E.; Bernhardt, E. S., Decreasing Uncertainties in Assessing Environmental Exposure, Risk, and Ecological Implications of Nanomaterials. *Environ. Sci. Technol.* **2009**, *43* (17), 6458-6462.
- (19) Henn, K. W.; Waddill, D. W., Utilization of Nanoscale Zero-Valent Iron for Source Remediation—A Case Study. **2006**, *16* (2), 57-77.
- (20) Barnes, R. J.; Riba, O.; Gardner, M. N.; Singer, A. C.; Jackman, S. A.; Thompson, I. P., Inhibition of biological TCE and sulphate reduction in the presence of iron nanoparticles. *Chemosphere* **2010**, *80* (5), 554-562.

- (21) Mueller, N. C.; Nowack, B., Exposure modeling of engineered nanoparticles in the environment. *Environ. Sci. Technol.* **2008**, *42* (12), 4447-4453.
- (22) Schaechter, M.; Ingraham, J. L.; Neidhardt, F. C., *Microbe*. 1 ed.; ASM Press: Washington, DC 20036, 2005; p 370.
- (23) Jiang, S.; Lee, J. H.; Kim, M. G.; Myung, N. V.; Fredrickson, J. K.; Sadowsky, M. J.; Hur, H. G., Biogenic Formation of As-S Nanotubes by Diverse *Shewanella* Strains. *Appl. Environ. Microbiol.* **2009**, *75* (21), 6896-6899.
- (24) Wang, H.; Law, N.; Pearson, G.; van Dongen, B. E.; Jarvis, R. M.; Goodacre, R.; Lloyd, J. R., Impact of Silver(I) on the Metabolism of *Shewanella oneidensis*. *J. Bacteriol.* **2010**, *192* (4), 1143-1150.
- (25) Kang, S.; Mauter, M. S.; Elimelech, M., Physicochemical determinants of multiwalled carbon nanotube bacterial cytotoxicity. *Environ. Sci. Technol.* **2008**, *42* (19), 7528-7534.
- (26) Phenrat, T.; Saleh, N.; Sirk, K.; Kim, H. J.; Tilton, R. D.; Lowry, G. V., Stabilization of aqueous nanoscale zerovalent iron dispersions by anionic polyelectrolytes: adsorbed anionic polyelectrolyte layer properties and their effect on aggregation and sedimentation. *J. Nanopart. Res.* **2008**, *10* (5), 795-814.
- (27) Cho, M.; Chung, H.; Choi, W.; Yoon, J., Linear correlation between inactivation of E-coli and OH radical concentration in TiO₂ photocatalytic disinfection. *Water Res.* **2004**, *38* (4), 1069-1077.
- (28) Elovitz, M. S.; von Gunten, U.; Kaiser, H. P., Hydroxyl radical/ozone ratios during ozonation processes. II. The effect of temperature, pH, alkalinity, and DOM properties. *Ozone-Sci. Eng.* **2000**, *22* (2), 123-150.
- (29) Haag, W. R.; Yao, C. C. D. In *Ozonation of U.S. drinking water sources: HO concentrations and oxidation-competition values*, Ozone in Water and Wastewater, San Francisco, CA, San Francisco, CA, 1993; pp S-17-119-125.
- (30) Westerhoff, P.; Aiken, G.; Amy, G.; Debroux, J., Relationships between the structure of natural organic matter and its reactivity towards molecular ozone and hydroxyl radicals. *Water Res.* **1999**, *33* (10), 2265-2276.
- (31) Langlais, B.; Reckhow, D. A.; Brink, D. R., *Ozone in Water Treatment: Applications and Engineering*. Lewis Publishers: 1991.
- (32) Wang, L. L.; Chin, Y. P.; Traina, S. J., Adsorption of (poly)maleic acid and an aquatic fulvic acid by goethite. *Geochim. Cosmochim. Acta* **1997**, *61* (24), 5313-5324.
- (33) Xie, B.; Xu, Z. H.; Guo, W. H.; Li, Q. L., Impact of natural organic matter on the physicochemical properties of aqueous C-60 nanoparticles. *Environ. Sci. Technol.* **2008**, *42* (8), 2853-2859.

Chapter 6: SUMMARY, CONCLUSIONS, RECOMMENDATIONS FOR FUTURE RESEARCH AND IMPLICATIONS

6.1 Summary

Nanomaterials may be accidentally or intentionally released into natural systems where they can interact with their chemical and biological environment and potentially result in detrimental effects. Since bacteria play a central role in environmental processes such as element cycling and human activities such as waste treatment, understanding the interactions between nanoparticles and bacteria will be important for developing models that incorporate the fate and transport of nanoparticles as well as assessing their potential risk to human and environmental health. Previous studies have described interactions between nanoparticles and bacterial cells for NZVI (1-2), nano-TiO₂ (3-4), AgNP (5-6), fullerene (7-8), and carbon nanotubes (9). These studies show that interactions with bare NP may lead to cyto- and eco-toxic effects in bacterial cells and communities. Another emergent theme from these studies is that the surface chemistry of the NP determines the physiochemical interaction(s) between the NP and the cells (10-12).

Although bare NP have been the focus of many prior studies of the interactions between NP and bacteria, nanomaterials used in commercial products are rarely bare (uncoated) and typically coated with polymer to enhance their stability and mobility or create a desired functionality. Additionally, bare nanoparticles may also become coated with natural organic matter after release into the environment (13). These coatings modify the physicochemical properties of nanoparticles (14-15) and by extension affect

the cell-particle interactions as well. The overarching hypothesis addressed in this research is that natural and engineered organic coatings are determinates of the nanoparticle-microorganism interaction.

This body of work examines the effect of coatings on the physicochemical and biological interactions between nanoparticles and bacteria. We assess the effects that organic macromolecular coatings such as synthetic polymers and natural organic matter have on interactions between nanoparticles and bacteria for three nanoparticles that exhibit distinctly different means of exerting cytotoxicity towards bacteria. The findings from these studies will aid with the assessment of risk associated with fate, transport, and toxicity of nanomaterials as well as guide the manufacturing of nanoparticles and their coatings for optimal utility and decreased potential for deleterious environmental impacts.

6.2 Conclusions

6.2.1 NZVI

E. coli cells were exposed to coated, uncoated, and oxidized nano-scale zero valent iron (NZVI). Cell numbers were monitored and transmission electron microscopy performed to better understand the impacts of coatings on cytotoxicity and cell-particle interactions. Previous studies postulated that reductive decomposition of protein functional groups in the cell membrane cause toxicity due to strong reducing conditions at the NZVI surface (2). This proposed mechanism requires physical association between the NP and cells.

E. coli was exposed to bare, polymer-, or NOM-modified NZVI. Exposures under anaerobic conditions and aerobic conditions were conducted. The minimal inhibitory concentrations, dispersed iron concentrations in *E. coli* exposure tubes were measured and the aggregation and sedimentation of particles examined. The physical interaction between *E. coli* cells and NZVI was visualized using TEM. The key findings of this study were:

- Bare NZVI under anaerobic conditions was cytotoxic at 100 mg/L.
- Aerobic conditions greatly reduced the cytotoxicity of bare NZVI.
- Adsorbed poly(styrene sulfonate) (PSS), poly(aspartate) (PAP), or NOM on NZVI decreased its toxicity.
- Bare NZVI adhered to cells while adsorbed polyelectrolyte or NOM on NZVI prevented adhesion.

Similar tests were conducted for *S. oneidensis*, a dissimilatory iron reducing bacteria that may be found in natural aqueous and terrestrial environments. *S. oneidensis* was exposed to bare, polymer- or NOM-modified NZVI under anaerobic conditions. Similar findings were observed:

- Bare NZVI under anaerobic conditions was cytotoxic; a dose response for NZVI toxicity was observed.
- Adsorbed NOM or polymeric modifier decreased its toxicity.

Overall the study suggests that polyelectrolyte coatings and NOM will decrease the physical interaction between NZVI and bacterial and mitigate cytotoxicity. Although a correlation existed between initial Fe^0 content and cytotoxicity, oxidation of the Fe^0 under aerobic conditions nearly eliminated its cytotoxic effects.

6.2.2 Titanium Dioxide Nanoparticles

TiO₂ nanoparticles were studied to understand the effects of organic coatings on a nanomaterial that produces toxic reactive oxygen species. Nano-TiO₂ may express toxicity through photocatalytic and non-photocatalytic mechanisms. Reactive oxygen species (ROS) generated from photocatalyzed reactions of TiO₂ in water is the primary route for cytotoxicity towards bacteria.

E. coli was exposed to bare, polymer-, or NOM-modified nano-TiO₂, with a nano-TiO₂ concentration of 100 mg/L. Exposure with and without UV irradiation was conducted. Cytotoxicity of nano-TiO₂ contributed by ROS was investigated by conducting exposure tests with the addition of ROS scavengers. Hydroxyl radical concentrations were measured to understand its importance for nano-TiO₂ toxicity.

- Bare nano-TiO₂ with UV irradiation was toxic to *E. coli* and hydroxyl radical or/and hydrogen peroxide were the toxic agents
- Adsorbed NOM decreased nano-TiO₂ toxicity
- Adsorbed polyaspartate (PAP) had no impact on the toxicity of nano-TiO₂.
- The NOM coating interfered with the reactivity of produced hydroxyl radicals more than the PAP coating.

Similar tests were conducted for *S. oneidensis*. *S. oneidensis* was exposed to bare, polymer- or NOM-modified nano-TiO₂. Similar findings were observed:

- Bare nano-TiO₂ with UV irradiation was toxic to *S. oneidensis*; a dose response for nano-TiO₂ was observed.
- Adsorbed NOM decreased nano-TiO₂ toxicity; however, adsorbed PAP had no impact on nano-TiO₂ toxicity.

In contrast to the NZVI studies, this work with TiO₂ shows that the type of coating and not merely its existence on the NP is an important determinate of the interaction between bacteria and the particle. It is likely that the aromatic functional groups on NOM (lacking on the PAP coating) are responsible for scavenging ROS (16). The findings suggest that the detrimental impacts of nanoparticles that produce ROS may be lessened in the presence NOM. It is also perhaps significant to note that despite the organic polymer coating (e.g. PAP), ROS produced by TiO₂ were able to be produced and escape from the surface and coating to be reactive against bacteria in solution.

6.2.3 Silver Nanoparticle

Silver nanoparticles were studied to understand how coatings affect the interactions between cells and AgNP which are known to release toxic ions into solution. Although ROS may be produced by AgNP, the primary cytotoxic agent is believed to be the released Ag⁺ ions, which may damage protein and DNA (17-19).

E. coli was exposed to polymer- or NOM-modified AgNP as well as polymer and silver ion controls. NOM with different sulfur contents were examined to explore the importance of sulfur as a silver ion scavenger. The major findings from this study are:

- Bare, PVP- and NOM-modified AgNP at 1 ppm and Ag⁺ at 0.2 ppm were all toxic to *E. coli*.
- Adsorbed polymeric and NOM coatings did not affect AgNP cytotoxicity.
- Dissolved NOM significantly reduced AgNP toxicity and delayed Ag⁺ cytotoxic activities
- CMC and PVP did not affect Ag⁺ cytotoxicity.

Dissolved NOM was able to reduce Ag^+ concentrations for both AgNP and AgNO_3 as a dissolved Ag^+ source while CMC and PVP did not. This suggests that NOM may reduce AgNP toxicity by scavenging Ag^+ . A correlation between sulfur content of NOM effects on AgNP toxicity was observed. NOM with lower sulfur content (0.44%) reduced AgNP cytotoxicity less than the NOM containing high sulfur content (2.42%). The findings suggest that in natural systems where NOM exists, toxicity of AgNP may not be as significant as previous studies have suggested. Results also suggest that the Ag^+ scavenging effects may be attributed to the sulfur content. Where NOM is high in sulfur, the impact of AgNP release into natural systems may be quite small.

6.2.4 Inorganic coatings: Sulfidation Effects on AgNP Cytotoxic Properties

In addition to organic coating effects, inorganic coating affected nanoparticle cytotoxicity as well. It has been shown that inorganic sulfide play an important role in AgNP toxicity (20). Inorganic sulfide may scavenge Ag^+ to form Ag_2S , which has extremely low bioavailability. *E. coli* was exposed to bare, PVP coated or sulfidized AgNP, with an AgNP concentration of 50 ppm. *E. coli* cell concentrations were measured at 0, 15, 45, 90, and 180 minutes.

Sulfide exposure decreases growth inhibition effects from bare and PVP coated particles compared to PVP AgNPs that have not been sulfidized. Cell mortality is most significantly caused by aqueous Ag^+ . There is a correlation between degree of Ag-sulfidation and toxicity. Aggregated engineered AgNPs form a passivated Ag_2S layer, thus limiting the remaining Ag^0 from dissolving.

6.3 Recommendations for Future Research

6.3.1 Model Microorganisms

E. coli is a well-studied, model organism well suited to laboratory investigations and its interactions with NP may not reflect those observed in more complex bacterial communities or with other organisms in natural system. Future studies should examine the interactions of bare and coated NZVI with microbial communities and common soil bacteria such as members of the *Geobacteraceae* family. This family of bacteria has resistance to metals and may use electrons from reduced metals for respiration.

In addition, both *E. coli* and *S. oneidensis* are Gram-negative bacteria. However, Gram-positive bacteria may interact with nanoparticles differently than Gram-negative bacteria; hence coating effects may be different. The outer membrane of Gram-negative bacteria contains lipopolysaccharides (LPS). LPS are large molecules consisting of a lipid and a polysaccharide, joined by covalent bonds. LPS contributes greatly to the structural integrity and protects the membrane from certain chemical attack. In contrast, Gram-positive bacteria do not have outer membrane. Instead, they have a thicker multilayered peptidoglycan layer. As a result, Gram-negative and Gram-positive bacteria are likely to experience different interactions with similar NP or coatings on NP. Future studies should examine the interactions of nano-TiO₂ or AgNP with Gram-positive bacteria.

6.3.2 Metal Ion Releasing Nanoparticles

ZnO and CuO are well known to exert toxicity through the release of toxic metal ions. Further studies should investigate the ability of coatings to affect the interactions

and toxicity of zinc and copper oxide NP. Results show that the scavenging of silver ions by NOM may be sulfur dependent. This finding should be verified with additional, well-characterized NOM and engineered polymers with sulfur groups. ZnO and CuO nanoparticles may form sulfidized coatings. The stability and impact on microbial interactions with sulfidized ZnO and CuO should be examined.

6.4 Implications

Nanoparticle-microorganism interactions may be examined as models for more complex organisms and systems of organisms to guide NP design, implementation, managing risks and regulating the industry. This study shows that natural, engineered, and organic matter coatings may impact particle-cell interactions. The regulation of the interaction by the coating is dependent on the coating type as well as the mode of interaction of the bare particle with cells. Although the toxicity of the NP examined is expressed through different mechanisms, NOM is able to mitigate cytotoxicity for all nanoparticles in this study by interfering with the different modes of toxicity. These findings serve as a guide for ongoing nanotoxicity research, nanomaterial development and implementation, and regulation of the industry.

One of the important messages from this body of work is that the potential for detrimental effects of nanoparticles in natural systems may be lower than previously thought. Laboratory results with bare particles show distinct patterns of toxicity to both eukaryotes and prokaryotes. Our results show that the presence of natural organic matter, virtually ubiquitous in terrestrial systems, greatly reduces the toxicity of the particles, regardless of the mode of toxicity. Similar observations have been reported for NOM. A

previous study suggested that carbonaceous nanomaterials (e.g. carbon nanotube) have little impact on the microbial communities in soil where NOM is present, despite their well-known toxicity in lab (21). Our findings link inactivation to the presence of organic matter and shed first light on the mechanisms behind the inactivation of NP toxicity. What is clear is that the mechanisms of inactivation are closely linked to the mechanism of toxicity expression for the individual particles. Future research in nanotoxicity should closely examine the *in situ* or *in vivo* conditions expected for the expected exposure route.

Findings in this thesis are also useful for environmental policy makers and regulation of the nanotechnology industry. We demonstrate that NZVI, nano-TiO₂, and AgNP are cytotoxic to *E. coli* and that the toxicity is concentration dependent. Nanomaterials have also been shown to be toxic to other microorganisms as well (3-5), including; algae (22-24), invertebrates (24), and mammalian cells (25). Clearly, nanomaterials may pose a risk to individual organisms as well as populations and sensitive ecosystems. As a result, regulation for nanotechnology may be necessary for managing the potential risks. However, management of risk is challenging with limited nanotoxicology data, difficulty detecting and measuring nanoparticles in natural systems, and limited knowledge about the fate and transport of the materials. That said, as described above, particle toxicity is greatly reduced by the presence of coatings, and in particular natural organic matter. Regulators should carefully consider the impacts of environmental transformations such as NOM adsorption, on the fate, transport and toxicity of the particles.

Finally, our findings may be used to guide the nanotechnology industry towards design and use of materials with reduced potential for adverse environmental impacts.

The finding that the inactivation of toxicity is closely tied to the chemistry of both the coating and particle demonstrates that there is no panacea for the design of innocuous materials; the industry will need to design coatings with the surface chemistry of the particle in mind.

6.5 References

- (1) Auffan, M.; Achouak, W.; Rose, J.; Roncato, M. A.; Chaneac, C.; Waite, D. T.; Masion, A.; Woicik, J. C.; Wiesner, M. R.; Bottero, J. Y., Relation between the redox state of iron-based nanoparticles and their cytotoxicity toward *Escherichia coli*. *Environmental Science & Technology* **2008**, *42* (17), 6730-6735.
- (2) Lee, C.; Kim, J. Y.; Il Lee, W.; Nelson, K. L.; Yoon, J.; Sedlak, D. L., Bactericidal effect of zero-valent iron nanoparticles on *Escherichia coli*. *Environmental Science & Technology* **2008**, *42* (13), 4927-4933.
- (3) Adams, L. K.; Lyon, D. Y.; Alvarez, P. J. J., Comparative eco-toxicity of nanoscale TiO₂, SiO₂, and ZnO water suspensions. *Water Research* **2006**, *40* (19), 3527-3532.
- (4) Maness, P. C.; Smolinski, S.; Blake, D. M.; Huang, Z.; Wolfrum, E. J.; Jacoby, W. A., Bactericidal activity of photocatalytic TiO₂ reaction: Toward an understanding of its killing mechanism. *Applied and Environmental Microbiology* **1999**, *65* (9), 4094-4098.
- (5) Fabrega, J.; Fawcett, S. R.; Renshaw, J. C.; Lead, J. R., Silver Nanoparticle Impact on Bacterial Growth: Effect of pH, Concentration, and Organic Matter. *Environmental Science & Technology* **2009**, *43* (19), 7285-7290.
- (6) Morones, J. R.; Elechiguerra, J. L.; Camacho, A.; Holt, K.; Kouri, J. B.; Ramirez, J. T.; Yacaman, M. J., The bactericidal effect of silver nanoparticles. *Nanotechnology* **2005**, *16* (10), 2346-2353.
- (7) Fang, J. S.; Lyon, D. Y.; Wiesner, M. R.; Dong, J. P.; Alvarez, P. J. J., Effect of a fullerene water suspension on bacterial phospholipids and membrane phase behavior. *Environmental Science & Technology* **2007**, *41* (7), 2636-2642.
- (8) Lyon, D. Y.; Adams, L. K.; Falkner, J. C.; Alvarez, P. J. J., Antibacterial activity of fullerene water suspensions: Effects of preparation method and particle size. *Environmental Science & Technology* **2006**, *40* (14), 4360-4366.
- (9) Simon-Deckers, A.; Loo, S.; Mayne-L'Hermite, M.; Herlin-Boime, N.; Menguy, N.; Reynaud, C.; Gouget, B.; Carriere, M., Size-, Composition- and Shape-Dependent Toxicological Impact of Metal Oxide Nanoparticles and Carbon Nanotubes toward Bacteria. *Environmental Science & Technology* **2009**, *43* (21), 8423-8429.
- (10) Ginzburg, V. V.; Balijepailli, S., Modeling the thermodynamics of the interaction of nanoparticles with cell membranes. *Nano Lett.* **2007**, *7* (12), 3716-3722.

- (11) Kang, S.; Mauter, M. S.; Elimelech, M., Physicochemical determinants of multiwalled carbon nanotube bacterial cytotoxicity. *Environmental Science & Technology* **2008**, *42* (19), 7528-7534.
- (12) Nel, A. E.; Madler, L.; Velegol, D.; Xia, T.; Hoek, E. M. V.; Somasundaran, P.; Klaessig, F.; Castranova, V.; Thompson, M., Understanding biophysicochemical interactions at the nano-bio interface. *Nature Materials* **2009**, *8* (7), 543-557.
- (13) Johnson, R. L.; Johnson, G. O.; Nurmi, J. T.; Tratnyek, P. G., Natural Organic Matter Enhanced Mobility of Nano Zerovalent Iron. *Environmental Science & Technology* **2009**, *43* (14), 5455-5460.
- (14) Phenrat, T.; Saleh, N.; Sirk, K.; Kim, H. J.; Tilton, R. D.; Lowry, G. V., Stabilization of aqueous nanoscale zerovalent iron dispersions by anionic polyelectrolytes: adsorbed anionic polyelectrolyte layer properties and their effect on aggregation and sedimentation. *J. Nanopart. Res.* **2008**, *10* (5), 795-814.
- (15) Saleh, N.; Sirk, K.; Liu, Y. Q.; Phenrat, T.; Dufour, B.; Matyjaszewski, K.; Tilton, R. D.; Lowry, G. V., Surface modifications enhance nanoiron transport and NAPL targeting in saturated porous media. *Environ. Eng. Sci.* **2007**, *24* (1), 45-57.
- (16) Westerhoff, P.; Aiken, G.; Amy, G.; Debroux, J., Relationships between the structure of natural organic matter and its reactivity towards molecular ozone and hydroxyl radicals. *Water Research* **1999**, *33* (10), 2265-2276.
- (17) Lok, C. N.; Ho, C. M.; Chen, R.; He, Q. Y.; Yu, W. Y.; Sun, H. Z.; Tam, P. K. H.; Chiu, J. F.; Che, C. M., Proteomic analysis of the mode of antibacterial action of silver nanoparticles. *J. Proteome Res.* **2006**, *5* (4), 916-924.
- (18) Sonidi, I.; Salopek-Sonidi, B., Silver nanoparticles as antimicrobial agent: a case study on E-coli as a model for Gram-negative bacteria. *J. Colloid Interface Sci.* **2004**, *275* (1), 177-182.
- (19) Wigginton, N. S.; De Titta, A.; Piccapietra, F.; Dobias, J.; Nesatty, V. J.; Suter, M. J. F.; Bernier-Latmani, R., Binding of Silver Nanoparticles to Bacterial Proteins Depends on Surface Modifications and Inhibits Enzymatic Activity. *Environmental Science & Technology* **2010**, *44* (6), 2163-2168.
- (20) Choi, O.; Cleuenger, T. E.; Deng, B. L.; Surampalli, R. Y.; Ross, L.; Hu, Z. Q., Role of sulfide and ligand strength in controlling nanosilver toxicity. *Water Research* **2009**, *43* (7), 1879-1886.
- (21) Tong, Z. H.; Bischoff, M.; Nies, L.; Applegate, B.; Turco, R. F., Impact of fullerene (C-60) on a soil microbial community. *Environmental Science & Technology* **2007**, *41* (8), 2985-2991.
- (22) Aruoja, V.; Dubourguier, H. C.; Kasemets, K.; Kahru, A., Toxicity of nanoparticles of CuO, ZnO and TiO₂ to microalgae *Pseudokirchneriella subcapitata*. *Sci. Total Environ.* **2009**, *407* (4), 1461-1468.
- (23) Huang, C. P.; Cha, D. K.; Ismat, S. S. *Short-term Chronic Toxicity of Photocatalytic Nanoparticles to Bacteria, Algae, and Zooplankton*; 2005.
- (24) Sharma, V. K., Aggregation and toxicity of titanium dioxide nanoparticles in aquatic environment-A Review. *J. Environ. Sci. Health Part A-Toxic/Hazard. Subst. Environ. Eng.* **2009**, *44* (14), 1485-1495.

- (25) Jeng, H. A.; Swanson, J., Toxicity of metal oxide nanoparticles in mammalian cells. *J. Environ. Sci. Health Part A-Toxic/Hazard. Subst. Environ. Eng.* **2006**, *41* (12), 2699-2711.

APPENDIX A: NOTATION

A.1 Abbreviations

Abbreviation	Description
AAS	atomic absorption spectrometry
AgNP	silver nanoparticle
BET	Brunauer-Emmett-Teller
BOD	biochemical oxygen demand
CFU	colony forming units
CMC	carboxy methyl cellulose
CNT	carbon nanotube
DI	deionized
DLS	dynamic light scattering
<i>E. coli</i>	<i>Escherichia coli</i>
GC	gas chromatograph
<i>G. sulfurreducens</i>	<i>Geobacter sulfurreducens</i>
HPLC	high-performance liquid chromatography
MFC	microbial fuel cell
μ MFC	sub- μ L volume MFC
MIC	minimum inhibitory concentration
MRNIP2	RNIP modified by olefin maleic acid
nC ₆₀	fullerene nanoparticle
NOM	natural organic matter
NZVI	nano-scale zero-valent iron

PAP	polyaspartate
PCE	tetrachloroethene
<i>p</i> CBA	<i>p</i> -chlorobenzoic acid
PDMS	poly(dimethylsiloxane)
PSS	polystyrene sulfonate
ppm	parts per million
PVP	polyvinylpyrrolidone
RNIP	reactive nano-scale iron particles
ROS	reactive oxygen species
SEM	scanning electron microscope
<i>S. oneidensis</i>	<i>Shewanella oneidensis</i>
SOD	superoxide dismutase
TCE	trichloroethene
TEM	transmission electron microscopy

A.2 Symbols

<u>Symbols</u>	<u>Unit</u>	<u>Description</u>
$k_{\text{OH}, p\text{CBA}}$	$\text{mass}^{-1} \text{ time}^{-1}$	The second order rate constant for the reaction between OH radical and <i>p</i> CBA
k_{exp}	time^{-1}	Experimental rate constant for <i>p</i> CBA degradation
Re	(---)	Reynolds number

APPENDIX B: SUPPORTING INFORMATION FOR CHAPTER 2

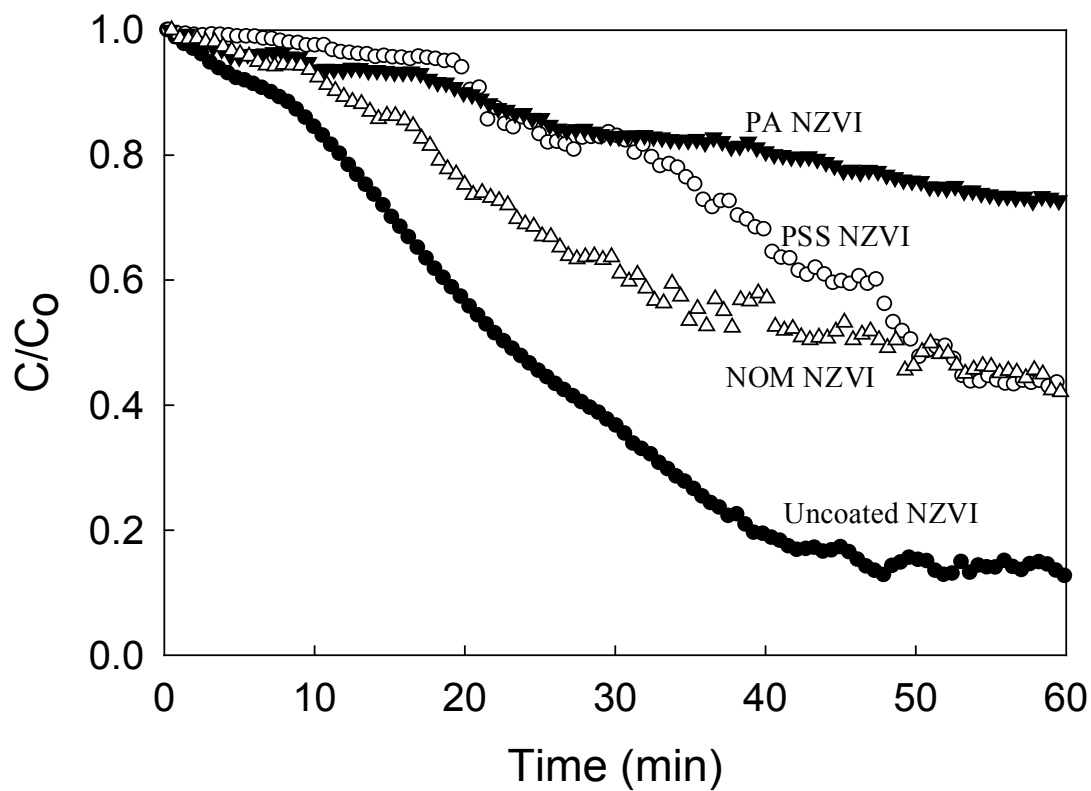


Figure B.1. Aggregation and sedimentation of bare and polymer coated NZVI particles in 5 mM sodium bicarbonate. Bare particles rapidly aggregate and sediment without mixing. Particle concentration is 100 mg/L in all cases.

APPENDIX C: SUPPORTING INFORMATION FOR CHAPTER 3

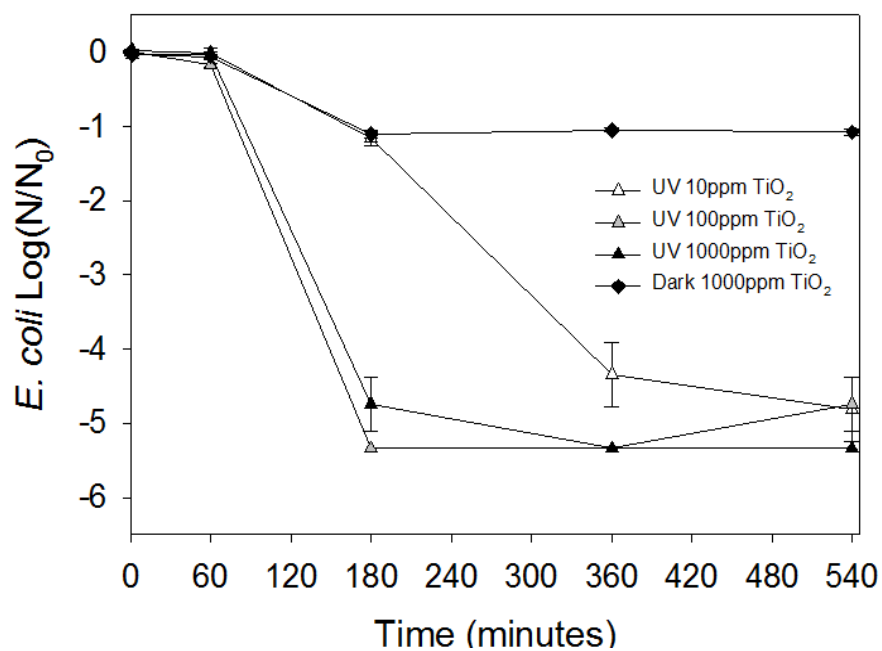


Figure C.1. Exposure of *E. coli* to 10ppm, 100ppm, and 1000ppm bare nano-TiO₂ under UV irradiation, and exposure to 1000ppm bare nano-TiO₂ under dark condition.

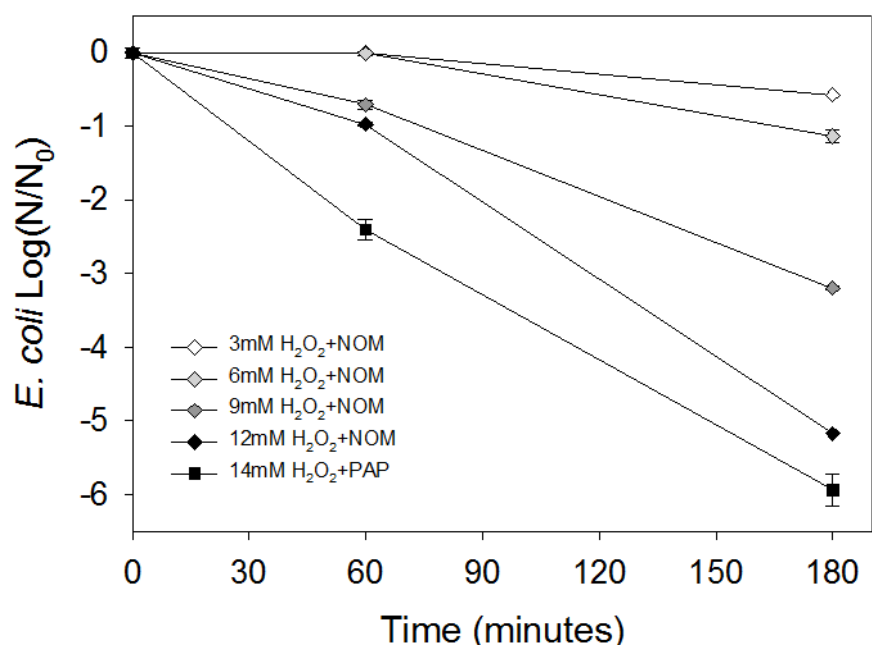


Figure C.2. Exposure of *E. coli* to 3, 6, 9, and 12 mM H_2O_2 with 100 mg/L NOM and 100 mg/L PAP.

APPENDIX D: METHODS

D.1 Coating Adsorption Protocol

Typical particle/polymer concentrations during adsorption are 3 g/L particle +1 g/L polymer.

1. Start with a 30 g/L stock suspension of particles. Sonicate using ultrasonication probe for 30 minutes. Tip should be towards the bottom of the suspension, not in the middle.
2. Let suspension completely cool to room temperature before using.
3. A note on polymer stock solutions: if you are preparing your own solution by dissolving solid polymer in water, allow ~ 1 day for complete dissolution. This is especially important for high-molecular weight polymers.
4. Prepare reactors: first add water or buffer (e.g. 5mM NaHCO₃) to each reactor. If using oxidatively unstable particles, such as RNIP, you should be using water/buffer that has been purged with N₂. You should also briefly (1 or 2 minutes) purge the headspace of each reactor with N₂ before adding particles and polymer solution.
5. Shake the particle stock suspension before withdrawing aliquots, since the particles will have completely settled to the bottom during cooling. Add the appropriate aliquot of particle stock suspension to the first reactor, quickly followed by addition of the polymer stock solution. It is important to add polymer to particle, and not the reverse. Once particles have been added to a

reactor, the next steps of adding polymer, capping the reactor, and getting it on a rotator should be done as quickly as possible.

6. No matter what total volume you choose for each reactor (for example, 30 mL), always use the same volume. Different amounts of headspace in the reactors will give you different results.
7. Allow reactors to rotate for enough time for adsorption to be complete; ~ 1 – 2 days should be more than enough. Use the same adsorption time for all reactors that you want to compare to each other.
8. Remove reactors from rotator. Always shake a reactor vigorously before removing any samples in order to get the most representative samples. Particles will quickly begin to settle once agitation has stopped.
9. Reserve 50 – 200 μ L samples of each reactor for digestion with acid and AA. You will need the real particle concentration for calculating adsorbed mass.
10. Separate particles from excess polymer by ultracentrifugation. Centrifuge 20 mL samples of each suspension (this is close to the maximum volume of the polycarbonate centrifuge tubes) first at 27,500 rpm for 1 hour 20 minutes. Reserve sufficient supernatant for measurement of polymer concentration (typically by TOC analysis); it is a good idea to reserve more sample than is necessary, so aim for 10 mL. Be careful not to suck up traces of particles when you are pipetting supernatant out of the centrifuge tubes.
11. Wash particles: add 20 mL of water to each tube that now has only particles sedimented at the bottom and along the sides. Centrifuge again at 27,500 rpm for 40 minutes (the particles should not have re-dispersed much when you

added water). Discard this supernatant after centrifugation. This washing step is important because polymer-modified particles are usually not stable in the presence of excess polymer. Two centrifugation cycles are typically sufficient to remove excess polymer.

12. Don't forget to measure pH of the supernatant. pH is a critical parameter in adsorption experiments and should always be checked. Wait until after TOC analysis of your samples is complete, just in case you need more of the supernatant to repeat the measurement of polymer concentration.
13. Re-suspend washed particles: add 20 mL of water (or your aqueous medium of choice) to a centrifuge tube with washed particles. Sonicate using the ultrasonication probe for a few seconds in order to get most of the particles into suspension. Then pour the suspension from the centrifuge tube into the glass vial that you will be storing your suspensions in (you may have to pour back and forth a few times to get as much of the particles into the glass vial as possible). Sonicate this suspension for 5 minutes. You should always remove the suspension from the centrifuge tube before this final sonication step because it is damaging to the polycarbonate tubes, which are expensive to replace.
14. The tip of the ultrasonication tube should be towards the bottom of the suspension during sonication. Keep in mind that as the tip ages, the resulting stability of your suspensions will get worse, so you may not be able to compare a suspension that you prepared today with one from 6 months ago.

Note: if you are measuring adsorption isotherms, you can stop after step 9. You only need the polymer concentration in the supernatant, so the second washing step and re-suspension of the particles are unnecessary, unless you plan to do further experiments on one of the suspensions. You still need to measure pH of the supernatant.

I've been taking my uncoated particles through the same procedure as for the coated (shake in reactor for 2 days, centrifuge, wash twice) for consistency, and also I need to check if any organic matter comes off the bare TiO₂ when I do TOC.

If there's no organic matter, then you should just be able to make a 30 g/L solution of TiO₂ powder in water and sonicate (power level 3) for half an hour, then let it cool down several hours, and use that.

If I have a solution of particles that I've left sitting around for a while, I usually sonicate before I use or analyze it (10 minutes for concentrated solutions e.g. 2 g/L, or 5 minutes for dilute solutions). TiO₂ is pretty stable in water so it should be easy to use.

D.2 Culture Preparation

E. coli (ATCC strain 33876) was inoculated in 60 mL of LB Miller broth medium and grown at 37 °C for 12 h. The bacteria were harvested by centrifugation at 5000g for 10 minutes. The supernatant was decanted, the cells were resuspended in 5 mM sodium bicarbonate (pH=8.2 ±0.1), then centrifuged again at 5000g for 10 minutes. This washing step was repeated. The *E. coli* stock was prepared by resuspending the bacteria pellets in 15 ml of 5 mM sodium bicarbonate. The stock concentration of *E. coli* was determined to be in the range of 1 x 10⁹ to 2 x 10⁹ colony forming units (CFU) /mL by the spread plate method using LB agar plates incubated at 37 °C for 12 hours.

Shewanella oneidensis MR-1 (ATCC 700550) was cultured in liquid LB (Luria-Bertani) medium with 20 mM lactate as electron donor under aerobic conditions at 30°C for 12 hr. The bacteria were harvested by centrifugation at 5,000 g for 30 min. After decanting the supernatant, 5 mM sodium bicarbonate (pH=7.0) was added to resuspend the bacteria and then centrifuged again at 5,000 g. This process was repeated 3 times to achieve completed harvesting of bacteria. To get a *S. oneidensis* stock for experiments, its pellets were resuspended with 15 mL of 5 mM sodium bicarbonate. Through the spread plate (LB and Agar) method at 30°C for 24 h, 6.0×10^8 to 9.4×10^8 colony forming units (CFU) was determined as the stock concentration of *S. oneidensis*.

D.3 Plate Count

Serial dilutions of suspension of bacteria are plated onto LB agar solid medium. For the method of serial dilution of sample, we could have 10^{-1} to 10^{-8} or more dilutions of the sample. Dilution procedure influences overall counting process. The suspension is spread over the surface of solidified growth medium (LB agar). The plates are incubated so that colonies are formed. Multiplication of a bacterium on solid media results in the formation of a macroscopic colony visible to naked eye. It is assumed that each colony arises from an individual viable cell.

Total number of colonies is counted and this number multiplied by dilution factor to find out concentration of cells in the original sample. Counting plates should have 30-300 colonies at least. A major limitation in this method is selectivity.

The nature of the growth medium and the incubation conditions determine which bacteria can grow and thus be counted. Viable counting measures only those cells that are

capable of growth on the given medium under the set of conditions used for incubation. Sometimes cells are viable but not culturable.

LB agar medium compositions are shown in Table D.1. Medium is heated to dissolve ingredients, and autoclave 20 min at 121°C. Final pH is around 7.0 ± 0.2 . Then medium is dispensed 20 ml portions into sterile 15 x 100 mm petri dishes.

Table D.1. Plate count agar compositions

Tryptone	5 g
Yeast extract	2.5 g
Dextrose	1 g
Agar	15 g
Distilled water	1 liter

APPENDIX E: MICROBIAL ELECTRICITY GENERATION VIA MICROFLUIDIC FLOW CONTROL

E.1 Abstract

Next generation battery technology is rapidly evolving to meet the demand for higher power densities and smaller footprints through novel catalysts and battery architecture. We present a μ -scale, biological fuel cell which utilizes microbial electricity generation enabled by microfluidic flow control to produce power. The new fuel cell, the smallest of its kind, with a total volume of 0.3 μ L, produces scalable and controllable electrical energy from organic matter which is sustained through microbial respiration and laminar flow separation of the electrolytes. Electrical currents are dependent on specific biofilm formation on the anode, the concentration of electron donor, and a diffusion-limited flow regime. A maximum current density of 18.40 ± 3.48 mA m⁻² (92 ± 17 A m⁻³) was produced by *Geobacter sulfurreducens*, and 25.42 mA m⁻² (127 A m⁻³) by *Shewanella oneidensis*. The μ -scale biological fuel cell introduces the necessary small size and fuel flexibility for applications in *in vivo* and *in situ* sensors which may be remotely-deployed and self-powered.

Keywords: biosensing; geobacter; lab on a chip; microfluidics; microbial fuel cell.

E.2 Introduction

The demand for creating small scale power sources has been rapidly expanding due to the need in applications ranging from in vivo clinical and in situ environmental sensing to the development of microanalytical, field-deployable devices. For example, advanced lithium-ion chemistry (1) and nanostructuring (2, 3) is enabling development of micron-scale batteries for portable and implantable electronics. Regardless of their size, conventional batteries are finite energy sources and prone to self-discharge. If remotely deployed or deployed for spatially high-resolution applications, maintenance and replacement of the power source is too invasive and costly for conventional batteries. Moreover, chemical batteries may introduce human and/or environmental risk associated with the toxicological impacts from the rupture of the power-cell.

A potential solution may lie in the application of biological materials and systems for battery technology. Energy generation from biological systems, such as microbial fuel cells (MFC) (4, 5), take advantage of the broad metabolic capabilities of bacteria to utilize a broad variety of electron donors, including renewable sources such as waste organic matter without the need for expensive catalysts or extreme temperatures (4, 5). In brief, MFC are galvanic electrochemical cells in which pure cultures or consortia of bacteria catalyze the oxidation of electron donor and transfer electrons liberated during their metabolic processes to the anode. In this manner, the anode serves as the electron acceptor for microbial oxidation of the donor in the fuel cell. In comparison to conventional batteries, MFC offer a more environmentally benign footprint for powering remotely deployed devices (6, 7). The evolution of MFC technology has largely been motivated by the potential for renewable energy sources and waste biomass to serve as a

fuel for large-scale electricity generation (4). However, interest in battery technology for portable electronic devices and sensors has driven miniaturization of MFC to meet this growing energy need. For example, small-scale (1-10 mL reactor volume and 1-10 cm² geometric surface area electrodes) have increased power densities (8-11) as compared to larger MFC (9). Micromanufacturing technology has given rise to still smaller (under 20 μ L-range) (12, 13) MFC with volumes down to 1.5 μ L, as reported by Qian et al (14). Additionally, micromanufacturing has led to the development of a variety of cellular and sub-cellular biotechnologies (15-17), including recently described high-throughput screening technology utilizing a MFC array to identify microbes which may be respire or otherwise be electrochemically reactive on the anode of a fuel cell (18).

Here we describe the micromanufacturing and operation of the first sub- μ L volume MFC (μ MFC). In contrast to previously described chemical fuel cells which are enabled by microfluidic flow control (19, 20), the μ MFC is first whole-cell biological application to utilize similar separation of anolyte and catholyte fluids by laminar flow rather than semi-permeable membranes or diffusion limitations through a biofilm (Figure D.1). We demonstrate the ability to create power using bacteria in a simple and scalable system of microfluidics with an anode area of 1.4 mm² and anode volume of 0.3 μ L. The power was dependent on microbial colonization of the anode, availability and concentration of electron donor, and the maintenance of diffusion-limited conditions through manipulation of the microfluidic flow regime. The μ MFC technology was validated using two different bacterial strains capable of respiration in a MFC, *Geobacter sulfurreducens* and *Shewanella oneidensis*. Scanning electron microscopy imaging shows the specific colonization of the anode by pure cultures of bacteria. This novel

approach for MFC technology introduces the opportunity for sub- μL -scale biological power devices which may be deployed for certain niche electronics, such as remote and biological sensing where conventional battery technology may not be optimal.

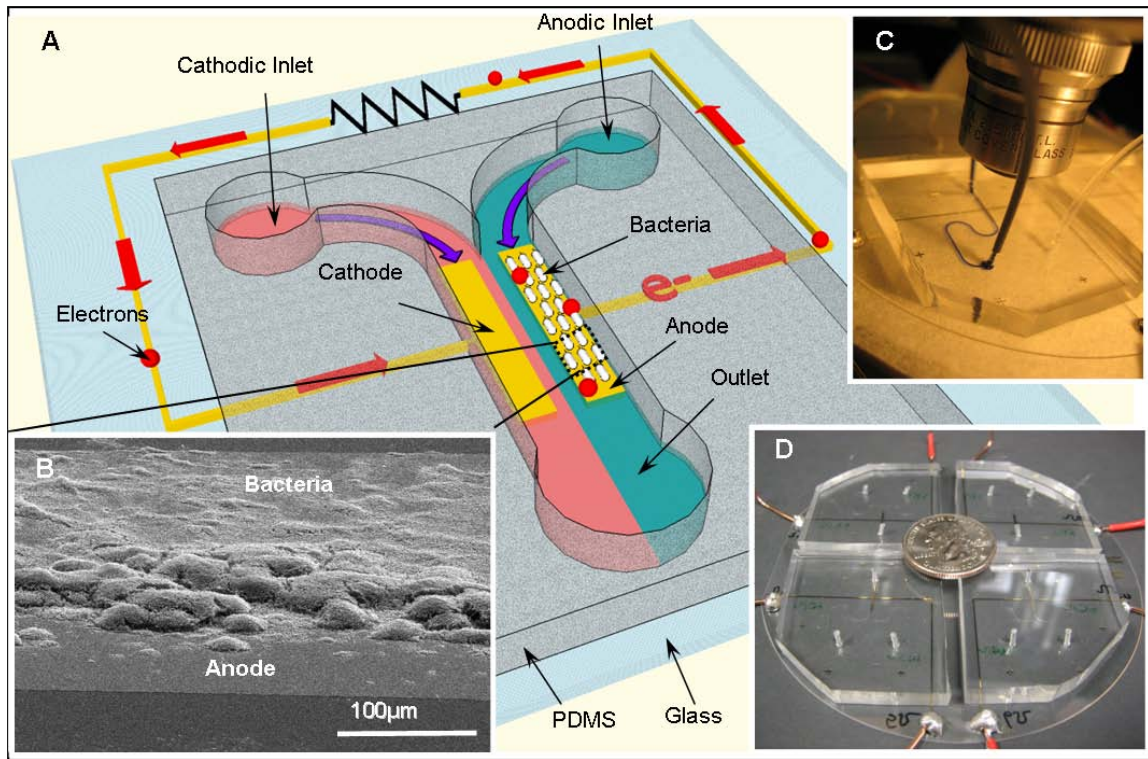


Figure D.1. The microfluidic microbial fuel cell (μMFC). An illustration of the essential components for μMFC : (A) two inlets and one outlet, two gold microelectrodes connected with gold wires, and (B) SEM image of bacteria colonized on the anode. Images of the fabricated μMFC including (C) the μMFC with blue dye in one inlet confirming the ability to establish laminar flow conditions in the μMFC and (D) multiple μMFC units on one glass wafer confirming our ability to multiplex this system using lithographic techniques.

E.3 Materials and Methods

E.3.1 Bacterial Strains and Culture Media

Geobacter sulfurreducens PCA (ATCC 51573) were grown in freshwater (FW) medium (21) with 20 mM acetate as the electron donor and 20 mM fumarate as the electron acceptor under strict anaerobic conditions as described previously (22). During colonization and growth in the μ MFC, *Geobacter* cultures were grown in identical FW medium. *Shewanella oneidensis* MR-1 (ATCC 700550) was cultured in liquid LB (Luria-Bertani) medium with 20 mM lactate as electron donor under aerobic conditions (23). Prior to inoculation into the μ MFC, MR-1 cultures were grown aerobically in yeast extract at 30 °C overnight to obtain a high-density culture which was then centrifuged, washed, and resuspended three times using an isotonic phosphate buffer solution. The cell pellet was re-suspended in anaerobic (FW) (21) medium amended with 20 mM lactate as the electron donor and 0.5% yeast extract (w/w).

E.3.2 Fabrication of Microfluidic Fuel Cells

Microelectrodes. Glass wafers (diameter 4 inch) were purchased from AGTEC (Gilroy, CA). Chromium and gold were sputtered at 10^{-6} Torr to achieve a total thickness of 50 nm and 100 nm on the glass wafer, sequentially. Figure.D.2 A is a schematic of the photolithography and metal etching techniques used to fabricate the μ MFC. The microelectrode and electrical wire pattern was designed in a CAD program and printed on a transparency at high resolution (5080dpi). Photoresist AZ 4110 (Shipley Company Inc., Newton, MA) was spin-coated on the gold-coated glass wafer, with a thickness of

~1 μm . Then ultraviolet light exposure through the patterned transparency mask was performed for the photoresist-coated wafer. The pattern was transferred to the photoresist layer after using AZ photoresist developer. Chromium and gold that will form electrodes and wires were prevented from being etched off by the photoresist, while those in the remaining area were dissolved through using a chromium etchant type TFD and gold etchant type TFA (Transene Inc., Danvers, MA). The overlaying photoresist was washed off using acetone to obtain the desired electrodes. Each electrode was 175 μm wide and 8 mm long, with a 200 μm separation between two electrodes.

Microchannels. The soft-lithography approach (Figure.D.2 B) was used to fabricate the microfluidic system (24, 25). A silicon wafer was spin-coated with 50 μm -thick SU-8 50 (MicroChem Corp., Newton, MA), and exposed to ultraviolet light with a patterned transparency mask. SU-8 was developed in SU-8 developer to transcribe the pattern onto the photoresist and used as the mold for the microfluidic channel. Poly(dimethylsiloxane) (PDMS) was poured on the patterned photoresist and cured to form the desired microchannel, with a length of 1 cm, a width of 600 μm , and a height of 50 μm . The channel length was chosen to minimize the impacts of diffusional mixing between the anolyte and catholyte (19, 20). The PDMS slab with microchannel and the glass wafer with microelectrodes were assembled together underneath a microscope to ensure accurate alignment. To achieve better adhesion, the PDMS slab and glass wafer may be pretreated in plasma oxidation chamber prior to assembly. After assembling the μMFC , blue dye was passed through one of the inlet channels while water was in the other inlet to image the interface between the two streams and visually verify laminar flow conditions (Figure D.2 C, D).

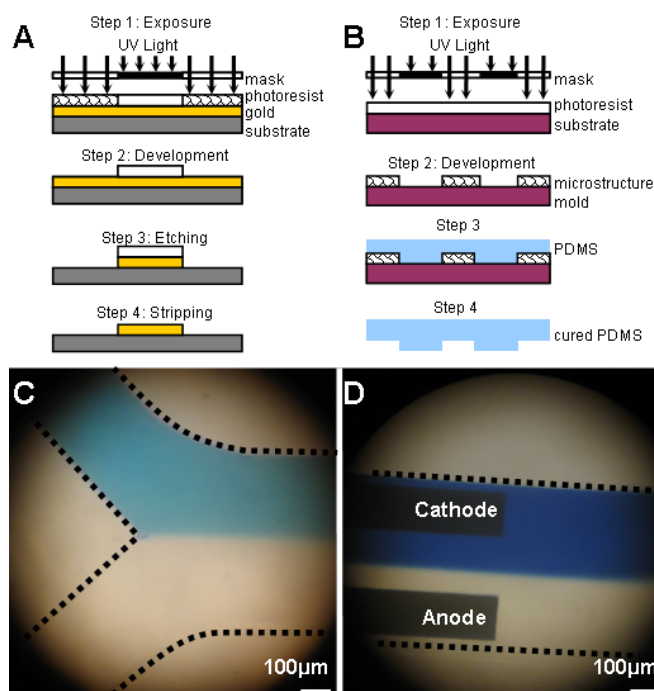


Figure D.2. Schematic of μ MFC fabrication process and laminar flow condition verification. (A) Photolithography and metal etching techniques were employed for fabrication of the gold microelectrodes. A photoresist layer on top of the gold with desired pattern was created by exposing to UV light (step 1 and 2). The gold uncovered with photoresist on a glass wafer was etched off to form the microelectrodes and wires. (B) The microstructure channel was fabricated using conventional soft lithography. PDMS with a 10:1 ratio of base to curing agent was used and cast against the mold (step 3 and 4), which was created by exposing photoresist on a silicon wafer to UV light (steps 1 and 2). (C) Image at the convergence of the anolyte and catholyte channels and (D) the outlet of the microfluidic fuel cell channel showing that the laminar flow separation persists well along the length of the channel.

E.3.3 Inoculation and Operation of Microfluidic Microbial Fuel Cells

Prior to inoculation, the microfluidic microbial fuel cell was rinsed for 15 minutes with 1 N NaOH, 1 N HCl, 10% Bleach, 70% ethanol, and sterile DI water for removal of proteins, metals, and sterilization before introduction of the cultures. Flow to the anode and cathode sides of the μ MFC was provided by a syringe pump (KD Scientific 780230) at a flow rate of $45 \mu\text{L min}^{-1}$. This flow rate resulted in a Reynolds number (R_e) of 4.62,

well below the threshold for laminar conditions in the μ MFC. R_e is a dimensionless number defined in Equation (1) which indicates the relative importance of convective mixing in the flow.

$$R_e = \frac{\rho V D}{\mu}, \text{ Equation (1).}$$

Biofilms were established on the anodes of the μ MFC through inoculation of mid-log growth cultures of *G. sulfurreducens* or *S. oneidensis* into the anolyte reservoir containing growth medium under electron acceptor limited conditions. Colonization of the anode was determined by the passage of current across the fuel cell. Once current was observed, the anode reservoir was filled with fresh, sterile, anaerobic medium which lacked electron acceptor and was amended with the appropriate electron donor; 20 mM acetate or 20 mM lactate for *G. sulfurreducens* or *S. oneidensis*, respectively. The reservoirs were replenished with fresh, sterile, anaerobic medium as needed. For all conditions tested, an isotonic phosphate buffer solution (pH 6.8) saturated with O_2 was used as the catholyte with an identical flow rate to the anolyte.

E.3.4 Imaging of Microfluidics and Biofilm Cultures

A μ MFC reactor with *S. oneidensis* was sacrificed during experimentation for imaging of the biofilms using Scanning Electron Microscopy (SEM). In order to expose the biofilm for fixation and imaging, the PDMS channel was carefully separated from the electrodes. The exposed biofilm was fixed to the microelectrodes with 4% para-formaldehyde phosphate buffer (pH 7.2) overnight. The electrodes were then washed in para-formaldehyde-free phosphate buffer (PBS) for 1 hour. After 3 washes with PBS, the

specimens were fixed for one hour in 1% OsO₄ buffered with PBS. The OsO₄ was removed and washed three 5 minutes with dH₂O, followed by dehydration in an ascending series of ethanol (50%, 70%, 80%, 90%, and 3 changes of 100%). The specimens were dried in a Pelco CPD2 critical point dryer using CO₂, at 1200 psi, and 42 °C. Dried specimens were attached to SEM stubs using double sided tape, and sputter-coated with gold using a Pelco SC-6. Specimens were examined using a Hitachi 2460N Scanning Electron Microscope at 25 kV. Digital images were obtained using Quartz PCI Image management system software. Images were adjusted only for brightness or contrast in Adobe ® Photoshop.

E.3.5 Current Dependence on Electron Donor Concentrations

To investigate the relationship between current and electron donor concentration, a μ MFC experiment was conducted at variable acetate concentrations. μ MFC was inoculated with *G. sulfurreducens* as described above. Growth medium with a series of acetate concentrations (0 mM, 5 mM, 10 mM, and 20 mM) was fed into the μ MFC as the anolyte at a constant flow rate, subsequently. At each concentration, a constant medium feeding was maintained for 3-4 hours after a stationary phase current was reached. The current was averaged for each stationary phase and plotted vs. the corresponding concentrations.

E.3.6 Analytical Methods

Current was measured with a Keithley 6485 Picoammeter and data were collected using ExceLINX (Keithley Instruments Inc.). Concentrations of acetate, lactate, and fumarate were analyzed using an Agilent 1100 HPLC equipped with an Eclipse XDB-C18 column and UV detector (210nm). Adequate separation was achieved with a flow rate of 1 mL min⁻¹ at 25°C, using mobile phase of 3% methanol and 97% 20 mM (NH₄)₂HPO₄ at pH 2.2.

E.4 Results and Discussion

E.4.1 *Geobacter sulfurreducens*: Current Production and Sensing

We used a microfluidic fuel cell approach utilizing bacteria to demonstrate electricity generation and amperometric sensing via microbial respiration in the μ MFC with *Geobacter sulfurreducens* (Figure D.3), a dissimilatory iron-reducing bacterium that produces electricity in at the anode of a fuel cell (5, 26). The principle behind the electricity generation is the oxidation of electron donor by the bacterium coupled with respiration of the anode as its terminal electron acceptor (26, 27). Current was produced by *G. sulfurreducens* approximately 3 days after the inoculation of a culture into the anode inlet. Current steadily increased over several days indicating adaptation to anode respiration and growth on electrode (26, 27) (Figure D.3.A).

The dependence of electricity production on laminar flow conditions was observed by uniformly decreasing the flow rate across the anode and cathode of μ MFC after 6.5 d (Figure D.3 A). Current density decreased with flow rate and the stoppage of

flow entirely on day 8 resulted in a cessation of electricity generation and slight reversal of current from anode to cathode. Restoration of flow through the channels on day 9 immediately reestablished the laminar flow regime and hence the potential gradient and current production (Figure D.3 A) from the μ MFC with its maximum power density achieved shortly thereafter. These observations demonstrate that separation of anolyte and catholyte fluids (Figure D.3 C, D) is necessary to maintain the voltage gradient between the electrodes and that separation is maintained by the diffusion barrier created by the laminar flow regime. The diminished current density with flow rate through the μ MFC may be attributed to a gradual broadening of the downstream liquid-liquid interface and mixing of anolyte and catholyte fluids at cathode and anode, respectively. The broadening of the mixing zone with increased diffusion results in gradual depolarization of fuel cell (19, 20, 28).

Utilizing acetate as the electron donor *G. sulfurreducens* produced a maximum current density of $18.40 \pm 3.48 \text{ mA m}^{-2}$ ($92 \pm 17 \text{ A m}^{-3}$) over 15 hours. After swapping the electron donor to H_2 , the maximum current density was 708 mA m^{-2} ($3,300 \text{ A m}^{-3}$) with a typical range of $333 \pm 45 \text{ mA m}^{-2}$ ($1,500 \pm 240 \text{ A m}^{-3}$) (Figure E.1). Our volumetric current density is higher than previous reports from micron-scale MFC, but similar on a geometric electrode area basis (11, 13, 14).

The μ MFC approach is possible because members of the family *Geobacteraceae* conserve energy for growth through respiration of the anode electrode in a fuel cell with nearly stoichiometric recovery of electrons as electricity (5, 29). They grow as an attached biofilm on electrodes and without required contributions by planktonic cells to the current (26). An understanding of how *Geobacteraceae* externalize electrons

generated in central metabolism during electron donor oxidation is continually evolving (30), however anode respiration likely involves multiple c-type cytochromes (31) and conductive pili (32); both of which are required for optimal current production. The conductive pili of *Geobacteraceae* are necessary for biofilm formation (33) and are hypothesized to enable respiration of the anode by cells which are not in direct contact with the anode. Similar mechanisms of electricity production by *Geobacteraceae* biofilms likely occur in the μ MFC with the sole difference of an additional requirement of diffusion-limited conditions between the anolyte and catholyte in order to maintain the potential gradient between the electrodes.

A significant advantage for the potential deployment of μ MFC in clinical and environmental sensing is imparted by the small size of the device and its scalable electrical response. The suitability of a precolonized μ MFC with *G. sulfurreducens* for sensing was investigated through analyses of the amperometric response under various influent electron donor (acetate) concentrations. Figure D.3 presents raw current (Figure D.3 C) and reduced (Figure D.3 D) data confirming the dependence of current on acetate concentration. The current response to variation of acetate concentration was rapid and repeatable with a coefficient of determination (R^2) of 0.98. The response of the electricity producing biofilm of *Geobacter* was approximately linear with acetate concentration whether increasing or decreasing the influent concentrations; this suggests a similar, robust approach for MFC sensor applications as previously described for lactate measurement (34, 35), Biochemical Oxygen Demand (BOD) monitoring (36), and microbial activity monitoring (37, 38).

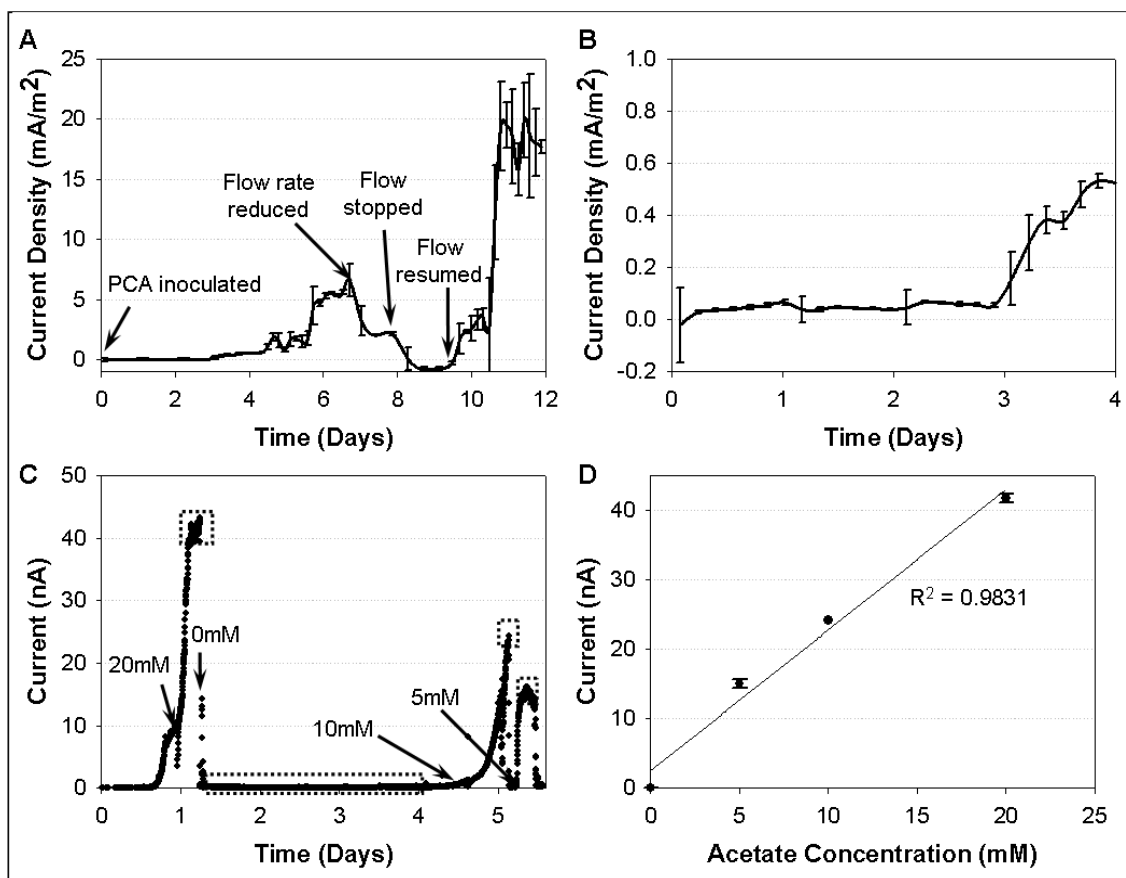


Figure D.3. Electricity production by *G. sulfurreducens* in the μ MFC. (A) Electrical current as a function of time showing microbial growth and adaptation to electrode respiration was dependent on diffusion limited conditions maintained by laminar flow through the fuel cell. (B) Magnification of x axis to show the onset of the earliest current after inoculation of the cells. (C) Electrical current as a function of time with varying concentrations of electron donor (acetate) (i.e. 0 mM, 5 mM, 10 mM and 20 mM). (D) Current response plotted as a function of varying electron donor concentration.

E.4.2 *Shewanella oneidensis*: Current Production and Biofilm Imaging

The performance and robustness of μ MFC was further evaluated by examining biofilm formations and current production on the micromanufactured electrodes using *Shewanella oneidensis*. Like *Geobacteraceae*, members of the family *Shewanellaceae* may conserve energy for growth during dissimilatory iron reduction and may also

produce conductive pili structures (39). However, *Shewanellaceae* may grow aerobically and exhibit a distinctly alternate mechanism from *Geobacteraceae* for externalizing electrons to electrode surfaces which involves planktonic cells as well as attached biofilm cells (40). Recently, Marsili *et al* (41) identified flavin compounds produced by *S. oneidensis* which mediate electron transfer to electrodes and may enable planktonic cells of *S. oneidensis* to respiration when not in contact with the biofilm or electrode. In the μ MFC flow-through system, planktonic cells would not be expected to contribute significantly to current production, but the electron mediating flavin compounds may attach to the electrode and facilitate electron transfer (41).

The μ MFC was inoculated with *S. oneidensis* and lactate was provided as the electron donor at the same flow rate. *S. oneidensis* produced current after 36 hours, about 24 hour earlier than *G. sulfurreducens* and achieved a maximum current density 25.42 mA m⁻² (127 A m⁻³) with an average current density 21.00 ± 2.00 mA m⁻² (105 ± 10 A m⁻³) over 15 hours (Figure D.4 A). Both volumetric and electrode surface area current densities of our μ MFC are similar to the maximum current densities in other μ L-scale fuel cells with *Shewanella* (11, 14). The more rapid onset of current production by *Shewanella* in the μ MFC may have been an artifact of the higher cell density of the aerobically-grown inoculation culture (40). Fresh, sterile medium with lactate was introduced on day 3. As soon as current production resumed and was observed to increase, the μ MFC was sacrificed for Scanning Electron Microscopy (SEM) imaging of the anode and cathode.

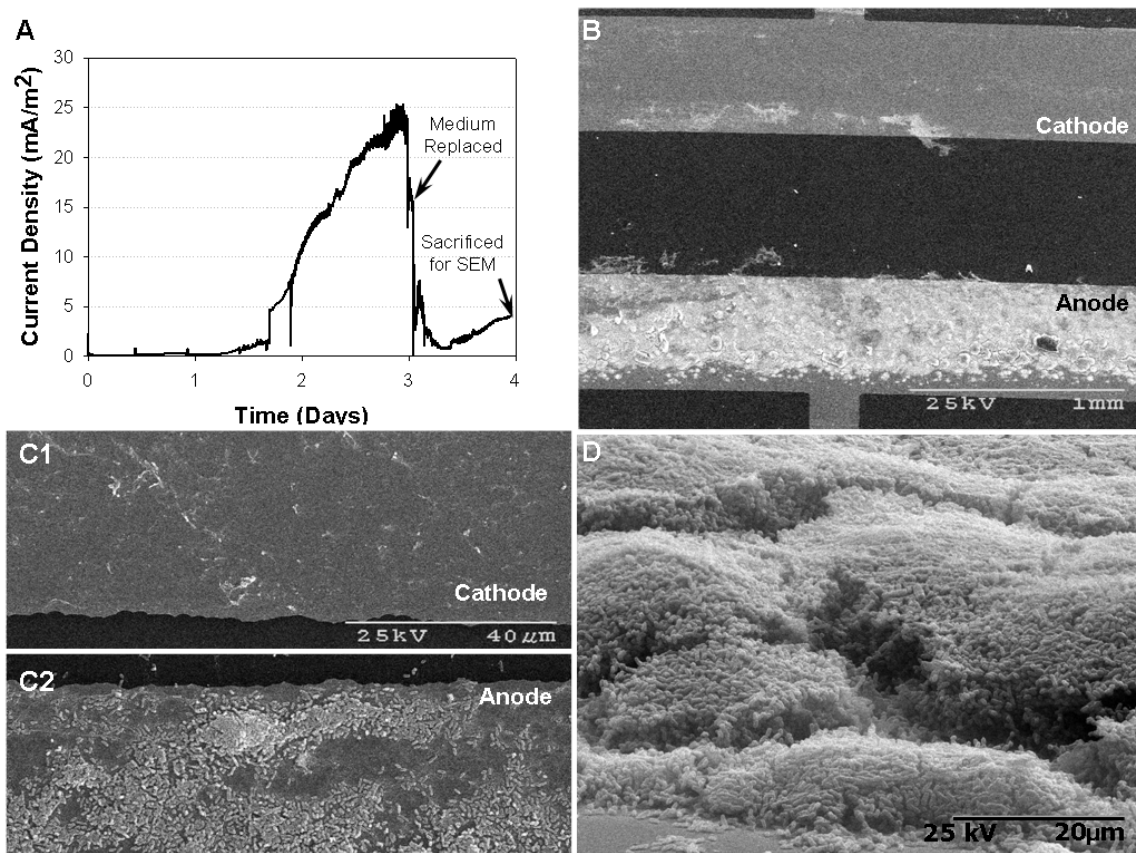


Figure D.4. Current production by *S. oneidensis* and SEM images of *S. oneidensis* growing on a gold electrode in a μ MFC. (A) Electrical current as a function of time. Reactors were sacrificed for imaging after 4 days of continuous operation in (A). (B) Anode and cathode at low magnification shows biofilm growth on the anode surface, while almost no biofilm was formed on the cathode. (C) Higher magnification images of the anode and cathode. (D) Higher magnification images of biofilm growth on the anode at a 75° tilted angle view.

SEM images of the gold microelectrodes were obtained in order to determine the location of colonization of *S. oneidensis* in the μ MFC. Figures D.4 B and C reveal that cells specifically colonized the anode with nearly complete and confluent coverage of the electrode. In addition, the images show a robust, a three-dimensional biofilm structure. Conversely SEM examination of the cathode shows that the cathode was not colonized by *Shewanella* (Figure D.4 B, C1, and E.2). The observation of a thick and mature

biofilm structure with extensive coverage of the gold electrodes reported here is consistent with the study by Qian *et al* (14), differing from the sparsely colonized *S. oneidensis* biofilm observed on graphite electrodes in batch experiments with carbon electrodes in a μ L-scale MFC (11). Although electrode materials are likely to impact the biofilm, hydrodynamics in the microchannel may also contribute to the different biofilm structures observed among anode-grown *S. oneidensis* cultures (42). Under higher magnification and visualized at a 75° angle (Figure D.4 D), *S. oneidensis* biofilms were observed to have a pillar thickness of over 30 μ m. These characteristics are typical of *S. oneidensis* biofilms which may extend as high as 200 μ m into the bulk fluid medium (42). The pillar height in the μ MFC is confined by the channel height of 50 μ m. Additionally, it is likely that some of the biofilm which was in contact with the top of the PDMS channel walls was removed during separation of the PDMS from the electrodes while preparing the electrode biofilm for SEM imaging.

E.5 Conclusions

Microbial fuel cells are emerging as promising technology for energy supply in applications where maintenance is risky or expensive and the power requirements are low (7, 43). We describe the first microbial fuel cell based on laminar flow separation of the anolyte and catholyte. The fuel cell employs microfluidic flow control to achieve diffusion-limited condition. Each electrode in the μ MFC had a surface area of 1.4×10^{-6} m² and each channel a volume of 0.12 μ L under the flow conditions tested; the smallest MFC to date. Diffusional mixing along the length of the channel has the impact of

reducing the current. Flow rate also affects the power output by affecting Reynolds Number and therefore expected mixing conditions and diffusion in the channel. This deleterious effect may be minimized through an application-specific optimization of the channel length and Reynold's Number. We have operated the fuel cell for as long as 2 weeks after stable biofilms formed and have noted two phenomena that need further investigation and optimization for specific applications: 1) nutrients conditions and electron donor supply, and 2) prevention of biofilm overgrowth when nutrients are in great abundance.

Laminar-flow based current was produced by *Shewanella* and *Geobacter* spp, both capable of electricity production in MFC but with distinct mechanisms of electron transfer to the anode, and tolerances for oxygen (44). These different physiological capabilities and strategies for reducing the anode suggest that ample opportunity exists to design μ MFC architecture guided by the physiology of the organism. Raw current was low, relative to conventional fuel cells. Normalized to the surface area of the anode or volume of the microfluidic channels, currents were similar to and greater than previous reports for μ L-scale microbial fuel cells. Current in MFC may be optimized through design of microbe-electrode interface for maximal capture rates of electrons from cells (45), minimization of internal resistances through modification fuel cell architecture (8, 46), and metabolic engineering of cells for higher rates of respiration (47). In the μ MFC, current and power can be greatly increased through multiplexing where microfluidics is ideally suited described by Yang et al. (17).

From a sensing perspective, the strong dependence of current on electron donor concentrations in the anolyte solution suggests that a micron-scale MFC may serve as a

small-scale sensing device for a variety of applications. For example, acetate is a key intermediate substrate during anaerobic biodegradation of organic matter and bioremediation (48). The calibration curve was linear as would be expected from a steady-state deep biofilm at low substrate concentration (49). MFC-based sensors have been proposed for a variety of applications, however, a microfluidic biosensor offers significant technological advantages, especially with respect to minimization of measurement artifact introduced by the size of the sensor.

Generating multiple small scale microfluidic based units in parallel within a confined area has been demonstrated by several groups (16, 50); using this unit approach with microbes in microfluidics is a direct extension of these approaches. Furthermore, building these systems in three dimensions would also realize further increases in energy production for the same area on a single device thus increasing the energy return on the battery size, which is a tremendous limitation in many current applications. In this manner, the natural and engineered metabolic diversity of microorganisms may be harnessed to enable the design of microfluidic and micron-scale MFC which serve as independent energy sources, self-powered sensing devices in a variety of deployments. Moreover, the small size of the μ MFC offers much greater flexibility by limiting potential disturbances to the sensed or powered environment and offering high-throughput screening via whole cell lab-on-a-chip technology. The micron-scale biological fuel cell introduces the necessary flexibility and sustainability for in vivo and in situ sensors which may be remotely-deployed and self-powered.

E.6 Acknowledgements

The authors thank Dr. Joseph Suhan at the Carnegie Mellon University Electron Microscopy facility for taking SEM images and Carsen Klein at the Carnegie Mellon University Nanofabrication facility for enabling the fabrication of microelectrodes and microchannels in these experiments. We would like to express our gratitude to the Jidian Liang Fellowship for supporting Li's work.

E.7 References

- (1) Loeb, G. E.; Richmond, F. J. R.; Olney, S.; Cameron, T.; Dupont, A. C.; Hood, K.; Peck, R. A., Biontm bionic neurons for functional and therapeutic electrical stimulation. *Proc. 20th IEEE Engr. Med. Biol. Soc.* **1998**, 20, (5), 2305-2309.
- (2) Lee, Y. J.; Yi, H.; Kim, W.-J.; Kang, K.; Yun, D. S.; Strano, M. S.; Ceder, G.; Belcher, A. M., Fabricating genetically engineered high-power lithium-ion batteries using multiple virus genes. *Science* **2009**, 324, (5930), 1051-1055.
- (3) Nam, K. T.; Wartena, R.; Yoo, P. J.; Liao, F. W.; Lee, Y. J.; Chiang, Y. M.; Hammond, P. T.; Belcher, A. M., Stamped microbattery electrodes based on self-assembled m13 viruses. *Proc. Nat. Acad. Sci. U.S.A.* **2008**, 105, (45), 17227-17231.
- (4) Logan, B. E., Exoelectrogenic bacteria that power microbial fuel cells. *Nat. Rev. Microbiol.* **2009**, 7, (5), 375-381.
- (5) Lovley, D. R., Bug juice: Harvesting electricity with microorganisms. *Nat. Rev. Microbiol.* **2006**, 4, 497-508.
- (6) Reimers, C. E.; Tender, L. M.; Fertig, S.; Wang, W., Harvesting energy from the marine sediment-water interface. *Environ. Sci. Technol.* **2001**, 35, (1), 192-195.
- (7) Tender, L. M.; Gray, S. A.; Groveman, E.; Lowy, D. A.; Kauffman, P.; Melhado, J.; Tyce, R. C.; Flynn, D.; Petrecca, R.; Dobarro, J., The first demonstration of a microbial fuel cell as a viable power supply: Powering a meteorological buoy. *J. Power Sources* **2008**, 179, (2), 571-575.
- (8) Fan, Y. Z.; Hu, H. Q.; Liu, H., Enhanced coulombic efficiency and power density of air-cathode microbial fuel cells with an improved cell configuration. *J. Power Sources* **2007**, 171, (2), 348-354.
- (9) Nevin, K. P.; Richter, H.; Covalla, S. F.; Johnson, J. P.; Woodard, T. L.; Orloff, A. L.; Jia, H.; Zhang, M.; Lovley, D. R., Power output and coulombic efficiencies from biofilms of *Geobacter sulfurreducens* comparable to mixed community microbial fuel cells. *Environ. Microbiol.* **2008**, 10, (10), 2505-2514.

- (10) Richter, H.; McCarthy, K.; Nevin, K. P.; Johnson, J. P.; Rotello, V. M.; Lovley, D. R., Electricity generation by *geobacter sulfurreducens* attached to gold electrodes. *Langmuir* **2008**, 24, (8), 4376-4379.
- (11) Ringeisen, B. R.; Henderson, E.; Wu, P. K.; Pietron, J.; Ray, R.; Little, B.; Biffinger, J. C.; Jones-Meehan, J. M., High power density from a miniature microbial fuel cell using *shewanella oneidensis* dsp10 *Environ. Sci. Technol.* **2006**, 40, (8), 2629-2634.
- (12) Chiao, M.; Lam, K. B.; Lin, L. W., Micromachined microbial and photosynthetic fuel cells. *J. Micromech. Microeng.* **2006**, 16, (12), 2547-2553.
- (13) Crittenden, S. R.; Sund, C. J.; Sumner, J. J., Mediating electron transfer from bacteria to a gold electrode via a self-assembled monolayer. *Langmuir* **2006**, 22, (23), 9473-9476.
- (14) Qian, F.; Baum, M.; Gu, Q.; Morse, D. E., A 1.5 μ l microbial fuel cell for on-chip bioelectricity generation. *Lab Chip* **2009**, 9, (21), 3076-3081.
- (15) Takayama, S.; Ostuni, E.; LeDuc, P.; Naruse, K.; Ingber, D. E.; Whitesides, G. M., Laminar flows - subcellular positioning of small molecules. *Nature* **2001**, 411, (6841), 1016-1016.
- (16) Whitesides, G. M., The origins and the future of microfluidics. *Nature* **2006**, 442, 368-373.
- (17) Yang, J.; LeDuc, P., Three-dimensional molecular phase separation and flow patterns with novel multilevel fluidics. *Mol. Cell. Biomech.* **2006**, 3, (2), 69-77.
- (18) Hou, H. J.; Li, L.; Cho, Y.; de Figueiredo, P.; Han, A., Microfabricated microbial fuel cell arrays reveal electrochemically active microbes. *PLoS One* **2009**, 4, (8), 8.
- (19) Choban, E. R.; Markoski, L. J.; Wieckowski, A.; Kenis, P. J. A., Microfluidic fuel cell based on laminar flow. *J. Power Sources* **2004**, 128, (1), 54-60.
- (20) Ferrigno, R.; Stroock, A. D.; Clark, T. D.; Mayer, M.; Whitesides, G. M., Membraneless vanadium redox fuel cell using laminar flow. *J. Am. Chem. Soc.* **2002**, 124, (44), 12930-12931.
- (21) Lovley, D. R.; Phillips, E. J. P., Novel mode of microbial energy metabolism organic carbon oxidation coupled to dissimilatory reduction of iron or manganese. *Appl. Environ. Microbiol.* **1988**, 54, (6), 1472-1480.
- (22) Coppi, M. V.; Leang, C.; Sandler, S. J.; Lovley, D. R., Development of a genetic system for *geobacter sulfurreducens*. *Appl. Environ. Microbiol.* **2001**, 67, (7), 3180-3187.
- (23) Myers, C. R.; Nealson, K. H., Bacterial manganese reduction and growth with manganese oxide as the sole electron acceptor. *Science* **1988**, 240, 1319-1321.
- (24) Duffy, D. C.; McDonald, J. C.; Schueller, O. J. A.; Whitesides, G. M., Rapid prototyping of microfluidic systems in poly(dimethylsiloxane). *Anal. Chem.* **1998**, 70, (23), 4974-4984.
- (25) Quake, S. R.; Scherer, A., From micro- to nanofabrication with soft materials. *Science* **2000**, 290, (5496), 1536-1540.
- (26) Bond, D. R.; Lovley, D. R., Electricity production by *geobacter sulfurreducens* attached to electrodes. *Appl. Environ. Microbiol.* **2003**, 69, (3), 1548-1555.

- (27) Bond, D. R.; Holmes, D. E.; Tender, L. M.; Lovley, D. R., Electrode-reducing microorganisms that harvest energy from marine sediments. *Science* **2002**, 295, (5554), 483-485.
- (28) Kenis, P. J. A.; Ismagilov, R. F.; Whitesides, G. M., Microfabrication inside capillaries using multiphase laminar flow patterning. **1999**, 285, (5424), 83-85.
- (29) Tender, L. M.; Reimers, C. E.; Stecher, H. A.; Holmes, D. E.; Bond, D. R.; Lowy, D. A.; Pilobello, K.; Fertig, S. J.; Lovley, D. R., Harnessing microbially generated power on the seafloor. *Nat. Biotechnol.* **2002**, 20, (8), 821-825.
- (30) Lovley, D. R., Extracellular electron transfer: Wires, capacitors, iron lungs, and more. *Geobiology* **2008**, 6, (3), 225-231.
- (31) Kim, B. C.; Postier, B. L.; DiDonato, R. J.; Chaudhuri, S. K.; Nevin, K. P.; Lovley, D. R., Insights into genes involved in electricity generation in *geobacter sulfurreducens* via whole genome microarray analysis of the omcf-deficient mutant. *Bioelectrochemistry* **2008**, 73, (1), 70-75.
- (32) Reguera, G.; McCarthy, K. D.; Mehta, T.; Nicoll, J. S.; Tuominen, M. T.; Lovley, D. R., Extracellular electron transfer via microbial nanowires. *Nature* **2005**, 435, (7045), 1098-1101.
- (33) Reguera, G.; Nevin, K. P.; Nicoll, J. S.; Covalla, S. F.; Woodard, T. L.; Lovley, D. R., Biofilm and nanowire production leads to increased current in *geobacter sulfurreducens* fuel cells. *Appl. Environ. Microbiol.* **2006**, 72, (11), 7345-7348.
- (34) Kim, H. J.; Hyun, M. S.; Chang, I. S.; Kim, B. H., A microbial fuel cell type lactate biosensor using a metal-reducing bacterium, *shewanella putrefaciens*. *J. Microbiol. Biotechnol.* **1999**, 9, (3), 365-367.
- (35) Tront, J. M.; Fortner, J. D.; Plotze, M.; Hughes, J. B.; Puzrin, A. M., Microbial fuel cell technology for measurement of microbial respiration of lactate as an example of bioremediation amendment. *Biotechnol. Lett.* **2008**, 30, (8), 1385-1390.
- (36) Chang, I. S.; Jang, J. K.; Gil, G. C.; Kim, M.; Kim, H. J.; Cho, B. W.; Kim, B. H., Continuous determination of biochemical oxygen demand using microbial fuel cell type biosensor. *Biosens. Bioelectron.* **2004**, 19, (6), 607-613.
- (37) Tront, J. M.; Fortner, J. D.; Plotze, M.; Hughes, J. B.; Puzrin, A. M., Microbial fuel cell biosensor for in situ assessment of microbial activity. *Biosens. Bioelectron.* **2008**, 24, (4), 586-590.
- (38) Williams, K. H.; Nevin, K. P.; Franks, A.; Englert, A.; Long, P. E.; Lovley, D. R., Electrode-based approach for monitoring in situ microbial activity during subsurface bioremediation. *Environ. Sci. Technol.* **2010**, 44, (1), 47-54.
- (39) Gorby, Y. A.; Yanina, S.; McLean, J. S.; Rosso, K. M.; Moyles, D.; Dohnalkova, A.; Beveridge, T. J.; Chang, I. S.; Kim, B. H.; Kim, K. S.; Culley, D. E.; Reed, S. B.; Romine, M. F.; Saffarini, D. A.; Hill, E. A.; Shi, L.; Elias, D. A.; Kennedy, D. W.; Pinchuk, G.; Watanabe, K.; Ishii, S.; Logan, B.; Nealson, K. H.; Fredrickson, J. K., Electrically conductive bacterial nanowires produced by *shewanella oneidensis* strain mr-1 and other microorganisms. *Proc. Nat. Acad. Sci. U.S.A.* **2006**, 103, (30), 11358-11363.
- (40) Lanthier, M.; Gregory, K. B.; Lovley, D. R., Growth with high planktonic biomass in *shewanella oneidensis* fuel cells. *FEMS Microbiol. Lett.* **2008**, 278, (1), 29-35.

- (41) Marsili, E.; Baron, D. B.; Shikhare, I. D.; Coursolle, D.; Gralnick, J. A.; Bond, D. R., *Shewanella* secretes flavins that mediate extracellular electron transfer. *Proc. Nat. Acad. Sci. U.S.A.* **2008**, 105, (10), 3968-3973.
- (42) Thormann, K. M.; Saville, R. M.; Shukla, S.; Pelletier, D. A.; Spormann, A. M., Initial phases of biofilm formation in *shewanella oneidensis* mr-1. *J. Bacteriol.* **2004**, 186, (23), 8096-8104.
- (43) Rittmann, B. E., Opportunities for renewable bioenergy using microorganisms. *Biotechnol. Bioeng.* **2008**, 100, (2), 203-212.
- (44) Lin, W. C.; Coppi, M. V.; Lovley, D. R., *Geobacter sulfurreducens* can grow with oxygen as a terminal electron acceptor. *Appl. Environ. Microbiol.* **2004**, 70, (4), 2525-2528.
- (45) Yi, H.; Nevin, K. P.; Kim, B.-C.; Franks, A. E.; Klimes, A.; Tender, L. M.; Lovley, D. R., Selection of a variant of *geobacter sulfurreducens* with enhanced capacity for current production in microbial fuel cells. *Biosens. Bioelectron.* **2009**.
- (46) Cheng, S.; Liu, H.; Logan, B. E., Increased power generation in a continuous flow mfc with advective flow through the porous anode and reduced electrode spacing. *Environ. Sci. Technol.* **2006**, 40, (7), 2426-2432.
- (47) Izallalen, M.; Mahadevan, R.; Burgard, A.; Postier, B.; Didonato, R.; Sun, J.; Schilling, C. H.; Lovley, D. R., *Geobacter sulfurreducens* strain engineered for increased rates of respiration. *Metab. Eng.* **2008**, 10, (5), 267-275.
- (48) Lovley, D. R.; Holmes, D. E.; Nevin, K. P., Dissimilatory fe(iii) and mn(iv) reduction. In *Advances in microbial physiology*, vol. 49, Academic Press Ltd: London, 2004; Vol. 49, pp 219-286.
- (49) Rittmann, B. E.; McCarty, P. L., Model of steady-state-biofilm kinetics. *Biotechnol. Bioeng.* **1980**, 22, (11), 2343-2357.
- (50) Thorsen, T.; Maerkl, S. J.; Quake, S. R., Microfluidic large-scale integration. *Science* **2002**, 298, (5593), 580-584.

APPENDIX F: SUPPORTING INFORMATION FOR APPENDIX D

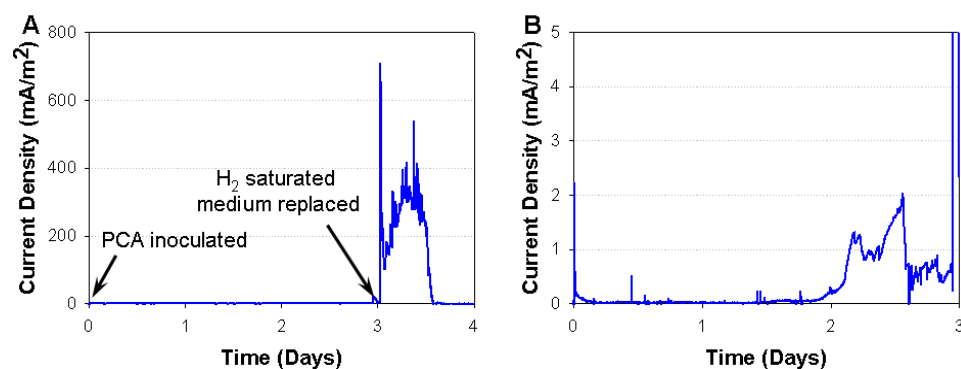


Figure E.1. Electricity production by *G. sulfurreducens* in the μ MFC with H₂ as the only electron donor. (A) High current density was observed when medium with acetate replaced with H₂ saturated medium. (B) Magnification of the axes in (A) to better show adaptation to electrode respiration and current production with acetate as electron donor.

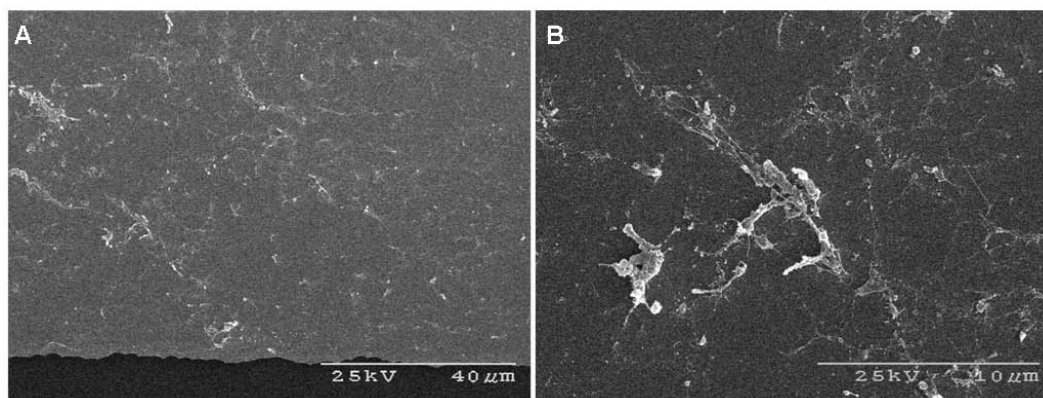


Figure E.2. SEM images for investigation of cell-like materials on cathode (Fig. 4 B, C1) at higher magnification.